Summer 8-13-2021

Delineation of New Mechanisms of DNA Damage Responses and Repair

YANQIU LI
University of Nebraska Medical Center

DELINEATION OF NEW MECHANISMS OF DNA DAMAGE RESPONSES AND REPAIR

By

Yanqiu Li

A DISSERTATION

Presented to the Faculty of

The Graduate College in the University of Nebraska

In Partial Fulfillment of the Requirements

For the Degree of Doctor Philosophy

Medical Science Interdepartmental Area

Graduate Program

(Oral Biology)

Under the Supervision of Professor Aimin Peng

University of Nebraska Medical Center

Omaha, Nebraska

August 2021

Supervisory Committee:

Aimin Peng, Ph.D. Gregory G. Oakley, Ph.D.

Jixin, Dong, Ph.D. Thomas M. Petro, Ph.D.

ACKNOWLEDGEMENTS

Funding support: The China Scholarship Council.

Much more important than the funding support, I would like to acknowledge the support and encouragement I received during my graduate study.

First of all, I'd like to give my giant thanks to my supervisor, Dr. Aimin Peng, for having me joined in his lab and for his continuous outstanding mentorship in the past five years. I respect him for his profound knowledge in DNA damage and his great dedication in scientific research, and feel most grateful for his support, inspiration and flexibility during my PhD study and research. I appreciate it for his easiness to get along with and his open-mindedness, which always makes me feel free to share every idea I have about my research.

I also owe my thanks to my committee members, Dr. Gregory G. Oakley, Dr. Jixin Dong and Dr. Thomas M. Petro, for their willingness to serve on my committee and for their endless support and encouragement, for their insightful comments and suggestions on my research, which broadened my viewpoints in research from different aspects. Special thanks to Dr. Gregory G. Oakley for helping me with flow cytometry analysis every week; thanks to Dr. Jixin Dong for generously providing us with plasmids and for helping me in phos-tag gel; thanks to Dr. Thomas M. Petro for donating us with antibodies of high quality.

I also thank my lab colleagues, Laura Fisher, Ling Wang and Songli Zhu for being willing to instruct me in the lab and helping me out when trouble troubles my research. Without them, I wouldn't have grown into a researcher as I am today.

My sincere thanks also go to Dr. James K. Wahl III, and Deborah J, Merritt, for their support during my study and IADR meeting registration. More thanks to Mrs. Phyllis

Kumm, Dr. Ali Nawshad and Dr. Peter J. Giannini for devoting their excellent expertise and suggestion to our immunohistochemistry analysis.

My deepest gratitude extended to my friends in the College of Dentistry UNMC, Dr. Yike Li and Ms. Bo Chao, for their accompaniment and support in the past years. It is super great to have friends as brilliant and helpful as them. I enjoy every gathering and hangout with them. More thanks also extended to my best friend in China, Shuang Yang, and her baby son, Shufan Wan, who continuously have my back and share all our feelings during the past twelve years.

Lastly, I could never forget to give my heartfelt appreciation to my family. I could not thank my parents too much for their endless love and raising me up as an honest, brave, integrity and hard-working girl. I also want to express my thanks to my boyfriend, Dr. Kun Jin, thank you so much for being with me in the past ten years.

I came here with my dream five years ago, now the dream is coming true. I appreciate every person who has helped and supported me along the way of my PhD study and training. They make me a better person, who is ready to meet her future full of confidence and hope.

ABSTRACT: DELINEATION OF NEW MECHANISMS OF DNA DAMAGE RESPONSES AND REPAIR

Yanqiu Li, Ph.D.

University of Nebraska Medical Center, 2021

Supervisor: Aimin Peng, Ph.D.

Upon DNA damage, cells promptly activate the cellular DNA damage response (DDR), a surveillance mechanism that leads to DNA repair, cell cycle arrest, and apoptosis. DDR deficiencies cause genomic instability, and are tightly associated with cancer predisposition, immunodeficiency, neurological diseases, and aging. On the other hand, radiation and many chemotherapeutics eliminate cancer cells by inducing DNA damage. Therefore, understanding the DDR and its involvement in cancer is a crucial step toward improving anti-cancer therapeutics. The overarching goal of this project is to delineate how cells respond to, and repair, DNA damage, thus to develop new strategies to overcome cancer resistance.

Microtubule associated serine/threonine kinase like (MASTL), also known as greatwall (GWL), was recently characterized as novel kinase that plays an important role in regulating mitosis. High-level of MASTL expression is frequently observed in various cancers, promoting cancer metastasis and resistance to therapeutics. However, little is known about how MASTL itself is regulated during replication stress and DNA damage, and whether MASTL is involved in immune response, requiring further research to answer these questions.

In the beginning of this project, we identified an E3 ubiquitin ligase that mediates MASTL protein degradation. Interestingly, we also highlighted that human cancer cells depleted of this enzyme exhibited weakened DNA damage checkpoints and faster cell

recovery from DNA damage. Afterwards, we examined the new function of MASTL in regulating innate immune response. This finding provides conceptual advances of MASTL in promoting tumorigenesis and evasion. Lastly, we characterized a novel function of Sm core proteins in DNA repair. Our research revealed that Sm proteins were associated with DNA damage and were required for homologous recombination (HR), an important mechanism to repair double strand breaks (DSBs).

Taken together, our studies delineated several novel mechanisms involved in the DNA damage response and repair, bringing better understandings of how cancer cells bypass DNA damage during tumorigenesis and treatment. Future investigations will potentially lead to new therapeutic strategies that predict cancer resistance and enhance treatment outcomes.

TABLE OF CONTENTS

LIST OF FIGURES

LIST OF ABBREVIATOINS

53BP1: p53-binding protein 1

ATM: ataxia-Telangiectasia-Mutated

ATR: ataxia telangiectasia and Rad3-related

BRCA1: breast cancer type 1 susceptibility protein

CDK: cyclin-dependent kinase

cGAS: cyclic GMP-AMP Synthase

ChIP: chromosome immunoprecipitation

CHK1: checkpoint 1

CHK2: checkpoint 2

DAPI: 4', 6-diamidino-2-phenylindole

DNA-PK: DNA-dependent protein kinase

DDR: DNA damage response

DMEM: Dulbecco's modified eagle medium

DSB: double strand break

E6AP: E6 associated protein

FACS: fluorescence-activated cell sorting

FBS: fetal bovine serum

FEN: flap endonuclease-1

GFP: green fluorescence protein

GST: glutathione-S-transferase

H2AX: H2A histone family member X

H2B: histone H2B

HaCaT: human aneuploid immortal keratinocyte cells

HeLa: human cervix carcinoma cells

HEK293: human embryonic kidney 293 cells

HR: homologous recombination

IF: immunofluorescence

IFN: interferon

IHC: immunohistochemistry

IP: immunoprecipitation

IR: ionizing radiation

IRF3: interferon regulatory factor 3

MASTL: microtubule associated serine/threonine kinase like

MBP: maltose binding protein

MDA-MB-231: human breast adenocarcinoma cell line (Caucasian)

MDA-MB-468: human breast adenocarcinoma cell line

NHEJ: non-homologous end joining

PARP1: poly (ADP-ribose) polymerase 1

Poly I: C: polyinosinic : polycytidylic acid

PP2A-B55α: protein phosphatase 2 regulatory subunit B alpha

P.S.: penicillin and streptomycin

qPCR: quantitative polymerase chain reaction

RAD51: homo sapiens RAD51 recombinase

RAW264.7: mouse monocyte macrophage cell line

RPA: replication protein A

SCC38: squamous cell carcinoma 38 (HPV-)

SDS-PAGE: sodium dodecyl sulfate-polyacrylamide gel electrophoresis

siRNA: small interfering RNA

Sm-D3: small nuclear ribonucleoprotein Sm D3

Sm-B/B’: small nuclear ribonucleoprotein-associated proteins B and B'

snRNP: small nuclear ribonucleoproteins

SSB: single strand break

STAT1: signal transducer and activator of transcription 1

STING: stimulator of Interferon Genes

TBK1: TANK binding kinase 1

UV: ultraviolet

UM-SCC38: squamous cell carcinoma 38 from University of Michigan

WB: western blotting

CHAPTER 1: E6AP REGULATES MASTL IN DNA DAMAGE AND REPLICATION STRESS

1.0 Abstract

MASTL (Microtubule associated serine/threonine kinase-like), also known as greatwall (GWL), was recently found to play a role as a required kinase to enter and maintain mitosis by activating its substrates ENSA/ARPP19, which inhibits PP2A-B55, a major phosphatase responsible for dephosphorylation of mitotic substrates to promote mitotic exit. Studies from our laboratory demonstrated a role of MASTL in promoting cell cycle resumption after replication stress and DNA damage. Consistent with these functions, MASTL is frequently overexpressed in various types of cancer, including head and neck cancer. However, compared to the function of MASTL, little is known about how MASTL itself is regulated in these important processes. Here we demonstrate a direct binding relationship between the E3 ubiquitin ligase E6AP and MASTL through their N-terminal domains, which could be disrupted by DNA damage and replication stress. We also proved that E6AP promotes MASTL protein degradation by ubiquitination. Finally, we found that E6AP knockout cells exhibited less accumulation of DNA damage response checkpoints but faster cell recovery capability from replication stress. Given the fact that cell cycle resumption promoted by MASTL has been suggested as a driver of cancer resistance to radiation and chemotherapy, our new findings may lead to clinically relevant information for cancer therapy.

1.1. Introduction

Microtubule associated serine/threonine kinase like (MASTL) is a master kinase to regulate mitosis and meiosis [1, 2]. It is required for both mitotic entry and mitotic maintenance and has the potential to phosphorylate many substrate proteins, including ARPP19 and ENSA [3]. At mitotic entry, cyclin-B–Cdk1 phosphorylates MASTL at its

kinase domain (residues T194 and T207), followed by subsequent MASTL autophosphorylation at residue S875 [4]. MASTL-regulated phosphorylation of ARPP19 and ENSA inhibits PP2A-B55, the phosphatase that antagonizes cyclin-B–Cdk1 activity and that is responsible for the dephosphorylation of mitotic substrates, thereby promoting a correct timing and progression of mitosis [4]. At mitotic exit, concomitantly with cyclin B degradation, MASTL activity is downregulated by dephosphorylation, which is regulated by three phosphatases – protein phosphatase 1 (PP1), PP2A-B55 and RNA polymerase II C-terminal domain phosphatase (Fcp1, also known as CTDP1), thus promoting effective mitotic exit [5-8]. In mouse zygotes, MASTL-ENSA-PP2A pathway regulates the timing of pronuclear formation onset, during which ribosomal S6 kinase regulates MASTL phosphorylation at residue T297 and enhances MASTL kinase activity even after CDK1 inactivation [9]. Recent evidence demonstrated that AKT also regulates MASTL phosphorylation at residue T299 in HEK293 cells [10]. Ablation of MASTL results in cell cycle dysregulation and loss of germ cells in mouse, which could be rescued by PP2A deletion [11]. Moreover, loss of function of MASTL was found correlated with reduced circulating thrombocytes in zebrafish [12].

Besides its function in cell cycle regulation, MASTL also shows its role in human disease progression. For instance, MASTL deficiency impairs megakaryocytes maturation and shortens the half-life of circulating platelets in mice [13]. MASTL dysfunction also seems to contribute to high UV signature mutation load, which is a primary environmental driver of melanoma [14]. Besides, high level of MASTL was expressed in thyroid tumor cells, while silencing MASTL in thyroid tumor cells induces less cell proliferation, more DNA damage, and higher cell sensitivity to cisplatin [15]. High MASTL level was also related with high-risk of colon cancer and lower survival probability, and silencing MASTL expression, which sensitized colon cancer cells to

chemotherapy, rendered cell arrest and apoptosis in vitro and inhibited xenograft-tumor growth in vivo [16]. Moreover, MASTL was frequently upregulated in estrogen receptor-positive (ER+) breast cancer, which was associated with higher metastatic relapse (MR) risk, worse MR-free survival and cancer resistance to chemotherapy [17, 18]. Other studies demonstrated that MASTL depletion impaired cells proliferation and resulted in cell cycle defects in breast cell lines and slower breast tumor growth in vivo, thus blocking breast cancer cells invasion, migration and metastasis [19, 20]. Knockdown MASTL re-sensitize non–small cell lung cancer (NSCLC) cells to radiotherapy [21], and has been predicted to be a promising target for cancer treatment [22].

While so much research has been focused on MASTL function, there is a great limitation in what is known about how MASTL expression is regulated, especially under the conditions of DNA damage and replication stress, which are the major mechanisms of current chemotherapy and radiotherapy to kill cancer cells.

E6AP, encoded by gene *UBE3A*, was initially discovered in 1993 and is the prototype HECT domain family of E3 ubiquitin protein ligases, which regulate protein expression [23]. As an E3 ubiquitin ligase, E6AP has been found to be related with viral infection, cancer development and neurodegenerative disorders [24]. Loss function of E6AP activity is the molecular etiology of Angelman syndrome (AS), a severe neurological disorder characterized by mental retardation, absent speech, ataxia, seizures and hyperactivity [25]. Complete deletion of *UBE3A* gene in rat could generate a model for AS, which phenotypically mirrors human AS [26]. A point mutation of E6AP at amino-terminal Zinc-binding (AZUL) domain impairs its ability to bind with 26S proteasome and contributes AS [27]. *UBE3A* gene copy number variation resulting overexpression of E6AP is directly linked to autism spectrum disorders [28].

In addition, dysfunction of E6AP was associated with a series of cancers. High level of E6AP was found in 60% of B-cell lymphoma and Burkitt's lymphoma, where E6AP acted as an E3 ligase to promote the degradation of the well-established tumor suppressor promyelocytic leukemia (PML) protein [29]. In prostate cancer, upregulated E6AP targeted both PML and p27 for their degradation, which was associated with regional metastasis, poor prognosis and relapse in prostate cancer patients [30]. Overexpression of E6AP triggered mesenchymal characteristics of prostate epithelial cells, while knockdown E6AP reduced metastasis potential and mesenchymal features of prostate cancer cells, which also promoted cellular senescence in vivo and sensitized prostate cancer cells to radiation-induced death [31, 32]. In human papillomavirus (HPV) infection, E6AP was hijacked by HPV E6 oncoprotein at the LXXLL peptide motif, then catalyzed the ubiquitination and proteolysis of p53, promoting HPV-induced cervical tumorigenesis [33, 34]. In addition to these known tumor suppressors, another set of proteins, including MAPK1, CDK1, CDK4, PRMT5, β-catenin, and UbxD8, have been found to be targets of E6AP for their ubiquitination and degradation [35]. In breast cancer cells, E6AP was found to interact with ENO1 and direct degradation of ENO1, a protein that has been shown to be associated with cancer cell invasion and metastasis, tamoxifen resistance and shorter overall survival in patients with breast cancers [36]. E6AP was also found highly expressed in hepatic stellate cells, which were essential for liver fibrosis derived from virus infection, chronic alcohol abuse and other etiology [37]. Other researchers demonstrated that E6AP also played a role in inhibiting HIV-1 replication by mediating viral protein Gag degradation [38].

Recent proteomic-transcriptomic measurements in prostate cancer cells exposed novel potential links of E6AP with DNA damage repair, DNA replication translation and centrosome regulation [39, 40]. Cells with E6AP depletion showed reduced capacity to

accumulate ROS and impaired senescent and apoptotic responses to oxidative DNA damage and stress [41]. In a xenograft model, downregulation of E6AP rendered transplanted tumors refractory to growth-suppressive effects of hydrogen peroxide [41]. Mouse embryonic fibroblasts (MEFs) lacking E6AP exhibited a range of transformed phenotypes, including the ability to grow under DNA damage, enhanced proliferation, anchorage independent growth and enhanced growth of xenografts in mice, suggesting that E6AP may act as an important regulator of the cellular response to stress [42].

Our recent proteomics assay revealed E6AP as a potential molecule that associates with MASTL, promoting study as to the relationship between E6AP and MASTL expression under conditions of DNA damage and replication stress.

1.2. Materials and methods

1.2.1. Cell lines and establishment of stable cell lines

Human cervix carcinoma (HeLa) and Human embryonic kidney 293 (HEK293) cell lines, authenticated by ATCC, were maintained in Dulbecco's modified Eagle medium (DMEM, Hyclone) with 10% fetal bovine serum (FBS, Hyclone). Human head and neck squamous cell carcinoma UM-SCC-38 cells were obtained from Dr. Thomas Carey (University of Michigan, Ann Arbor, MI) and maintained in DMEM (HyClone) with 10% FBS (HyClone).

For the generation of stable E6AP KO cell lines expressing different variants, HEK293 E6AP KO cells were transfected with plasmids as follows: pCDNA3.1 (+) EV, E6AP wild type (WT), E6AP S218A mutant. Transfections were performed using Lipofectamine 2000 (Thermo Fisher Scientific) and transfected cells were selected with G418 (800μg/mL) and cultured in the presence of lower concentration of G418 (400μg/mL). The expression level of E6AP variants were analyzed by Western blot.

1.2.2. Plasmid and siRNA transfections

As described previously [43], transfection of plasmid vectors was carried out using Lipofectamine 2000 (Invitrogen) following the manufacturer's protocol. siRNA targeting human *UBE3A* or human *MASTL* (Integrated DNA Technologies) was transfected into cells using Lipofectamine RNAi MAX (Invitrogen). A non-targeting control siRNA was used as a control. *UBE3A* siRNA sequence: 5'-3'AGGAAUUUGUCAAUCUUU; 5'-3' UCAGAAUAAAGAUUGACA. *MASTL* siRNA sequence: 5'-3'GUCUACUUGGUAAUGGAA; 5'-3' UAAGAUAUUCCAUUACCA.

1.2.3. Generation of E6AP knockout cell lines by CRISPR-Cas9

HeLa and HEK293 cell lines were used to build the E6AP knockout (KO) cell line using the established CRISPR-cas9 gene editing method with following single guide sequence: GCAAGCTGACACAGGTGCTG in lentiCRISPR v2 vector [44, 45]. In brief, cells were seeded in 35-cm dish before transfection of CRISPR-sgRNA targeting *E6AP* was introduced at 32°C. Twenty-four hours after transfection, the cells were digested with trypsin and single cell was seeded in 96-well plate. Selection was performed with G418 to get single colony, and the knockout efficiency was assessed by TIDE (Tracking of Indels by Decomposition) analysis using the web tool (https://tide.deskgen.com/) and confirmed by western blot.

1.2.4. Western blot analysis

Cell lysates or IP products were harvested in 1X Laemmli sample buffer (Bio-Rad) and boiled on 95 °C for 5 minutes before they were resolved by SDS-PAGE and electro-transferred to PVDF membranes (Millipore, Billerica, MA). Then membranes were blocked with 5% nonfat dry milk in 1× TBST (10mM Tris-HCl, pH7.5, 150mM NaCl, 0.05% Tween 20) for 30 mins at room temperature, followed by washing three times in 1× TBST and incubation with primary antibodies overnight at cold room. On the next

day, these first antibody-conjugated membranes were washed three times again in 1× TBST, and transferred into horseradish peroxidase (HRP)-conjugated secondary antibodies solution (Sigma) for 1 hour at room temperature before detection using an enhanced chemiluminescence (ECL) substrate kit (0.1M Tris-HCl, pH8.5, luminol, Couric acid, peroxide hydrogen).

1.2.5. Immunofluorescence

For immunofluorescence (IF), $1x10^6$ HeLa cells were seeded on 35-mm dishes with microscope cover glasses (Fisher Scientific, PA) on the bottom. After incubation in fresh medium for 24 hours, the cells were transfected with HA-tagged plasmid vector expressing E6AP. Then these microscope cover glasses were harvested, washed with PBS and fixed in 100% ethanol for 30 minutes on a rocker at room temperature, followed by incubation in 5% saponion for 30 minutes then in 10% goat serum for 30 minutes before they were immersed in the mixture of goat-anti rabbit HA or E6AP antibody (Cell Signaling Technology) and goat-anti mouse MASTL antibody overnight. The subsequent day, cells on the glasses were washed and incubated in Alexa Fluor secondary antibodies (Invitrogen, 1: 1,000) for 1 hour at room temperature before cells nuclei were stained with 4', 6-diamidino-2-phenylindole (DAPI). The stained cells were imaged using a Zeiss Axiovert 200M inverted fluorescence microscope at the Microscopy room of Dr. James K. Wahl's laboratory (University of Nebraska Medical Center, USA).

1.2.6. Antibodies for western blot and immunofluorescence

Mouse antibody to MASTL was purified as described previously [46]. α-tubulin (Santa Cruz Biotechnology, #sc-5286), E6AP (Bethyl Laboratories, Inc, A300-351-T), HA (self-purified), gamma H2AX/ phospho-histone H2A.X ser139 (Cell signaling technology #9718S), phospho-ATM/ATR substrate motif (Cell signaling technology, #6966S), phospho-SMC1 Ser957(Cell signaling technology, #58052), phospho-CHK1 Ser345

(Cell signaling technology, #2348), phospho-CHK2 (Cell signaling technology, #2197), RPA2 (Thermo Fisher Scientific Cat# PA5-22256), S5a (Boston Biochem,#SP-400), ubiquitin (Cell Signaling Technology, #3936), GFP (Cell Signaling Technology #2555).

1.2.7. Chemicals

The following chemicals were used: Hydroxyurea (HU, MP Biomedicals, LLC, Cat No.102023), doxorubicin (DOX, MilliporeSigma, CAS No. 25316-40-9), caffeine (Sigma-Aldrich, C0750), ATM/ATR inhibitor (ATM/ATRi, Sigma-Aldrich), ATM inhibitor (ATMi, Selleckchem, Cat No.S1092), ATR inhibitor (ATRi, Selleckchem, Cat No.S8007), cycloheximide (CHX, Fluka analytical, 01810), etoposide(Sigma Life Science, E1383), camptothecin (Sigma Life Science, C9911), G418 sulfate (Thermo Fisher Scientific, Cat No.10131035), MG132 (Calbiochem, CAS No.133407-82-6), cisplatin(R&D systems, CAS No.15663-27-1), propidium iodide (PI,Thermo Fisher Scientific, Cat No.P1304MP), nocodazole (Pubchem, CAS No. 31430-18-9), paclitaxel (taxol, LC Laboratories, Cat No. P-9600), Lambda protein phosphatase (lambda PP) were purchased from New England Biolabs (P0753S). Isopropyl-beta-D-thiogalactopyranoside (IPTG, RPI research products international, CAS No. 367-93-1).

1.2.8. Flow cytometry

Cell cycle progression were examined in HEK293 wild type (WT) cells and E6AP knockout (KO) cells. Briefly, cells were treated with either hydroxyurea or doxorubicin for 2 hours, then washed with 1X PBS and incubated in fresh medium and allowed for recovery up to 24 hours. Then cells were harvested at indicated times and fixed in 70% cold ethanol, washed with cold PBS at least once and stained with propidium iodide (20ug/ml propidium iodide and 200ug/ml RNAse A diluted in PBS with 0.1% Triton X100) at 37°C for 15 mins before analysis by flow cytometry.

1.2.9. Plasmid construction, protein expression and pulldown assay

Three segments of MASTL/ GWL (N, amino acids1-340; M, amino acids335-660; C, amino acids656-887) were fused into vector pGex 4T-1(GE Healthcare), while full-length E6AP was fused with pMBP vector as previously described [47]. Conversely, three segments of E6AP were also sub-cloned into pMBP vector and full-length MASTL/GWL was sublimed into pGex 4T-1 vector. The resulting constructs were transfected into BL21 bacteria strain for protein expression and purification. GST-tagged protein or fragments were purified and concentrated on glutathione-Sepharose beads (New England Biolabs) from BL21 bacteria lysates, while MBP-tagged ones were purified and enriched on Amylose resin. For GST pulldown assays, glutathione-Sepharose beads were firstly washed with GST washing buffer three times before overnight incubation with purified specific recombinant GST-tagged proteins. After washing away unbound proteins, those MBP-tagged proteins were introduced to the reaction system whether with addition of Xenopus egg extracts or not. The reaction system was then incubated at room temperature for 1hour with gentle rotation before the protein-bonded beads were isolated, washed and eluted for immunoblotting.

1.2.10. In vitro ubiquitination assay

Our in vitro ubiquitination assay was performed using the E6AP ubiquitin ligase kit (Boston Biochem, Cat#K-230) according to the protocol provided by manufacturer. All reactions were prepared on ice. Briefly, all protein reagents and buffers were quickly thawed with rapid back-and-forth rolling between palms and hands. Then His_6-S5a substrate protein (provided by the kit and used as positive control) or our self-purified GST-tagged MASTL protein and other reagents provided by the kit were added into a 1.5ml polypropylene tube following the recommended volumes and order of addition. Afterwards, the tube was spun and incubated at 37°C for up to 180 minutes. The

reaction was terminated by adding 8ul of 5X loading buffer and 1ul of 1M DTT, then heated to 95 °C for 5 minutes. The acquired samples were analyzed by western blot, while samples from reactions without Mg^{2+}-ATP were used as negative control.

1.2.11. Immunoprecipitation

HeLa cells which is continuously expressing GFP-tagged MASTL were seeded into 60-mm dishes at appropriate density. 24 hours after seeding, cells were treated with 10mM of hydroxyurea (HU) or 1xPBS overnight before they were harvested with lysis 250 buffer and stored at -80 degrees. In the meanwhile, anti-rabbit magnetic beads (Thermo Fisher) were washed thrice with 1XPBS and conjugated to GFP antibody (self-purified) overnight at cold room with gentle shaking. The unbounded GFP antibody was washed away before the magnetic beads were incubated with HeLa cell lysates prepared in earlier steps. After 1hour of reaction at room temperature, the beads were isolated on magnet racks and washed 3-5 times with 1XPBS and then eluted with Laemmli sample buffer for immunoblotting analysis.

1.2.12. Xenopus egg extracts

Cytostatic factor (CSF) extracts were prepared as described previously [48]. Eggs were dejellied with 2% cysteine in 1× XB (1 M KCl, 10mM MgCl2, 100mM HEPES (pH 7.7), and 500 mM sucrose) and washed in 1× XB (1M KCl, 11mM MgCl2, 100mM HEPES (pH 7.7), and 500mM sucrose). Eggs were packed in centrifuge tubes by low-speed centrifugation and then crushed by centrifugation at 10,000 × g. The cytoplasmic layer was collected and further separated by another centrifugation at 10,000 × g. For cycling extracts, eggs were rinsed with distilled water and then dejellied with 2% cysteine in 1× XB. The eggs were washed five times in 0.2× MMR buffer (100mM NaCl, 2mM KCl, 1mM MgCl2, 2mM CaCl2, 0.1mM EDTA, 10mM HEPES, and KOH to pH 7.8). The Ca2+ ionophore A23187 (MilliporeSigma,CAS No.52665-69-7) was added to 10ng/ml

until the animal poles rotated. The eggs were then washed and packed by low-speed centrifugation. The eggs were crushed by centrifugation at 10,000 × g. The cytoplasmic layer was transferred to new tubes, and energy mix (7.5mM creatine phosphate, 1mM ATP, and 1 MgCl2) was added. The cytoplasmic layer was further separated by another centrifugation at 10,000 × g and store at -80℃ freezer for later use.

1.2.13. Clone and site-directed mutagenesis

Human *MASTL* gene was cloned from a Homo sapiens cDNA library, and inserted into a pEGFP vector (Addgene) with an N-terminal MBP-tag. Plasmid vector HA-tagged human E6AP isoform II was obtained from Addgene (Plasmid #8658) and E6AP mutant variants were generated using site-directed mutagenesis (Agilent) following the protocol recommended by the manufacturer.

1.2.14. Purification of antibodies

Monoclonal antibodies recognizing human MASTL were generated as described before [46]. For antibodies to α-tubulin or phospho-E6AP S218, three 8- to 9-week-old female Balb/C mice were injected subcutaneously with 50–150mg of purified antigen per mouse. Intraperitoneal booster injections were given at 2-week intervals, followed by daily injections 3 days prior to sacrifice. Then mice splenocytes were isolated and fused with the mouse myeloma cell line P3/NS1/1-Ag4-1 (ATCC, Manassas, VA) in the presence of polyethylene glycol (ATCC). The complete fusion was plated in 30 96-well plates before unfused myeloma cells were eliminated with medium containing hypoxanthine, aminopterin, and thymidine the following day. Hybridoma supernatants were screened by immunoblotting analysis and positive hybridomas were cloned by limited dilution and maintained in Sigma HY medium supplemented with 20% FBS.

1.2.15. In vitro dephosphorylation assay

The dephosphorylation assay was completed following the manufacturer's protocol. In brief, 40µl of cell lysates were mixed with 5µl of 10X NEBuffer for Protein MetalloPhosphatases (PMP) and 5µl of 10mM MnCl2, with subsequent 1µl of Lambda Protein Phosphatase (New England Biolabs, Cat No. P0753S). Then the mixture was incubated at 30°C for 30 minutes to 1 hour before reactions were terminated by adding 1X Laemmli sample buffer (Bio-Rad) and boiled for immunoblotting.

1.2.16. Statistical analysis

Depending on specific conditions, either one-ANOVA analysis or student's t-test was used to compare the differences between means$\pm$standard deviation; only $p<0.05$ was considered as statistically significant.

1.3. Results

1.3.1. MASTL expression is upregulated after DNA damage or replication stress via protein stabilization

First, we examined the characteristics of MASTL expression upon DNA damage and replication stress induced by commercial DNA-damaging drugs. Western blot results showed that MASTL protein level was increased upon drug treatments, including doxorubicin (DOX), hydroxyurea (HU), camptothecin (CPT) (Figure 1.3.1A, B&D-J); so was that of phosphorylated RPA2, a subunit of replication protein A (RPA). Further protein stability assay revealed that MASTL up-regulation under replication stress and DNA damage was due to more protein stabilization, because MASTL protein level continued to increase in the HU-pretreated cells compared to continuous degradation in the control cells (Figure 1.3.1C).

A

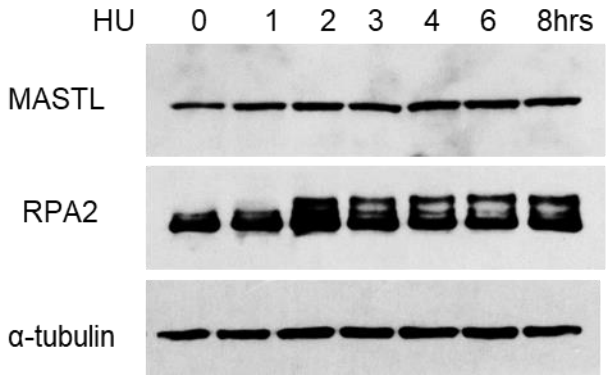
HU 0 1 2 3 4 6 8hrs
MASTL
RPA2
α-tubulin

B

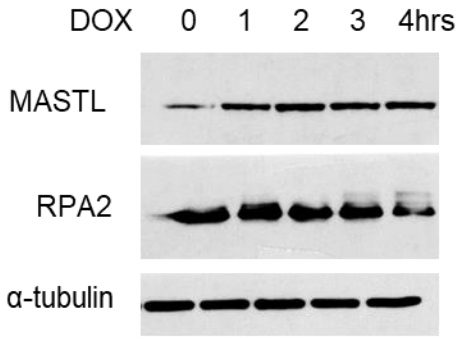
DOX 0 1 2 3 4hrs
MASTL
RPA2
α-tubulin

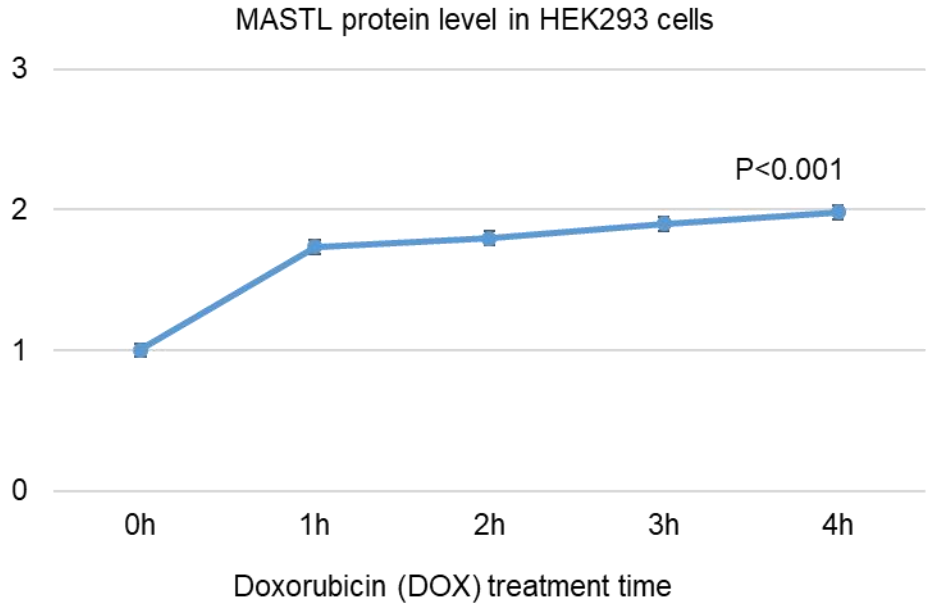
MASTL protein level in HEK293 cells
3
2
1
0
P<0.001
0h
1h
2h
3h
4h
Doxorubicin (DOX) treatment time

C

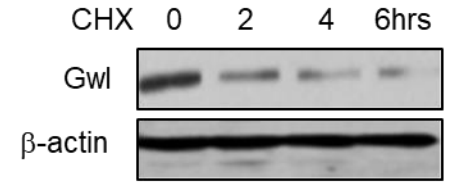
CHX 0 2 4 6hrs
Gwl
β-actin

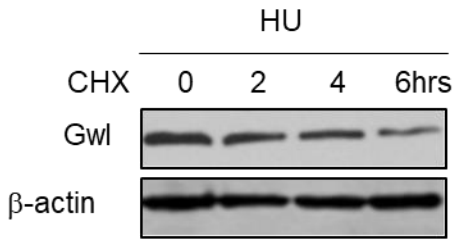
HU
CHX 0 2 4 6hrs
Gwl
β-actin

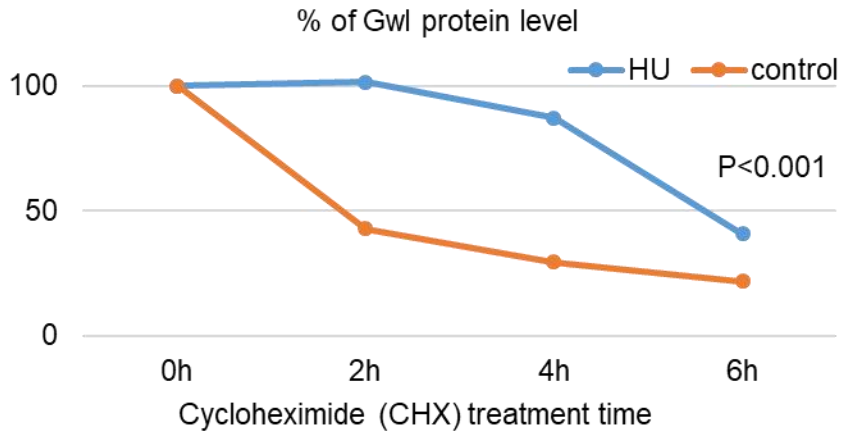
% of Gwl protein level
HU
control
100
50
0
P<0.001
0h
2h
4h
6h
Cycloheximide (CHX) treatment time

D

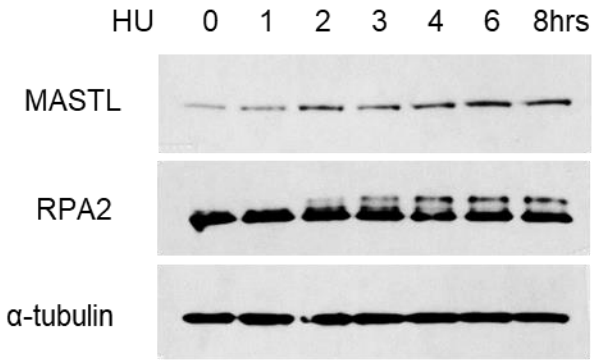
HU 0 1 2 3 4 6 8hrs
MASTL
RPA2
α-tubulin

E

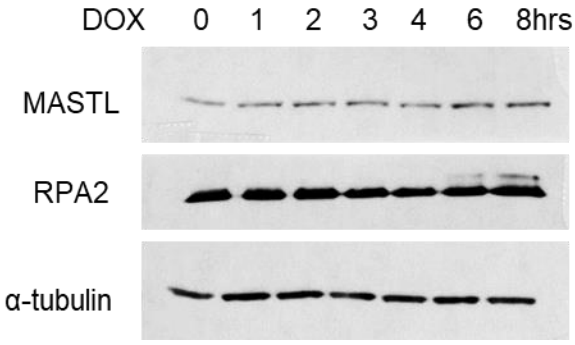
DOX 0 1 2 3 4 6 8hrs
MASTL
RPA2
α-tubulin

F

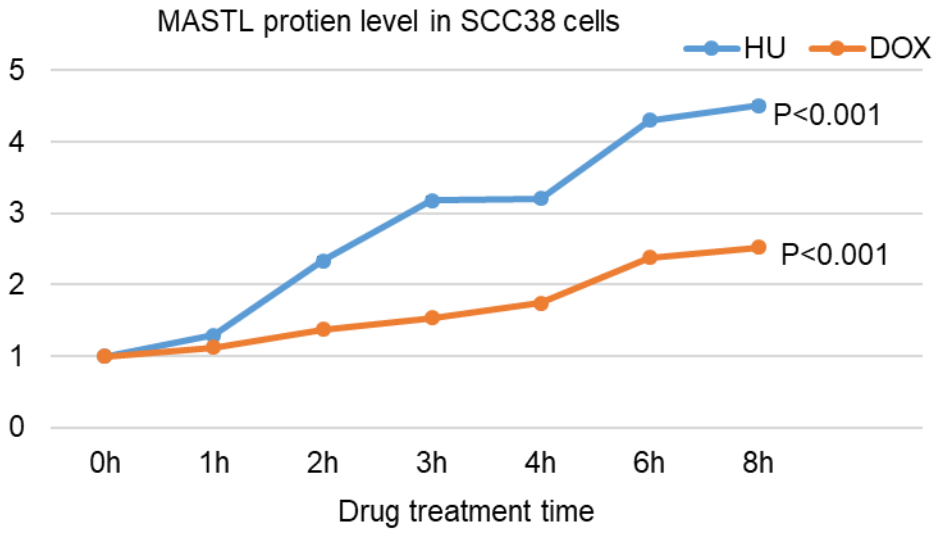
MASTL protien level in SCC38 cells
HU
DOX
P<0.001
P<0.001
5
4
3
2
1
0
0h
1h
2h
3h
4h
6h
8h
Drug treatment time

G

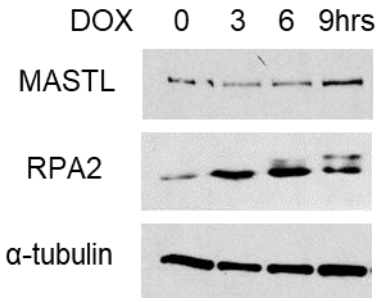
DOX 0 3 6 9hrs
MASTL
RPA2
α-tubulin

H

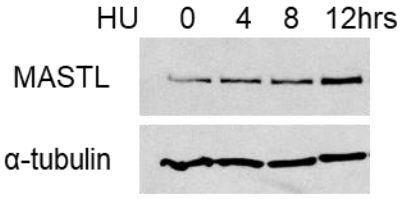
HU 0 4 8 12hrs
MASTL
α-tubulin

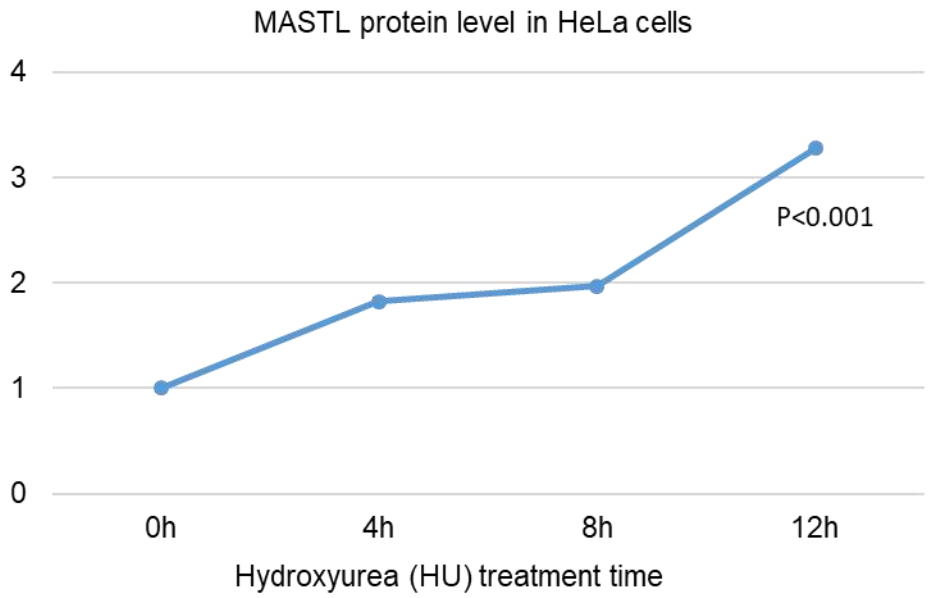
MASTL protein level in HeLa cells
4
3
2
1
0
P<0.001
0h
4h
8h
12h
Hydroxyurea (HU) treatment time

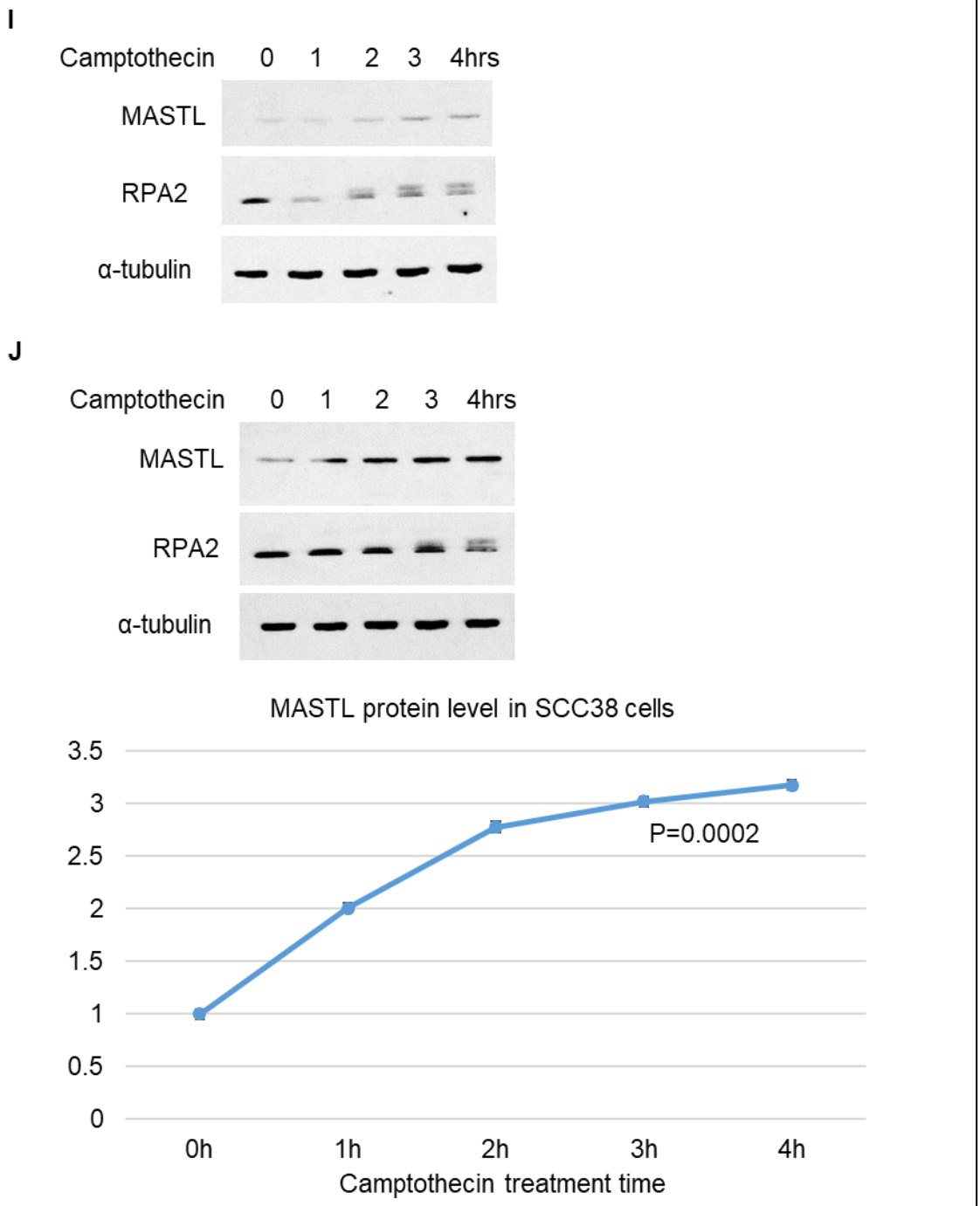

Figure 1.3. 1. MASTL expression is upregulated after DNA damage or replication stress via protein stabilization.

(**A**) HEK293 cells were treated with 10mM of hydroxyurea (HU) for indicated hours before cell lysates were collected for analysis by immunoblotting. (**B**) HEK293 cells were treated with 0.5μM of doxorubicin (DOX) for indicated hours; then cell lysates were harvested for western blot (left panel) and quantification of MASTL protein level

normalized to α-tubulin was shown as the right panel. (**C**) HeLa cells were treated with cycloheximide (CHX, 20μg/ml) alone (upper panel) or HU and cycloheximide (CHX 20μg/ml) (middle panel) for different time; then cell lysates were collected and MASTL, RPA2 and α-tubulin expression was determined by western blot. Quantification of MASTL protein level normalized to α-tubulin was shown as the lower panel. Data from Feifei Wang. (**D-F**) SCC38 cells were treated with 10mM of hydroxyurea (HU) (**D**) or 0.5μM of doxorubicin (DOX) (**E**) for indicated hours; then cell lysates were collected and MASTL, RPA2 and α-tubulin expression was determined by western blot. Quantification of MASTL protein level normalized to α-tubulin was shown as panel (**F**). (**G**) HeLa cells were treated with 0.5μM of doxorubicin (DOX), (**H**) HeLa cells were treated with10mM of hydroxyurea (HU) for indicated hours, then cell lysates were collected and MASTL, RPA2 and α-tubulin expression was determined by western blot (upper panel). Quantification of MASTL protein level normalized to α-tubulin was shown as the lower panel. (**I**) HeLa cells were treated with 10μM of camptothecin for up to 4 hours, and cell lysates were harvested for western blotting. (**J**) SCC-38 cells were treated with 10μM of camptothecin for up to 4 hours, and cell lysates were harvested for western blotting, and quantification of MASTL protein level normalized to α-tubulin was shown as the right panel. All experiments were carried out at least three times. Statistical analysis was performed using student's t-test and data were shown as mean ± standard deviation.

1.3.2. E6AP associates with MASTL and mediates MASTL degradation via ubiquitination

In order to find out candidate molecules that might bind or regulate MASTL protein expression, a proteomics mass spectrum was did and the result revealed multiple peptides from several proteins, including16 peptides of E6AP (Figure 1.3.2A), encoded by gene *UBE3A*, which suggested that E6AP might bind or regulate MASTL expression under DNA damage and replication. This hypothesis was firstly confirmed in pulldown assays in vitro (Figure 1.3.2B) and in HeLa cell lysates (Figure 1.3.2C). Further pulldown and immunoprecipitation assays revealed that the N-terminal domain of E6AP binds with the N-terminal domain of MASTL (Figure 1.3.2D&E). Then we studied the role of E6AP on MASTL expression. Our results showed that silencing or knockout of E6AP increased MASTL protein level (Figure 1.3.2F, I&J), while overexpressing E6AP in HeLa cells reduced MASTL protein level (Figure 1.3.2H&I). However, silencing UBE3A didn't

affect MAST mRNA transcription (Figure 1.3.2G). In addition, protein degradation results revealed that E6AP knockdown prolonged MASTL protein stability to over 12 hours compared to about 8 hours in the control cells (Figure 1.3.2K&L). As E6AP is an E3 ubiquitin ligase, we wondered if MASTL is a substrate of E6AP for ubiquitination. Surprisingly, our ubiquitination assay demonstrated that MASTL was ubiquitinated in a time-dependent manner (Figure 1.3.2N), confirming that MASTL is a substrate of E6AP for ubiquitination. The immuno-precipitation assays also uncovered that E6AP knockout in HeLa cell disrupted MASTL ubiquitination (Figure 1.3.2M), supporting the idea that MASTL ubiquitination is mediated by E6AP.

A

Protein	#peptide
GWL	55
E6AP	16

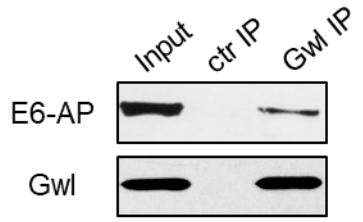

B

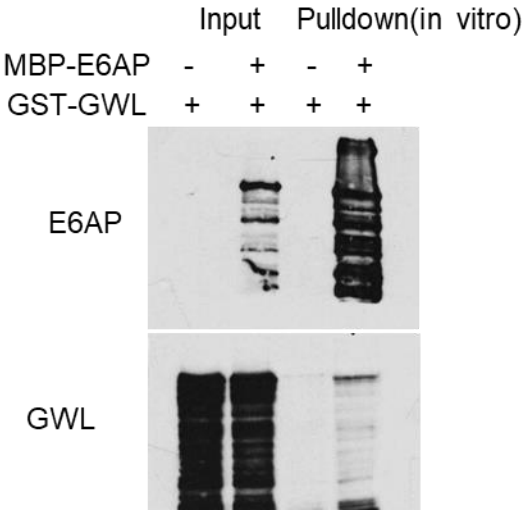

C

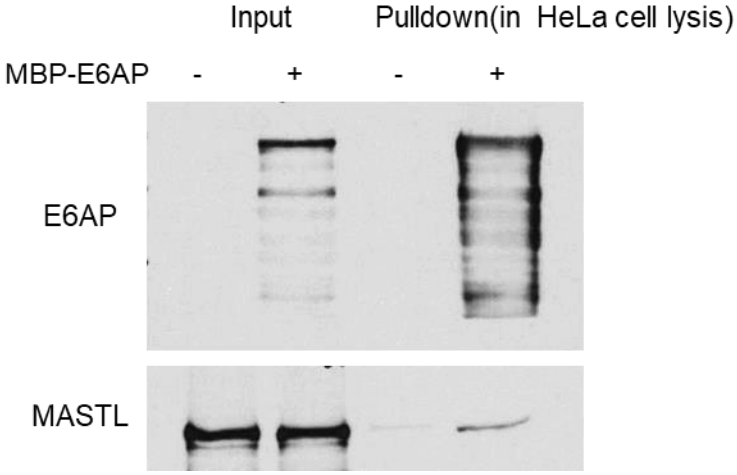

D

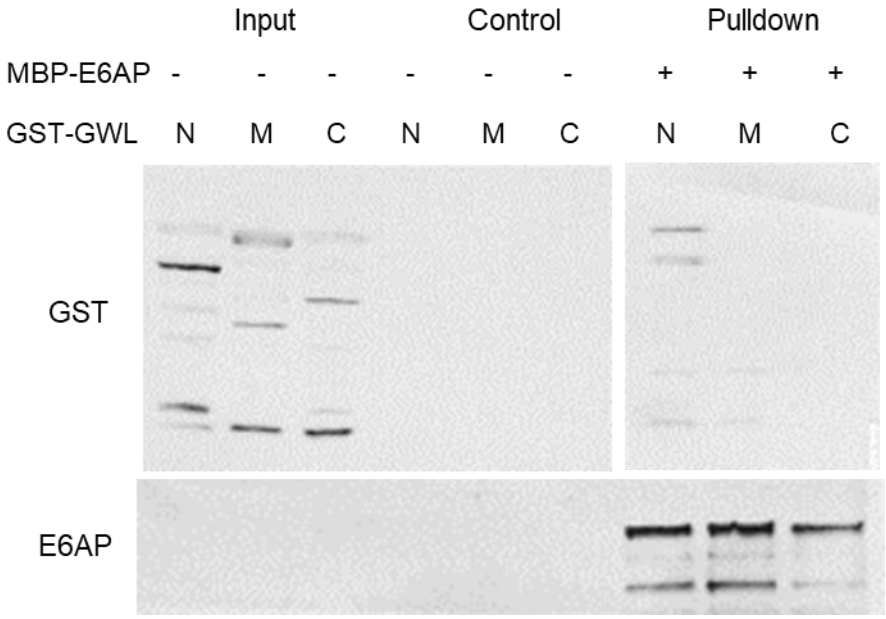
Input
Control
Pulldown
MBP-E6AP - - - - - - + + +
GST-GWL N M C N M C N M C
GST
E6AP

E

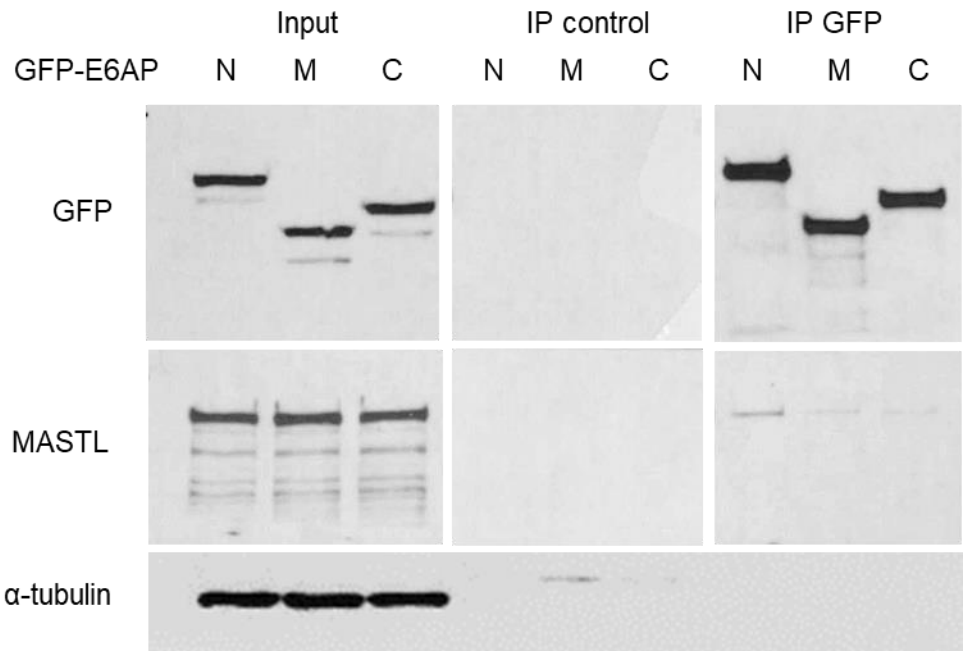
Input
IP control
IP GFP
GFP-E6AP N M C N M C N M C
GFP
MASTL
α-tubulin

F

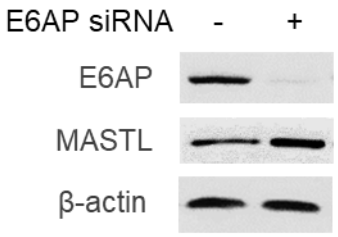
E6AP siRNA - +
E6AP
MASTL
β-actin

G

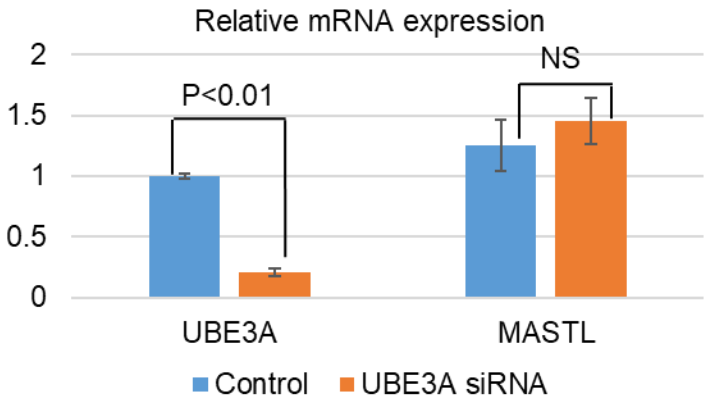
Relative mRNA expression
2
1.5
1
0.5
0
P<0.01
NS
UBE3A
MASTL
Control
UBE3A siRNA

H

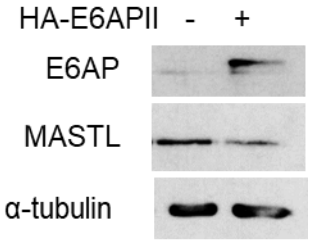
HA-E6APII - +
E6AP
MASTL
α-tubulin

I

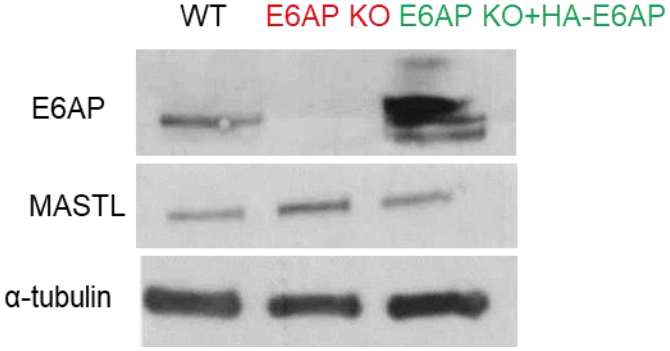
WT
E6AP KO
E6AP KO+HA-E6AP
E6AP
MASTL
α-tubulin

J

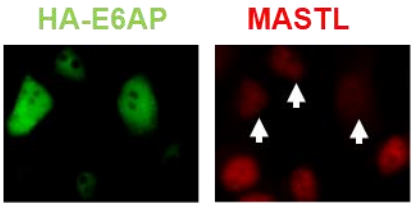
HA-E6AP
MASTL

K

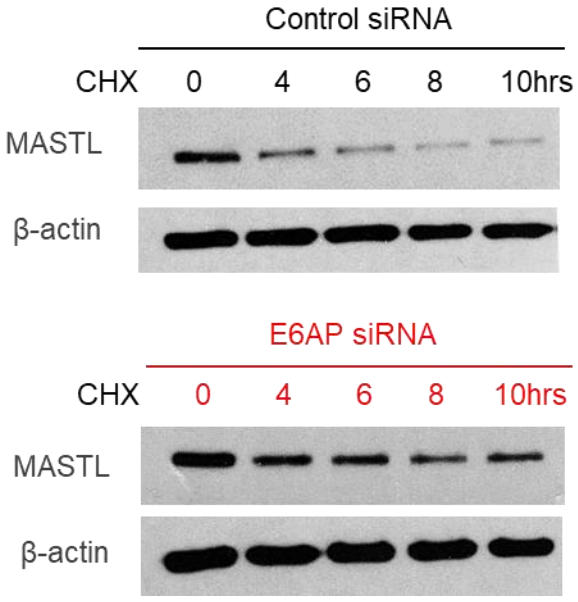
Control siRNA
CHX 0 4 6 8 10hrs
MASTL
β-actin
E6AP siRNA
CHX 0 4 6 8 10hrs
MASTL
β-actin

L

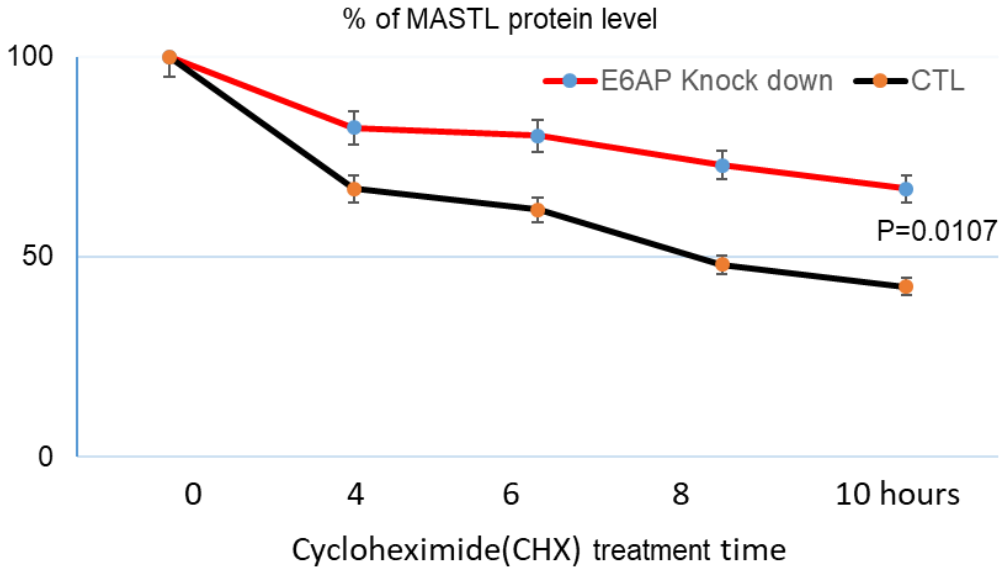
% of MASTL protein level
100
50
0
E6AP Knock down
CTL
P=0.0107
0
4
6
8
10 hours
Cycloheximide(CHX) treatment time

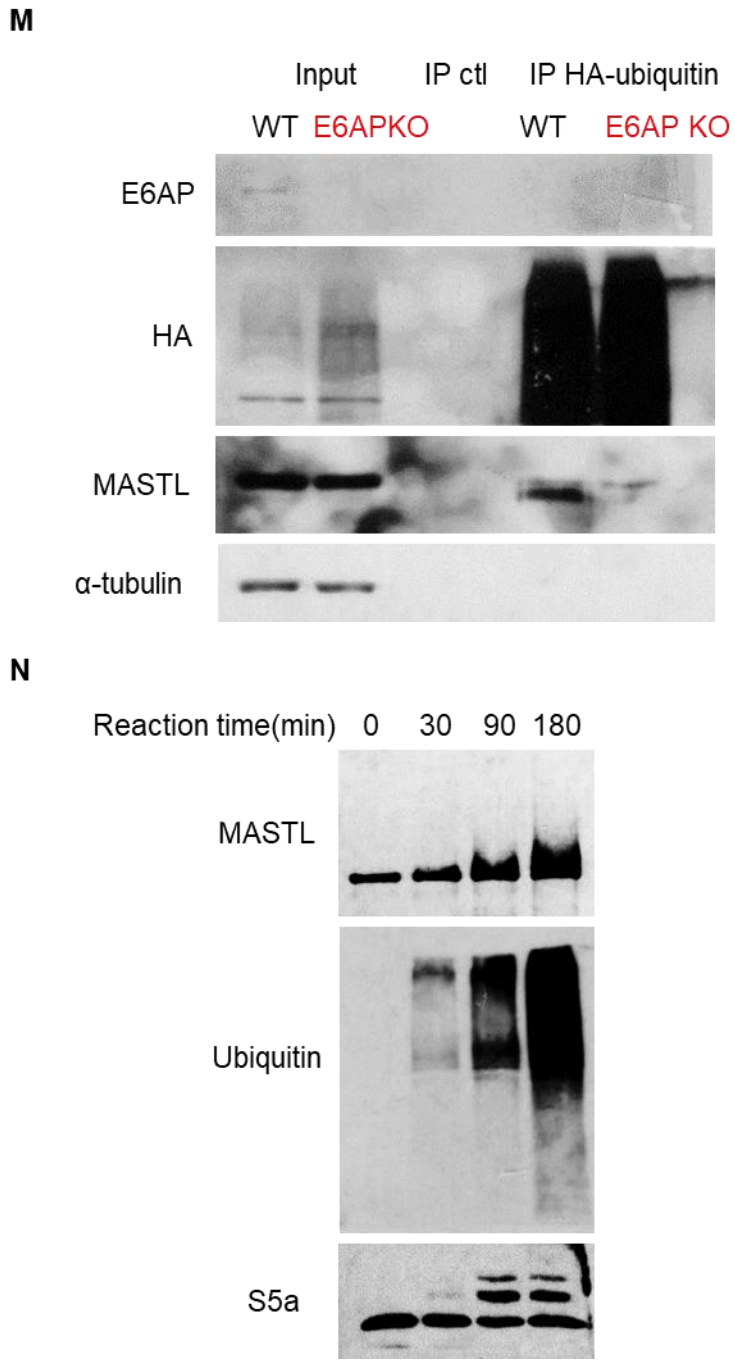

Figure 1.3. 2. E6AP associates with MASTL and mediates MASTL degradation.

(A) Proteomic mass spectrum results. Data from Feifei Wang. **(B)** A pulldown was performed using MBP-tagged full length E6AP in vitro. The pulldown product, cell lysates input, and a control (-) pulldown (using empty beads) were analyzed by immunoblotting for E6AP, GWL. **(C)** Another pulldown assay was performed using MBP-tagged full length E6AP in HeLa cell lysates. The pulldown product, cell lysate input, and a control (-) pulldown (using empty beads) were analyzed by immunoblotting for E6AP and MASTL. **(D)** A pulldown assay was performed using

MBP-tagged full length E6AP and GST-tagged truncated GWL in xenopus egg extract. The pulldown product, egg extract input, and a control (-) pulldown (using empty beads) were analyzed by immunoblotting for GST and E6AP. **(E)** An immunoprecipitation (IP) assay was performed using GFP-tagged truncated E6AP in HeLa cell lysates. The IP product, cell lysate input, and a control IP (using empty beads) were analyzed by immunoblotting for GFP, MASTL and α-tubulin. **(F&G)** HeLa cells were transfected with control or siRNA targeting *UBE3A* for at least 24 hours, then cells were collected and analyzed for either immunoblotting (**F**) or qPCR (**G**).for E6AP, MASTL and β-actin. (**H&J)** HeLa cells were transfected with HA-tagged E6AP (isoform II), then MASLT and E6AP/HA expression were analyzed by either western blot (**H**) or immunofluorescence (**J**). **(I)** MASTL, E6AP and α-tubulin expression were compared by western blot among wild type (WT) HeLa cells, E6AP knockout (E6AP KO) HeLa cells and E6AP KO cells with reconstruction of HA-tagged E6AP. **(K)** HeLa cells were transfected with control or siRNA targeting *UBE3A*. 24 hours after transfection, these cells were treated with cycloheximide (CHX, 20μg/ml) up to 10 hours, then cell lysates were harvested and determined by immunoblotting for MASTL and β-actin. **(L)** MASTL protein level normalized to β-actin in panel **(J)** was quantified to that before cycloheximide (CHX) treatment as time went by. $P=0.0107<0.05$ with paired t-test. **(M)** Wild type (WT) HeLa cells or E6AP knockout HeLa cells were transfected with HA-tagged ubiquitin for 12 hours, followed by 4 hours of 50μM of MG132 treatment. Then cell lysates were harvest for IP assay. The IP product, cell lysate input, and a control IP (using empty beads) were analyzed by immunoblotting for HA, MASTL, E6AP and α-tubulin. **(N)** In vitro E6AP-mediated ubiquitination of MASTL was performed as described in Materials and Methods *2.2.10*. The acquired samples were analyzed by western blot for MASTL, ubiquitin and S5a. All experiments were carried out at least three times. Statistical analysis was performed using student's t-test and data were shown as mean ± standard deviation.

1.3.3. E6AP and MASTL association is regulated by ATM/ATR-mediated DNA damage signaling

As we demonstrated earlier that MASTL was upregulated upon drug-induced DNA damage and replication stress (Figure 1.3.1), and that E6AP associated with MASTL and mediated MASTL ubiquitination (Figure 1.3.2), we wondered if such association would also be impacted by DNA damage or replication stress. As the immunoprecipitation results showed in Figure 1.3.3A, though MASTL protein level increased under HU-induced replication stress, its association with E6AP was dramatically disrupted. Considering that ATM/ATR pathways play in initiating activation of the DNA damage checkpoints, which leads to DNA damage repair [49], we further examined if these pathways involved in regulating the association between MASTL and E6AP under HU-induced replication stress. The results turned out that blocking ATM/ATR pathways by caffeine greatly rescued the association disruption induced by HU treatment (Figure 1.3.3B), suggesting that ATM/ATR pathways mediate MASTL association with E6AP under DNA damage and replication stress.

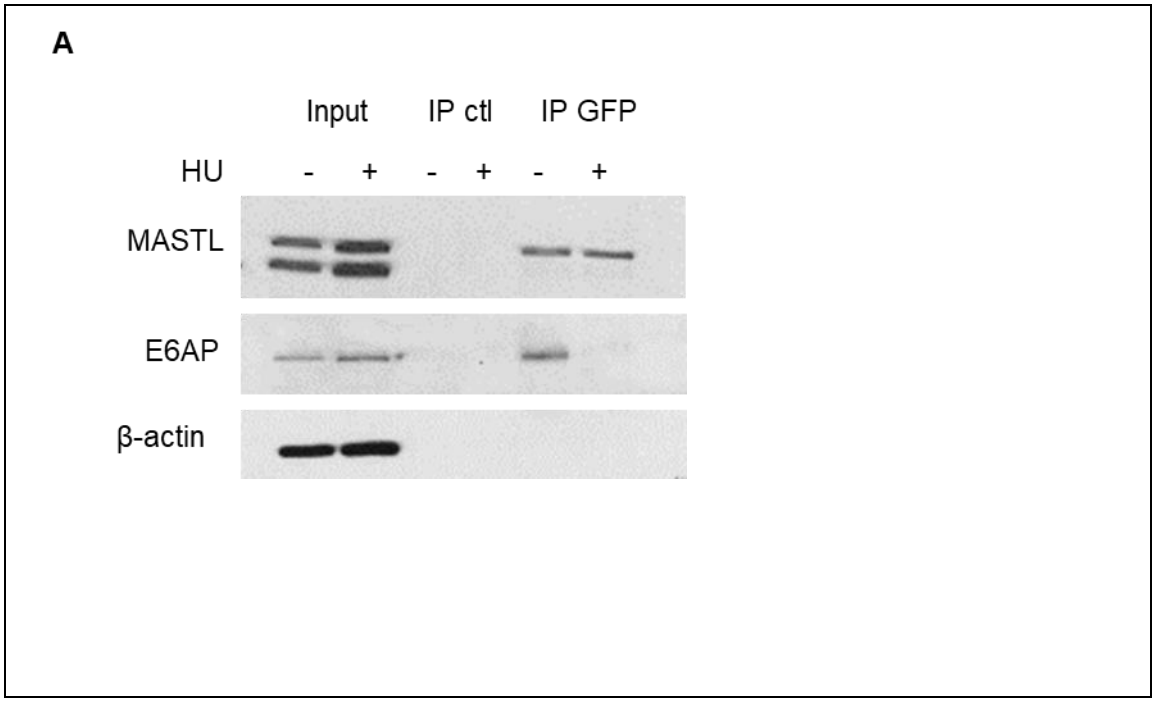

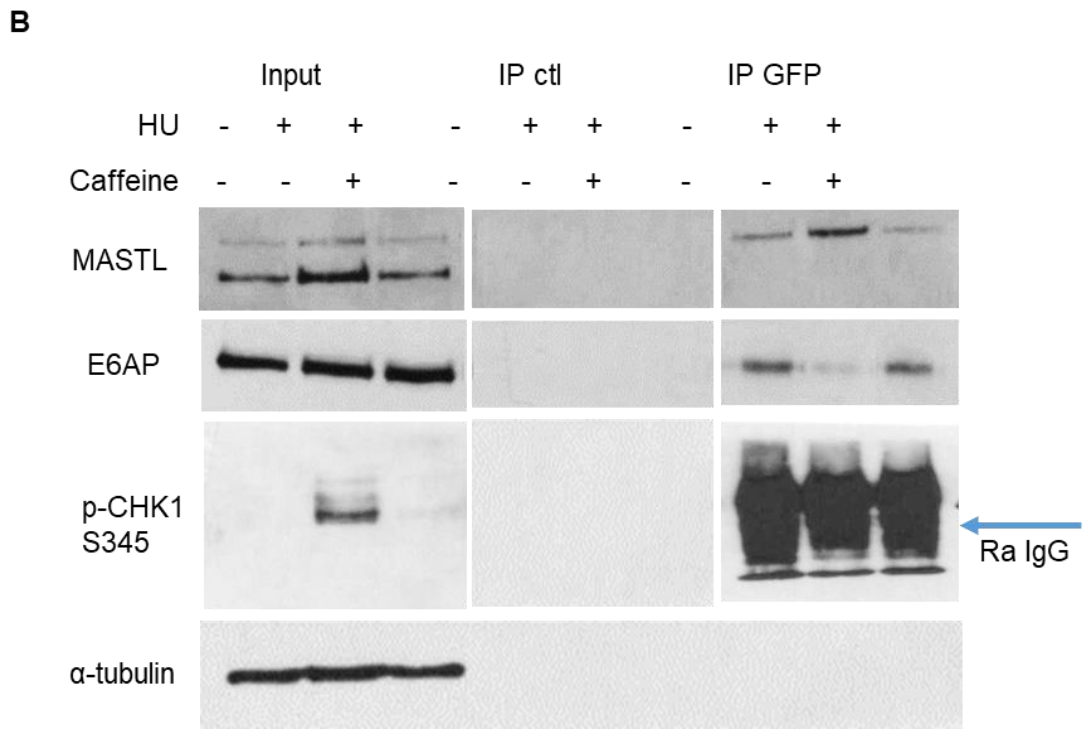

Figure 1.3. 3. E6AP and MASTL association is regulated by ATM/ATR-mediated DNA damage signaling.

(**A**) HeLa cells continuously overexpressing GFP-tagged MASTL were treated with or without 10mM of hydroxyurea (HU) overnight. Then celllysates were harvested for immunoprecipitation (IP) assay. The IP product, cell lysate input, and a control IP (using empty beads) were analyzed by immunoblotting for MASTL, E6AP and β-actin. (**B**) HeLa cells continuously overexpressing GFP-tagged MASTL were treated with each of 1x PBS, 10mM of hydroxyurea (HU) or 10mM of hydroxyurea (HU) combined with 4mM of caffeine. Then cell lysates were harvested for immunoprecipitation (IP) assay. The IP product, cell lysate input, and a control IP (using empty beads) were analyzed by immunoblotting for MASTL, E6AP, phosphor-CHK1 S345 and α-tubulin. All experiments were carried out at least three times.

1.3.4. ATM/ATR pathways mediate E6AP S218 phosphorylation to modulate E6AP and MASTL association

ATM/ATR are serine/threonine protein kinases that phosphorylate serine or threonine, thus serine/threonine residues would be an important characteristic for ATM/ATR substrates. Based on the results that ATM/ATR pathways regulated E6AP

association with MASTL under replication stress, we examined amino acid sequences of E6AP and MASTL trying to find potential motifs of ATM/ATR substrate. The sequencing data revealed that E6AP has conserved residue serine/threonine at amino acid 218 through all of three species (upper panel in Figure 1.3.4A) while no such conserved residue was found in MASTL. In addition, using self-purified antibody recognizing phosphorylated E6AP at S218, we further demonstrated that E6AP was phosphorylated at S218 under drug-induced DNA damage (Figure 1.3.4B&C). These data promoted us to hypothesize that DNA damage- and replication stress-induced association collapse between MASTL and E6AP was due to E6AP phosphorylation at S218. To verify this, two mutants of HA-tagged E6AP were sub-cloned for research: serine mutation to alanine at residue 218 (S218A), causing phosphorylation unavailable at this position, and serine mutation to aspartic at residue 218 (S218D), enabling consistent phosphorylation. To our surprise, mutant S218D lost its ability to associate with MASTL, while mutant S218A maintained such ability (lower panel in Figure 1.3.4A). More data showed that E6AP was phosphorylated at S218 under either HU or doxorubicin-induced DNA damage in both HeLa and HEK293 cells (Figure 1.3.4D&E). However, such DNA damage induced-phosphorylation of E6AP at S218 was eliminated by inhibiting ATM/ATR pathways, especially by ATM inhibitor (Figure 1.3.4F). Taken together, we demonstrated that, in response to DNA damage and replication stress, ATM/ATR

mediated E6AP phosphorylation at S218 modulates its association with MASTL, thus reducing MASTL ubiquitination for degradation to promote MASTL protein level.

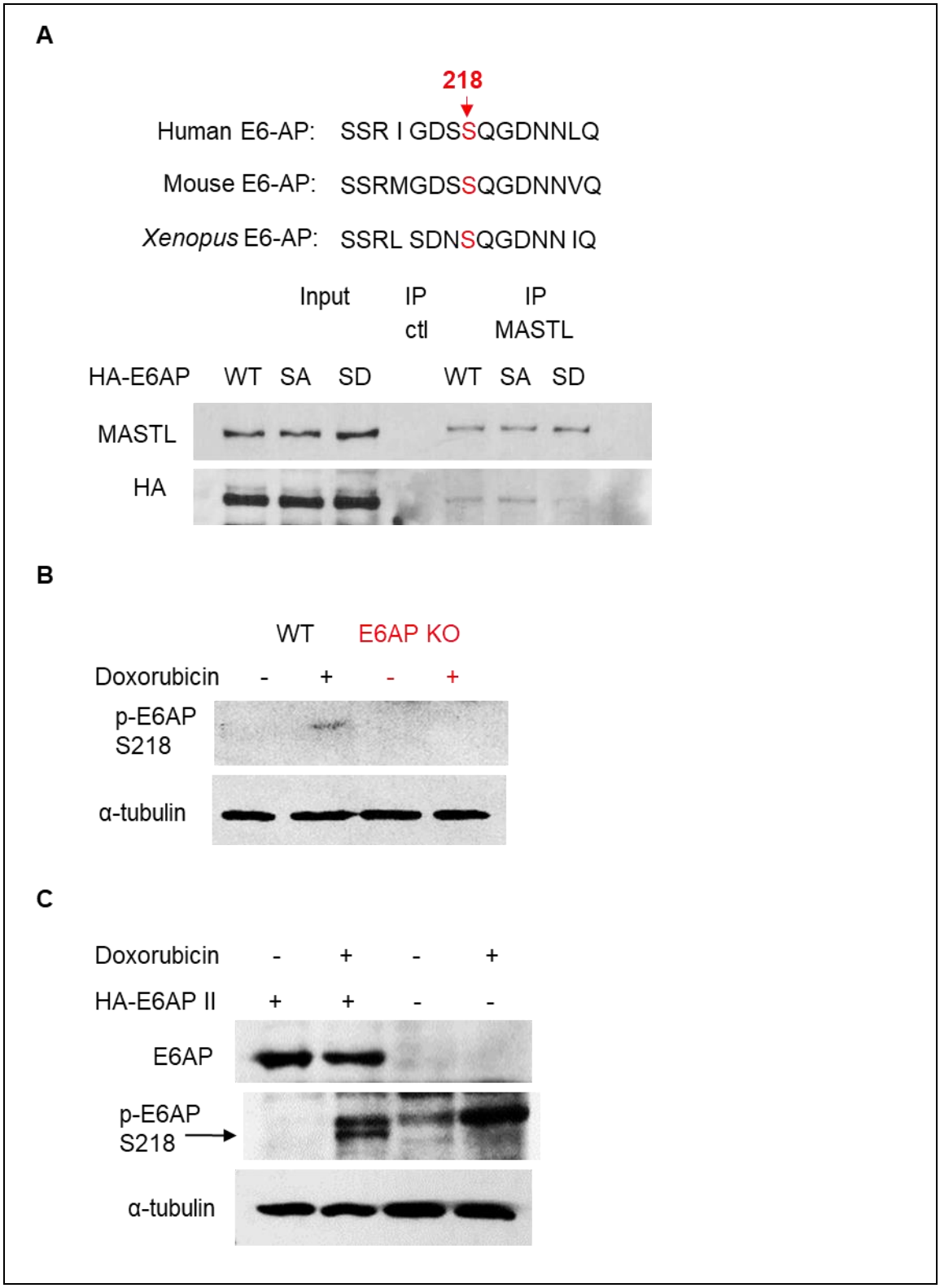

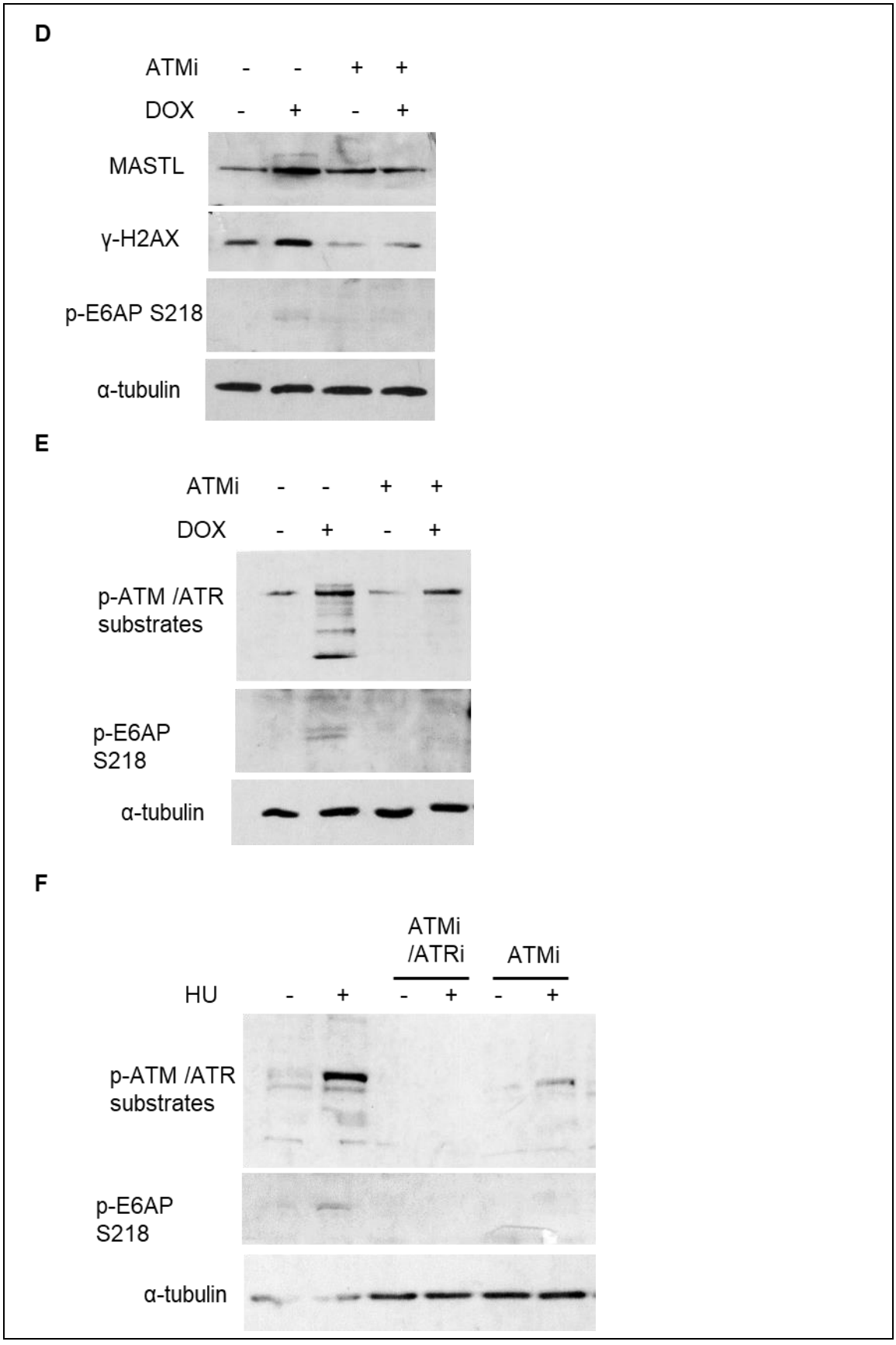
D
ATMi - - + +
DOX - + - +
MASTL
γ-H2AX
p-E6AP S218
α-tubulin
E
ATMi - - + +
DOX - + - +
p-ATM /ATR substrates
p-E6AP S218
α-tubulin
F
ATMi /ATRi
ATMi
HU - + - + - +
p-ATM /ATR substrates
p-E6AP S218
α-tubulin

Figure 1.3. 4. ATM/ATR-mediates E6AP S218 phosphorylation to modulate E6AP and MASTL association.

(A) Upper panel: amino acid sequence of E6AP in different species. Lower panel: HeLa cells were transfected with HA-tagged E6AP wild type, or S218 mutants. The cell lysates were harvest for immunoprecipitation (IP) assay. The IP product, cell lysate input, and a control IP (using empty beads) were analyzed by immunoblotting for MASTL and HA. **(B)** Wild type (WT) HEK293 cells or E6AP knockout (E6AP KO) HEK293 cells were treated with 0.5μM of doxorubicin for 4 hours. Then cells were harvested and determined by immunoblotting for phospho-E6AP S218 and α-tubulin. **(C)** E6AP knockout (E6AP KO) HEK293 cells were transfected with HA-tagged E6AP wild type for 24 hours, followed by 0.5μM of doxorubicin for 4 hours. Then cells were harvested and determined by immunoblotting for E6AP, phospho-E6AP S218 and α-tubulin. **(D)** HEK293 cells were treated with either 0.5μM of doxorubicin (DOX) alone or 0.5μM of doxorubicin combined with 4mM of ATM inhibitor (ATMi) overnight, then cell lysates were harvested for western blot. **(E)** HeLa cells were treated with 0.5μM of doxorubicin (DOX) alone or 0.5μM of doxorubicin combined with 4mM of ATM inhibitor (ATMi) for 3 hours, then cell lysates were collected for western blot. **(F)** HeLa cells were treated with 10mM of hydroxyurea (HU) alone, 10mM of hydroxyurea (HU) combined with 4mM of ATM/ATR inhibitor (ATM/ATRi) or 10mM of hydroxyurea (HU) combined with 4mM of ATM inhibitor (ATMi) for 12 hours, then cell lysate was collected and determined by immunoblotting for phospho-ATM/ATR substrates, phospho-E6AP S218 and α-tubulin. All experiments were carried out at least three times.

1.3.5. E6AP is required for the DNA damage checkpoints via MASTL modulation

To continue, the effect of E6AP on DNA damage checkpoints was examined between wild type (WT) and E6AP knockout (KO) HeLa cells. Our data showed that E6AP-depleted HeLa cells exhibited less DNA damage checkpoint signals, including phospho-ATM/ATR substrates, phospho-SMC1, phospho-CHK1, phospho-CHK2, and γ-H2AX under drug-induced DNA damage (Figure 1.3.5A). The dynamic kinetics of these checkpoints upon different DNA damaging drugs were also slower in E6AP knockout (KO) cells than that in the wild type (WT) HeLa cells (Figure 1.3.5B&C), indicating that E6AP was required for DNA damage checkpoints activation. Besides, our cell cycle analysis results revealed that the E6AP knockout (KO) cells recovered from drug-induced DNA damage faster than the wild type (WT) cells (Figure 1.3.5D&E).

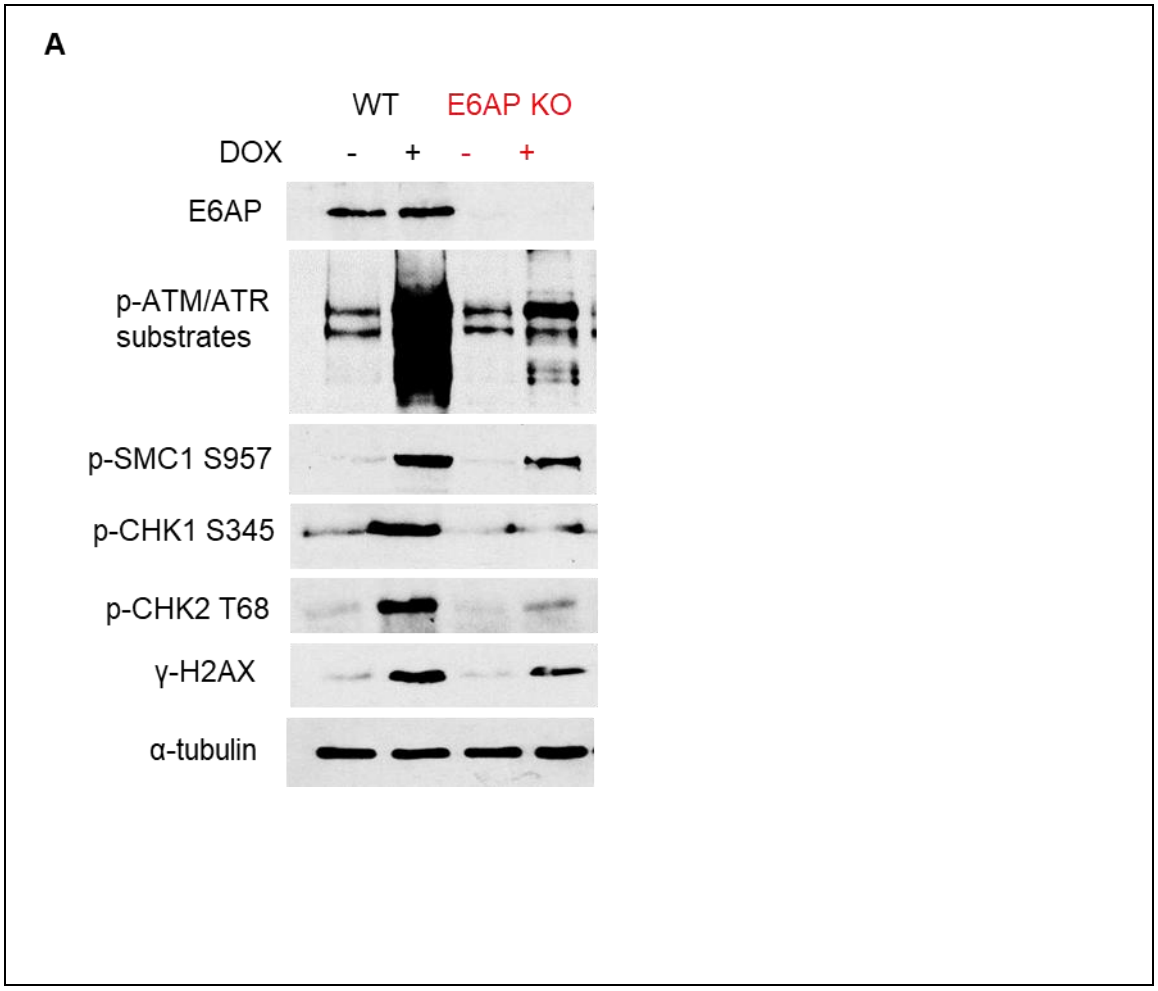

B

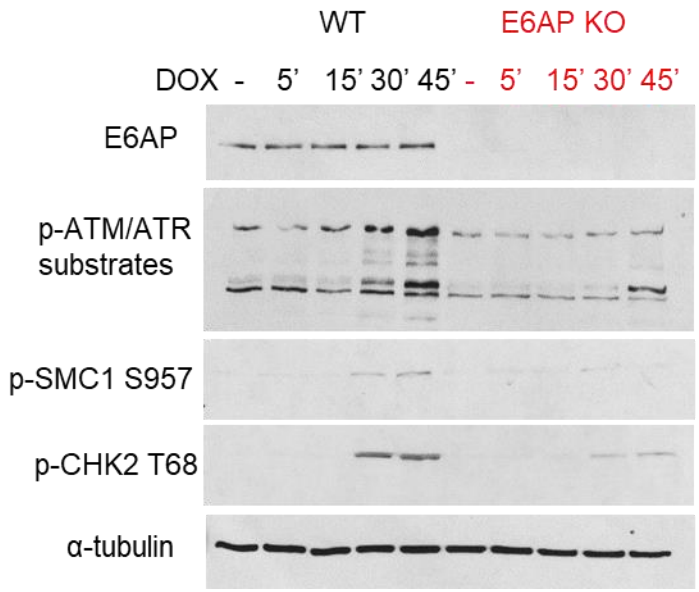
WT
E6AP KO
DOX - 5' 15' 30' 45' - 5' 15' 30' 45'
E6AP
p-ATM/ATR substrates
p-SMC1 S957
p-CHK2 T68
α-tubulin

C

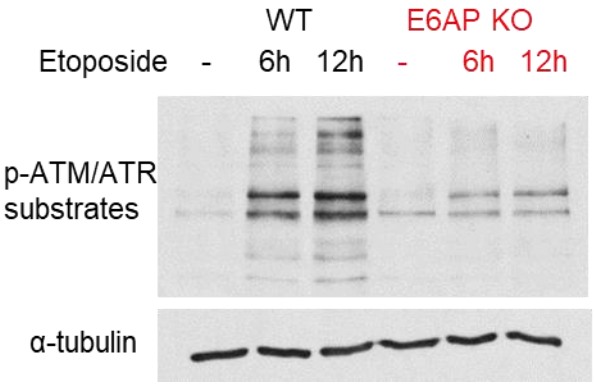
WT
E6AP KO
Etoposide - 6h 12h - 6h 12h
p-ATM/ATR substrates
α-tubulin

D

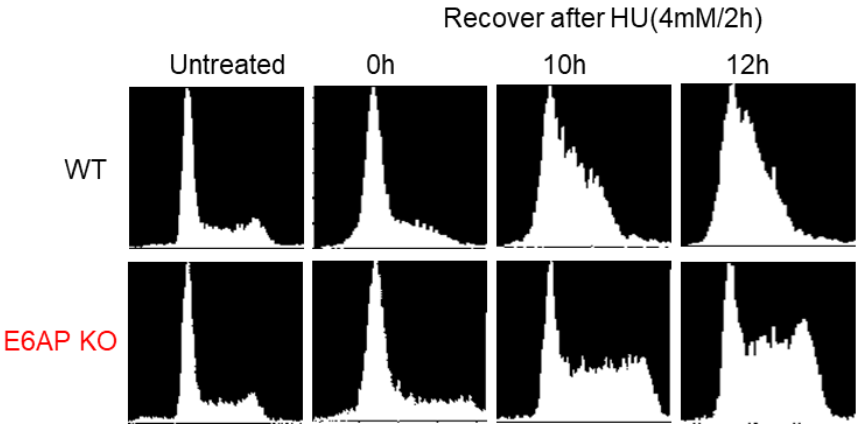
Recover after HU(4mM/2h)
Untreated
0h
10h
12h
WT
E6AP KO

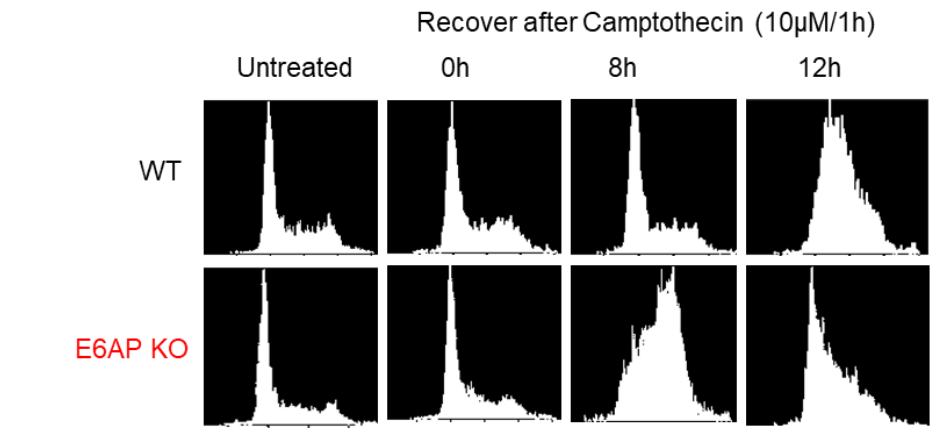

Figure 1.3. 5. E6AP is required for the DNA damage checkpoint via MASTL modulation.

(**A**) Wild type (WT) HeLa cells or E6AP knockout (KO) HeLa cells were treated with or without 0.5μM of doxorubicin (DOX) for 4 hours, then cells were harvested and determined by immunoblotting for E6AP, phospho-ATM/ATR substrates, phospho-SMC1 S957, phospho-CHK1 S345, phospho-CHK2 T68 and γ-H2AX and α-tubulin. (**B**) Wild type (WT) HeLa cells or E6AP knockout (KO) HeLa cells were treated with or without 0.5μM of doxorubicin (DOX), then cell lysates were harvested for western blotting to determine the dynamics of DNA damage response. (**C**) Wild type (WT) HeLa cells or E6AP knockout (KO) HeLa cells were treated with or without 0.1μM of etoposide; then cell lysates were harvested at different times for western blotting. (**D**) Wild type (WT) HEK293 or E6AP knockout (KO) HEK293 cells were treated with 4mM of hydroxyurea (HU) for 2 hours, then HU was removed and cells were allowed to recover up to 12 hours then fixed for flow cytometry. (**E**) Wild type (WT) HEK293 or E6AP knockout (KO) HEK293 cells were treated with 10μM of camptothecin (CPT) for 1 hour, then the drug was removed and replaced with fresh medium to allow cell recovery at indicated times before flow cytometry analysis. All experiments were carried out at least three times.

1.3.6 MASTL expression increases in M phase

A previous study demonstrated that MASTL was phosphorylated in M phase and plays important role in mitotic entry and maintaining mitotic [3]. Here, our data confirmed MASTL phosphorylation in M phase-arrested human cell lines (Figure 1.3.6A-D), such phosphorylation was sustained through M mitosis (Figure 1.3.6E&F). In addition, we also found that MASTL protein level was higher in M phase than that in interphase because

MASTL protein level increased in M phase after phosphate groups were removed from all proteins by lambda phosphatase (Figure 1.3.6A-D), indicating that MASTL was not only phosphorylated but also upregulated in M phase.

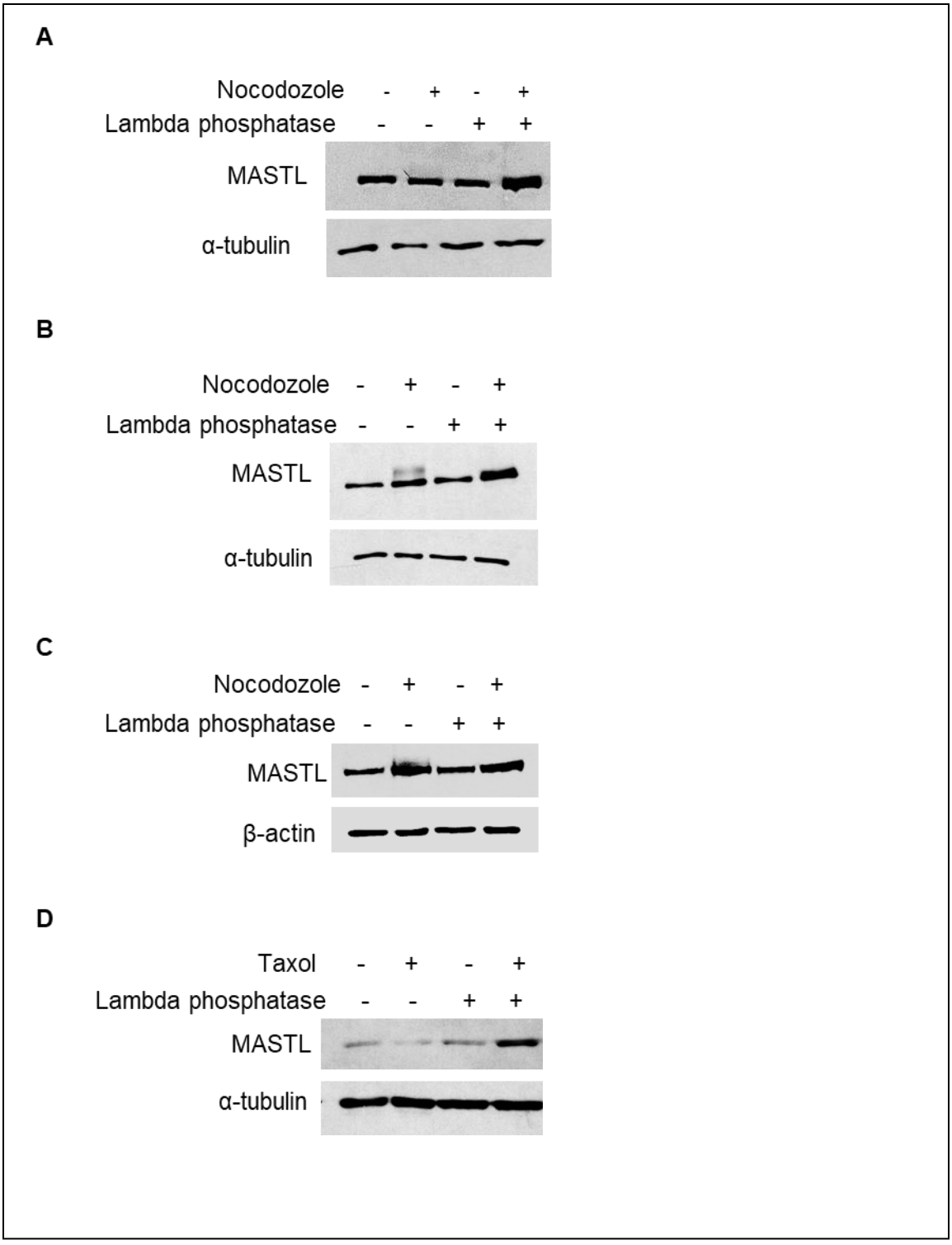

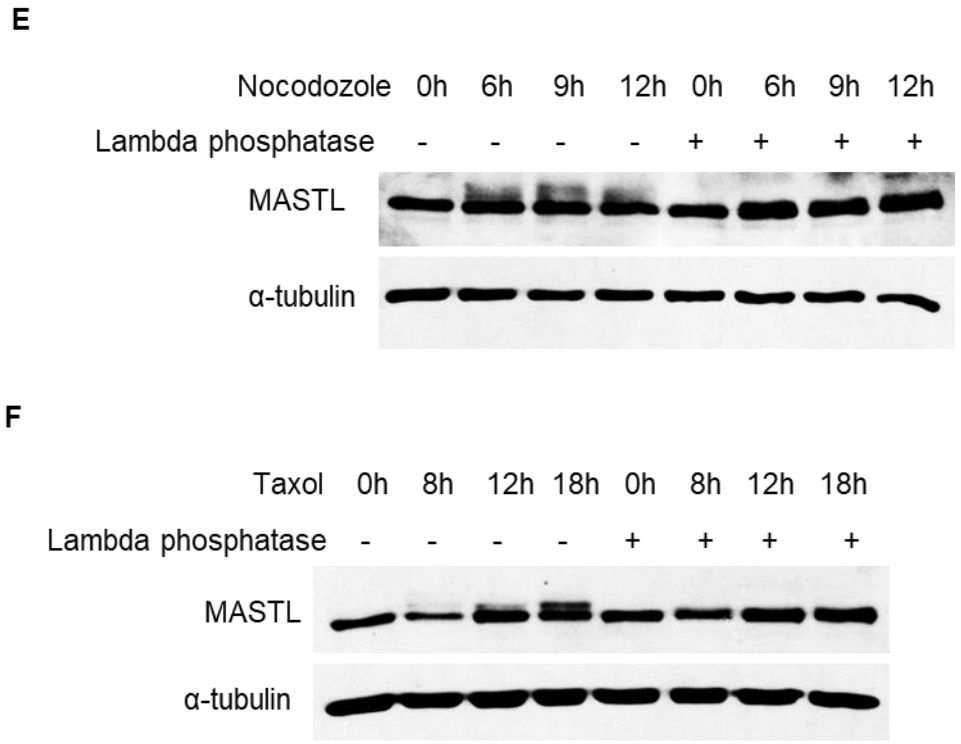

Figure 1.3. 6. MASTL expression increases in M phase.

(**A**) HEK293 cells, (**B**) SCC38 cells and (**C**) HeLa cells were arrested at M phase with 2μ g/ml of nocodazole for 24 hours, then cell lysates were harvested and treated with or without lambda phosphatase at 30℃ for 1 hour before analysis by immunoblotting. (**D**) HeLa cells were arrested at M phase with 100nM of paclitaxel (Taxol) for 16 hours, then cell lysates were harvested and treated with or without lambda phosphatase at 30℃ for 1 hour before analysis by immunoblotting. (**E**) HeLa cells were treated with 2μg/ml of nocodazole for different hours; (**F**) HeLa cells were treated with or without 100nM of paclitaxel (Taxol); then cell lysates were harvested and treated with or without lambda phosphatase at 30℃ for 1 hour before analysis to monitor the kinetics of MASTL upregulation in M phase. All experiments were carried out at least three times.

1.3.7. E6AP associates with MASTL and mediates MASTL degradation in M phase

Lastly, we verified the association between MASTL and E6AP in M phase. Our degradation assay revealed that MASTL protein degradation speeded up in M-phase arrested cells (Figure 1.3.7A). Immunoblotting demonstrated that the protein levels of both MASTL and E6AP were increased in M phase-arrested cells compared to that in control cells (Figure 1.3.7B). On the contrary, MASTL lost its association with E6AP in M phase compared to interphase as revealed by Co-IP assay (Figure 1.3.7C). Though E6AP knockout (KO) cells exhibited higher level of MASTL protein (Figure 1.3.7D)and retarded protein degradation of MASTL (Figure 1.3.7E), no further amplification of MASTL protein in M phase was observed in knockout (KO) cells compared with the wild-type (WT) cells (Figure 1.3.7D), suggesting that MASTL upregulation in M phase was dependent on E6AP.

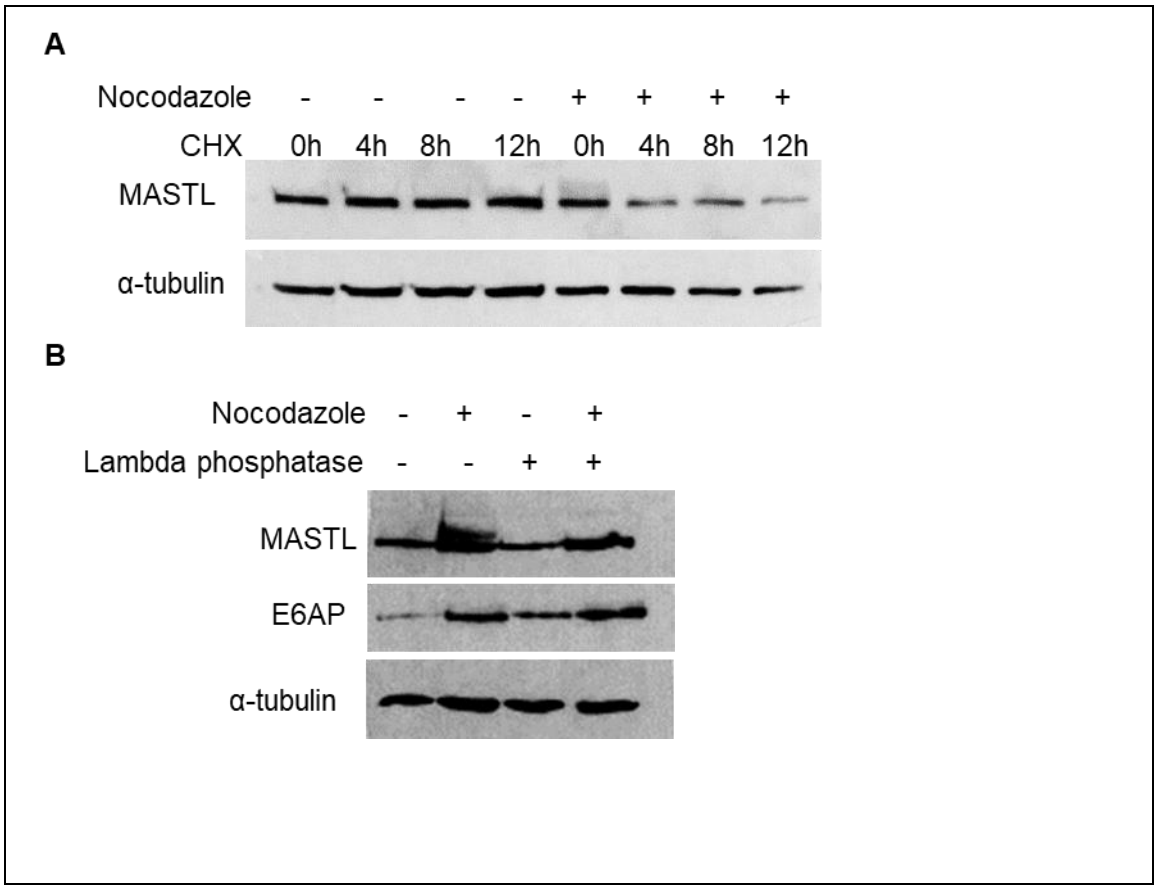

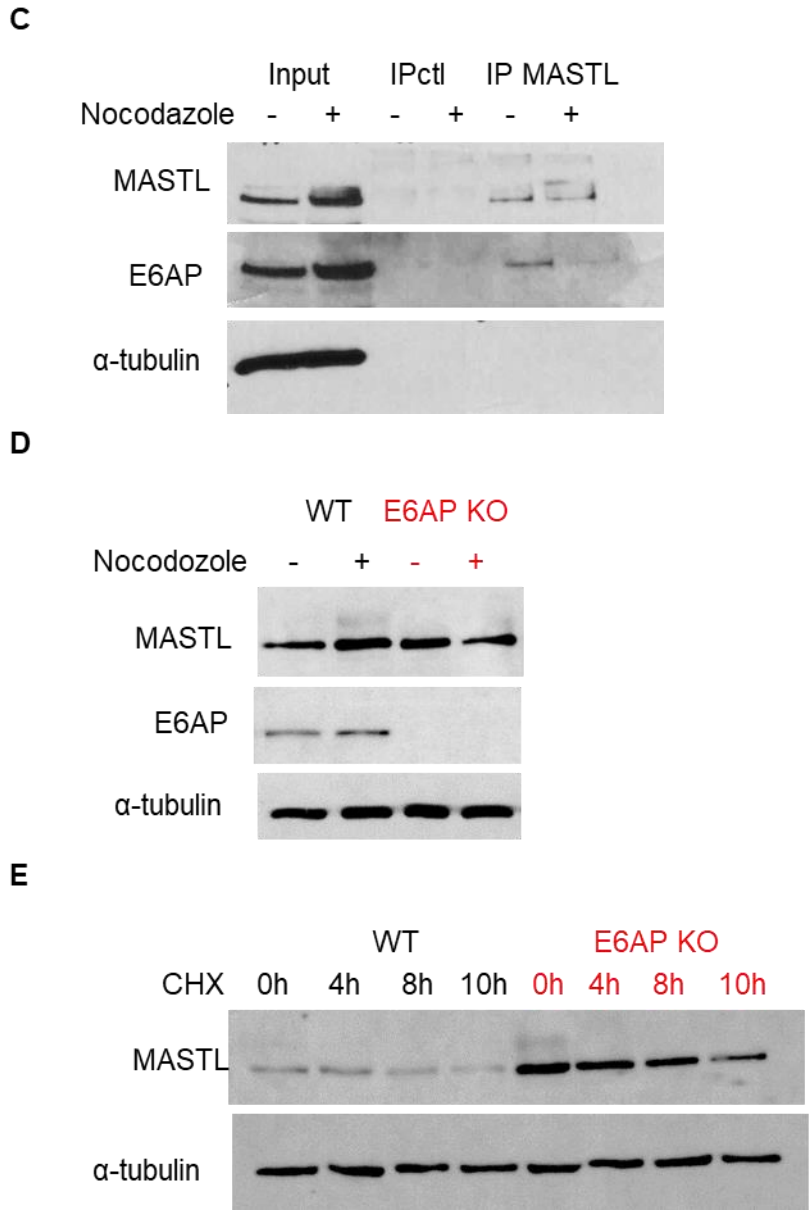

Figure 1.3. 7. E6AP associates with MASTL and mediates MASTL degradation in M phase.

(**A**) HeLa cells were pre-treated with or without 2μg/ml of nocodazole for 12 hours, followed by 20μg/ml of cycloheximide (CHX) treatment for up to 12 hours, then cell lysates were harvested for western blotting. (**B**) HeLa cells were arrested at M phase with 2μg/ml of nocodazole, then cell lysates were collected and incubated with/without lambda phosphatase at 30℃ for 1 hour before MASTL, E6AP and α-tubulin expression was determined with western blot. I: interphase, M: M phase arrested by nocodazole. (**C**) HeLa cells were treated with 2μg/ml of nocodazole overnight, then cell lysates were collected and used for immunoprecipitation (IP) with antibody against MASTL. The IP products, cell lysate input, and a control IP (using

empty beads) were analyzed by immunoblotting. (**D**) Wild type (WT) HeLa cells and E6AP knockout (KO) cells were arrested at M phase with 2μg/ml of nocodazole, then cell lysates were collected and MASTL, E6AP and α-tubulin expression was determined by western blot. (**E**) Wild type (WT) HeLa cells and E6AP knockout (KO) cells were treated with 20μg/ml of cycloheximide (CHX) treatment for up to 10 hours, then cell lysates were harvested for immunoblotting. All experiments were carried out at least three times.

1.4. Discussion

MASTL, with another known name, Greatwall kinase (GWL), is a novel kinase that has been demonstrated to play an important role in mitosis. Previous studies demonstrated that the localization, phosphorylation and activation of MASTL/GWL were precisely regulated during the cell cycle [4, 6, 7, 9, 10, 50]. Besides its function in cell cycle regulation, MASTL has been found to be upregulated in various human cancers [16, 19, 22, 51]. Overexpression of MASTL rendered cancer cell resistant to chemotherapy and was related with poor patient survival and tumor recurrence [19]. Even though, limited knowledge has been known about how MASTL expression itself is regulated in tumor, especially after chemotherapy and radiation therapy, which aims to triggering cancer cell death by inducing DNA damage and replication stress.

In this study, we firstly explored how MASTL expression was regulated in response to DNA damage and replication stress. Our data revealed that MASTL protein level was increased after both drug- and irradiation-induced DNA damage and replication (Figure 1.3.1A, B&D-J), resulting from more protein stability (Figure 1.3.1C). Consistent with a previous study stating that MASTL was phosphorylated in M phase [4], our current research also confirmed MASTL phosphorylation in multiple human cell lines arrested at M phase (Figure 1.3.6A-D). We also revealed that MASTL protein level was dynamically regulated depending on cell cycle progression, in that MASTL protein level was

significantly upregulated in M phase compared to interphase (Figure 1.3.6A-D), adding more clues on the regulation of MASTL expression during cell cycle.

As an E3 ubiquitin ligase, E6AP was found to play a role in regulating ubiquitination and degradation of many substrates [35, 39, 52]. Our proteomic assay identified possible molecules that regulate MASTL expression and found E6AP as one of the candidate regulators (Figure 1.3.2A). Further protein interaction analysis confirmed that MASTL directly associated with E6AP through their N-terminal domains (Figure 1.3.2B-E). To test function of E6AP on MASTL expression, we used siRNA targeting E6AP in human cancer cell lines and found that MASTL protein level was increased after E6AP silencing (Figure 1.3.2F, I&H), and such MASTL upregulation was associated with less E6AP-mediated ubiquitination and degradation of MASTL protein (Figure 1.3.2L&M). This line of evidence confirmed that E6AP directly bound with MASTL and mediated MASTL ubiquitination and degradation.

Besides its function in protein ubiquitination and degradation, E6AP was recently demonstrated to involve in DNA damage and replication stress [41, 42]. Here we discovered that E6AP lost its ability to bind with MASTL under DNA damage and replication stress (Figure 1.3.3A&B), which partially explained MASTL upregulation after chemotherapy treatment. Moreover, our data revealed that residue S218 of E6AP is a conserved motif that regulated its association with MASTL (Figure 1.3.4A). Using self-purified antibody to phospho-E6AP and pathway inhibitors, we demonstrated that ATM/ATR pathways regulated E6AP phosphorylation at S218 under DNA damage conditions (Figure 1.3.4D-F), making E6AP unable to bind with MASTL and mediate MASTL degradation.

Lastly, we examined E6AP function in DNA damage response, and found that E6AP was required for DNA damage response checkpoints. Human cell lines depleted

of E6AP showed less accumulation of DNA damage checkpoints but faster recover ability from drug-induced replication stress (Figure 1.3.5). Besides, our data revealed that protein level of both E6AP and MASTL were increased in M phase (Figure 1.3.7B&C), but their direct association was impaired in M phase, compared to that in interphase (Figure 1.3.7C), the mechanism of which remains to be uncovered.

In summary, our study found that MASTL was upregulated after DNA damage-induced drug treatment. We also recognized E6AP as a regulator of MASTL expression, which may lead to clinically relevant information for cancer therapy. Nevertheless, there are still more questions to be answered, such as whether E6AP is phosphorylated at M phase, whether such phosphorylation is dependent on any known DNA damage response signaling pathways. Thus, more efforts are needed to uncover the mechanisms.

CHAPTER 2: MASTL REGULATES DNA DAMAGE-INDUCED STAT1 PHOSPHORYLATION

2.0 Abstract

Microtubule associated serine/threonine kinase like (MASTL) is a novel kinase that plays important role in regulating mitosis and cell cycle. Overexpression of MASTL promotes cancer metastasis and resistance to radiation and chemotherapy, where antitumor immunotherapy is emerging as an alternative option for cancer treatment in recent decades. However, it is unclear how MASTL is involved in human immune response. In this study, we explored MASTL function in regulating innate immune response. We revealed that MASTL overexpression in human cancer cell lines inhibited immune response by negatively controlling cGAS/STING/TBK1/IRF3 pathway, resulting in decreased activation of STAT1 induced by DNA damage or interferon (IFN), which could be partially rescued by re-activating PP2A-B55α. Our study uncovered a new function of MASTL involved in immune response, suggesting MASTL as a potential target in immunotherapy to kill cancer cells that are resistant to classical treatments.

2.1

2.2 Introduction

Microtubule associated serine/threonine kinase like (MASTL) is a master kinase that regulates meiosis and mitosis [1-3]. At mitotic entry, MASTL phosphorylates and activates ARPP19 and ENSA, which inhibits PP2A-B55, thereby promoting a correct timing and progression of mitosis [4]. In mouse zygotes, MASTL-ENSA-PP2A pathway regulates the timing of pronuclear formation onset to delay pronuclear formation after oocyte activation [9]. MASTL ablation results in cell cycle dysregulation and loss of germ cells, which could be rescued by PP2A deletion [11]. MASTL deficiency also impairs megakaryocytes maturation and shortens the half-life of circulating platelets in mice [13].

Recent studies also revealed a role of MASTL involved in human cancer development and progression. MASTL was inducible by inflammatory cytokines, including interleukin 6 (IL-6) and tumor necrosis factor alpha (TNF-a) in liver cancer cells, suggesting that MASTL may relate to hepato-carcinoma development [53]. High level of MASTL has been found in lung cancer, thyroid tumor, breast cancer, gastric cancer and colon cancer. Overexpression of MASTL facilitates transformation of human fibroblasts, and promotes cell proliferation, migration and tumor growth in colon cancer through hyperactivating AKT oncoprotein [54]. In gastric cancer, increased MASTL was related to epithelial to mesenchymal transition (EMT) and poor patient survival [55]. In estrogen receptor-positive (ER+) breast cancer, upregulated MASTL expression reduced cisplatin-induced G2/M arrest and promoted chromosome instability and cancer resistance to chemotherapy [17]. High level of MASTL expression was associated with poor patient survival, higher metastatic relapse (MR) risk and worse MR-free survival [18, 19]. While depletion of MASTL impaired cancer cell proliferation, inhibited tumor growth, blocked cancer cell invasion, and sensitized cancer cells to chemotherapy and radiotherapy in various malignancy [15, 16, 19-21, 56], and MASTL has been predicted to be a promising target for cancer treatment in oral squamous cell carcinomas [22]. However, emerging cancer resistance has compromised efficiency of classical treatment options, including surgical removal, radiotherapy and chemotherapy, calling for new options to fight cancers. In recent decades, immunotherapy has been commonly used to treat allergies, autoimmune disorders and certain cancers. The study of the interaction between the immune system and cancer cells can lead to diagnostic tests and therapies to find and fight cancers.

The signal transducer and activator of transcription 1 (STAT1) is a pivotal transcription factor that contributes to modulating both innate and adaptive immune

immunity during type I interferon (IFN)-mediated lethal virus infection [57], enabling the transcription of genes that inhibit cell division and stimulate inflammation [58, 59]. IFNβ-dependent upregulation of STAT1 protects cells from viral infection and increases resistance to doxorubicin-induced DNA damage [60]. STAT1 activation by IL-6 contributes to controlling virus replication by inducing expression of IRF1, IRF7, and IRF9, which enhance IFN-γ expression, while knockdown of STAT1 significantly increased Theiler's murine encephalomyelitis virus (TMEV) RNA in macrophage [61].

In the brain, hypoxia triggers tyrosine phosphorylation of STAT1 at Y701, thus activating microglia cells towards M1 phenotype and resulting in oxidative stress and the release of pro-inflammatory cytokines [62]. DSBs caused by IR, etoposide or camptothecin (CPT) up-regulated IRF1 and STAT1 phosphorylation in U2OS and H1299 cells, which requires ATM/ATR/Chk1 activity [63, 64]. Besides, exposure to solar ultraviolet (SUV) leads to upregulation of IFN-γ and downstream pSTAT1/IRF-1/STAT1 signaling [65], while alkylating agent induces more DNA damage, including γ-H2AX and CHK2 T68 activation, and poor cell survival in STAT1-deficient human fibrosarcoma cell lines, indicating that STAT1 is involved in DNA damage response [66].

During antitumor response, STAT1 is an essential mediator through inhibition of myeloid derived suppressor cell accumulation and promotion of T-cell mediated immune responses in murine head and neck squamous cell carcinoma. STAT1 deficient mice displayed increased tumor growth and metastasis, impaired T-cell expansion and PD-1 overexpression, which was associated with enhanced T-cell exhaustion [67].The protein level phospho-STAT1 Y701 decreased with the increase of malignant grade of glioma. STAT1 overexpression suppressed the proliferation of glioma cells while STAT1 knockdown by siRNA promoted glioma cell growth [68]. In human breast cancer samples, progesterone receptor-positive (PR+) tumors exhibited lower levels of

phospho-STAT1 Y701 as compared to PR-negative (PR-) counterparts, indicating that this phosphorylation phenotype translates to human tumors [69]. Combined these data suggest a promising STAT1 involvement in antitumor therapy.

The cyclic GMP-AMP synthase (cGAS)-stimulator of interferon genes (STING) pathway is a component of the innate immune system that functions to detect the presence of cytosolic DNA, which is associated with tumorigenesis, viral infection, and bacteria invasion, thereby triggering expression of inflammatory genes, leading to senescence or activation of defense mechanisms. Upon binding cytosolic DNA, cGAS triggers reaction of GTP and ATP to form cyclic GMP-AMP (cGAMP), which binds to STING, inducing phosphorylation of IRF3 via TBK1. IRF3 can then dimerize prior to nuclear import for transcription of inflammatory genes, such as IFN-β.

The cGAS/STING/TBK1/IRF3 innate immunity pathway also plays a pivotal role in the DNA damage-induced innate immune response and helps to maintain chromosomal stability [70]. Depleting either component of this pathway resulted in decreased p21 level and chromosomal instability in HeLa and U2OS cancer cells [71]. STING is required for paclitaxel-induced pro-apoptotic response in breast cancer cells, which was impaired by depletion of either STING depletion or cGAS [72]. In mouse models, pharmacological activation of STING induced remarkable tumor regression by stimulating T cell proliferation and causing tumor vascular collapse, which contributes to tumor cell death and tumor-associated antigens release, indicating the role of the cGAS–STING pathway in cancer treatment [73]. However, the cGAS-STING pathway dysfunction was observed recently in lung cancer, which closely related with tumor stage and lymph node metastasis [74]. STING-deficient mice had higher number of large tumors at late stages of hepatocellular carcinoma (HCC) and exhibited less phospho-STAT1, autophagy, and cleaved caspase3. STING agonist cyclic dinucleotide (CDN)

treatment of mice after HCC development efficiently reduced tumor size, reinforcing that the cGAS-STING pathway is a therapeutic target in a preclinical model of hepatocellular carcinoma [75].

Herein, MASTL expression upon treatment with a DNA damage drug, as well as the IFN/Toll-like receptor 3 (TLR3) pattern recognition receptor (PRR) pathway activation, was firstly studied in this project, followed with MASTL's function on activation of STAT1 and the cGAS-STING pathway. Our data revealed that MASTL was increased after treatments of etoposide, IFN and poly I: C. Further experiments uncovered that MASTL negatively regulates STAT1 Y701 phosphorylation and the cGAS-STING pathway through inhibiting PP2A. In summary, we demonstrated a new role of MASTL in immune response, which might propose novel treatment options for antitumor therapy to fight cancers, especially those with higher MASTL expression, such as ER+ breast cancer and head and neck squamous cell carcinoma.

2.2. Materials and methods

2.2.1. Cell culture and transfection

Human aneuploid immortal keratinocyte (HaCaT) cells, human cervix carcinoma (HeLa) cells, human head and neck squamous cell carcinoma UM-SCC-38, and breast carcinoma MDA-MB-231 cell lines were maintained at Dulbecco's modified Eagle medium (DMEM, Hyclone) with 10% fetal bovine serum (FBS, Hyclone) and 1% of P.S. Human cell lines overexpressing CFP-MASTL were made as described before [22]. The HA-tagged PP2A-B55α expression vector was a gift from Dr. Xuan Liu (University of California Riverside) [76]. Human cell lines were seeding into 35-cm dishes at least 24 hours before transfection of HA-B55α vectors was carried out using Lipofectamine 2000 (Invitrogen). siRNA targeting gene ARPP19, ENSA or STING (Integrated DNA Technologies) was transfected into cells using Lipofectamine RNAi MAX (Invitrogen),

with a non-targeting control siRNA as a control. ARPP19 siRNA sequence: 5'-3'GAUUACAACAUGGCUAAA, 5'-3'UUUUUGCUUUAGCCAUGU; ENSA siRNA sequence: 5'-3'GUACUUUGACUCAGGAGA, 5'-3'GUUGUAGUCUCCUGAGUC; STING siRNA sequence: 5'-3'AAUCAGCAUUACAACAAC, 5'-3'GUAGCAGGUUGUUGUAA.

2.2.2. Immunoblotting

Sodium dodecyl sulfate-polyacrylamide gel electrophoresis (SDS-PAGE) and immunoblotting were carried out as previously described [43]. The following antibodies were used for immunoblotting: MASTL and α-tubulin self-purified by our laboratory [46]; STAT1, phospho-STAT1 Y701, phospho-STAT1 S727, IRF3, phospho-IRF3 (Cell Signaling Technology, Beverly, MA) kindly donated from Dr. Petro, T. M (University of Nebraska Medical Center) [61]; cGAS, PRA2, phospho-RPA2 s4/8, TBK1, phospho-TBK1, STING, and phospho-STING bought from Cell Signaling Technology (Beverly, MA).

2.2.3. Statistical analysis

According specific conditions, either one-ANOVA analysis or paired t-test was used to compare the differences between means$\pm$standard deviation; only $p<0.05$ was considered as statistically significant.

2.3. Results

2.3.1. MASTL upregulation upon DNA damage and immune-stimuli

Our previously unpublished data demonstrated that MASTL protein level was upregulated upon drug-induced DNA damage. A recent study revealed that IFN-γ and poly I: C reduced UM-SCC38 cell growth and reduced cyclin-D1 [77], a crucial kinase in mitosis regulation. Considering MASTL function in regulating mitosis entry and maintenance, we wondered if these immuno-stimuli would also affect MASTL expression. So, we firstly treated several human cell lines with either etoposide or IFN-γ

and poly I: C. We found that MASTL protein level was increased in a time-dependent manner after different treatments (Figure 2.3.1.A-J). Further protein stability analysis showed that MASTL upregulation after immune-stimulus and DNA damage was due to enhanced protein stability, as shown in as Figure 2.3.1K-L, both exogenous and endogenous MASTL protein degraded at a slower speed in the poly I: C or etoposide-pretreated cells than that in the control cells.

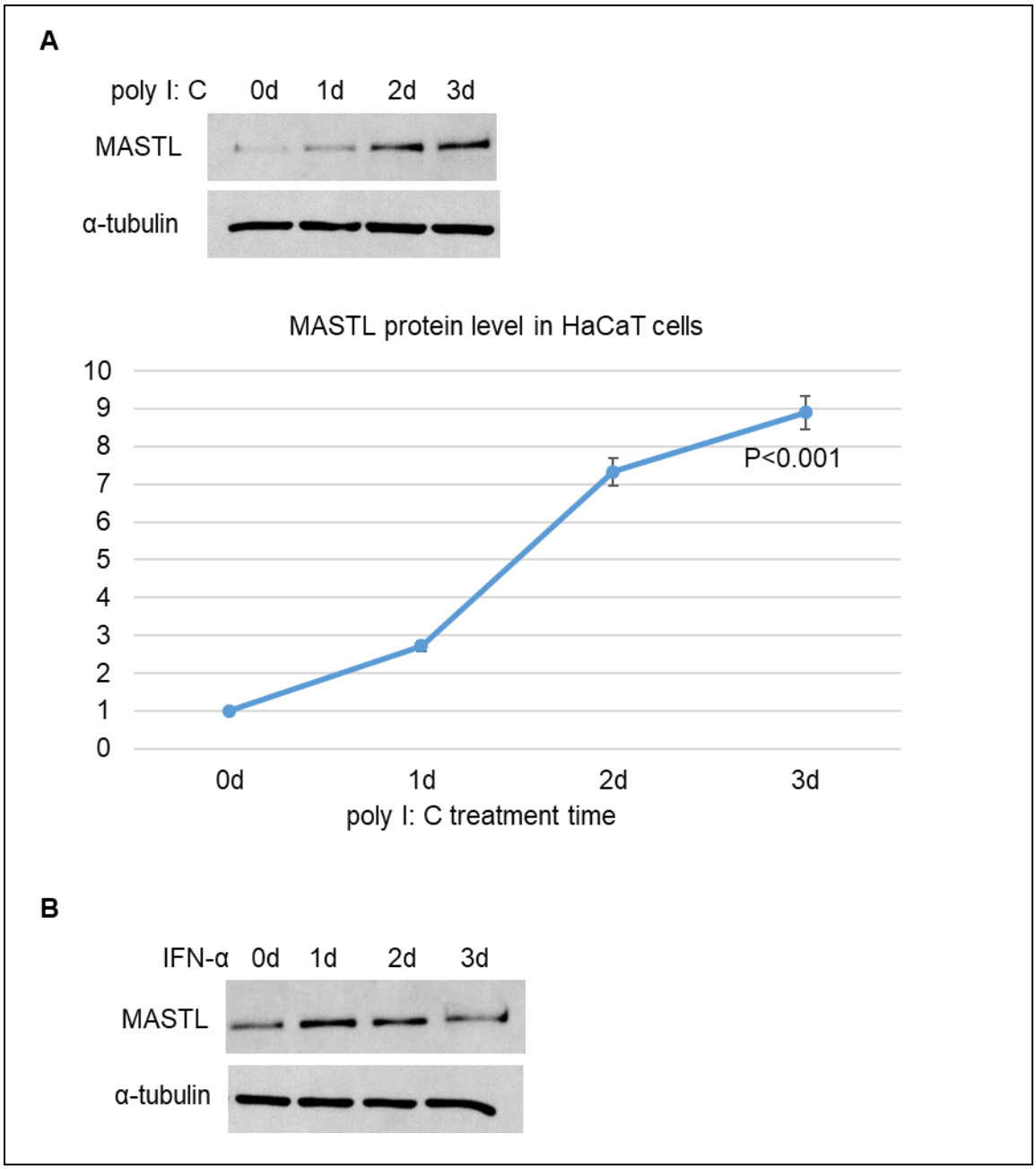

C

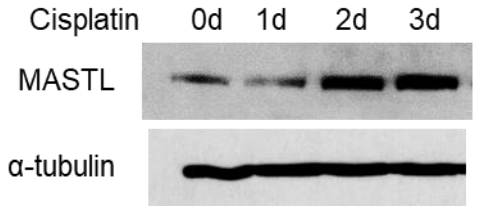
Cisplatin 0d 1d 2d 3d
MASTL
α-tubulin

D

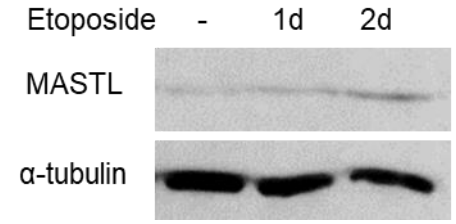
Etoposide - 1d 2d
MASTL
α-tubulin

E

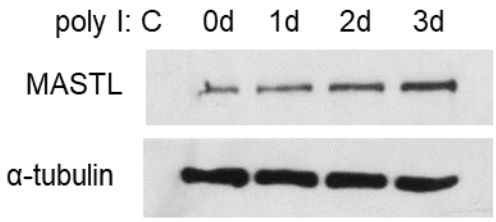
poly I: C 0d 1d 2d 3d
MASTL
α-tubulin

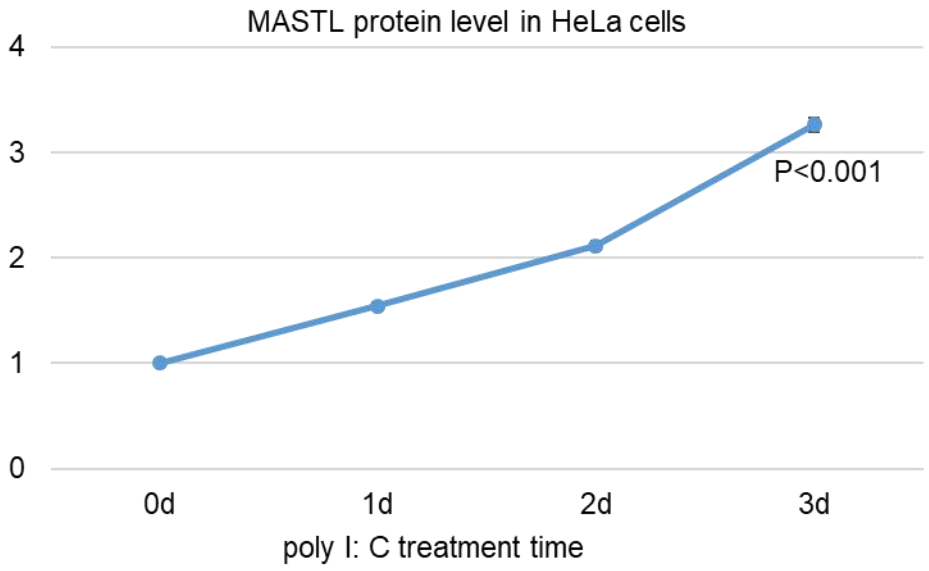
MASTL protein level in HeLa cells
4
3
2
1
0
P<0.001
0d
1d
2d
3d
poly I: C treatment time

F

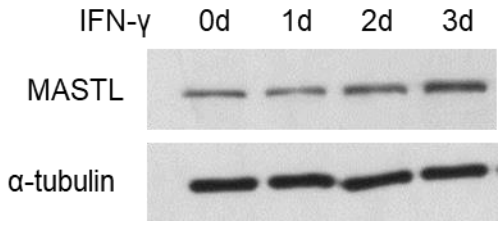
IFN-γ 0d 1d 2d 3d
MASTL
α-tubulin

G

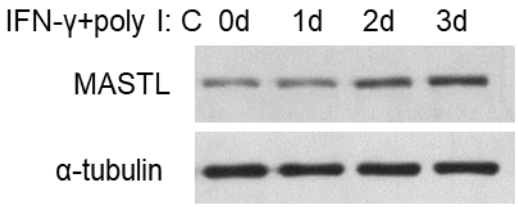
IFN-γ+poly I: C 0d 1d 2d 3d
MASTL
α-tubulin

H

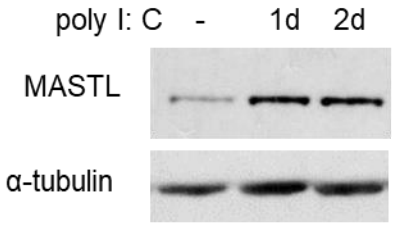
poly I: C - 1d 2d
MASTL
α-tubulin

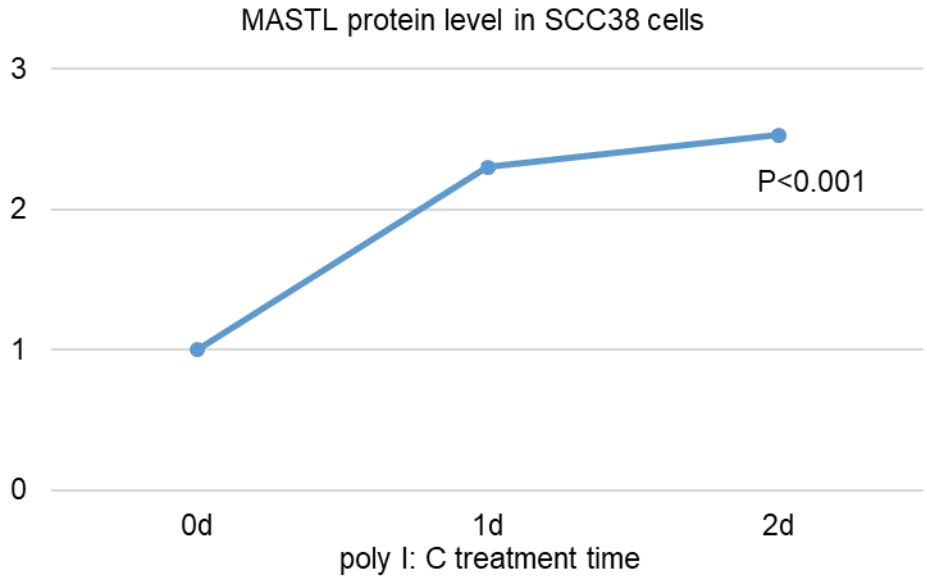
MASTL protein level in SCC38 cells
3
2
1
0
P<0.001
0d
1d
2d
poly I: C treatment time

I

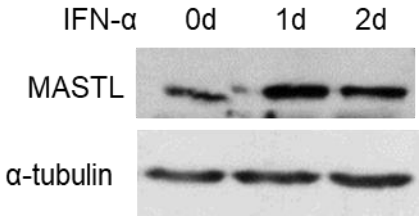
IFN-α 0d 1d 2d
MASTL
α-tubulin

J

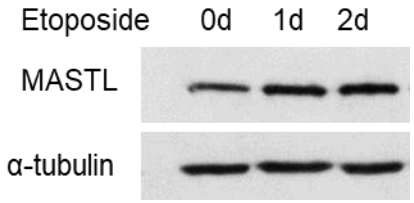
Etoposide 0d 1d 2d
MASTL
α-tubulin

K

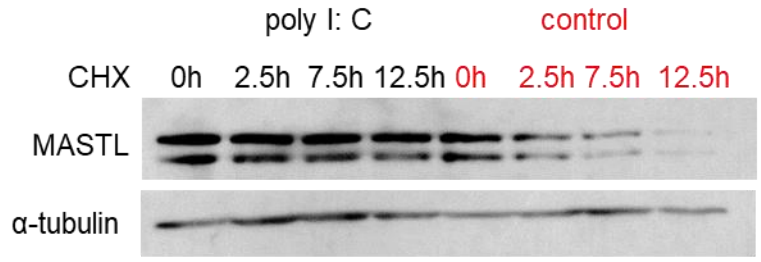
poly I: C
control
CHX 0h 2.5h 7.5h 12.5h 0h 2.5h 7.5h 12.5h
MASTL
α-tubulin

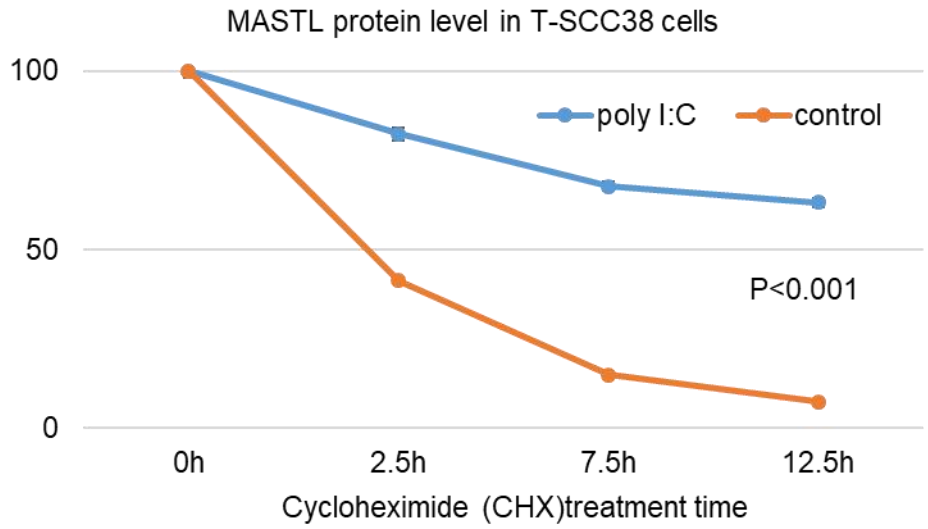
MASTL protein level in T-SCC38 cells
100
50
0
poly I:C
control
P<0.001
0h
2.5h
7.5h
12.5h
Cycloheximide (CHX)treatment time

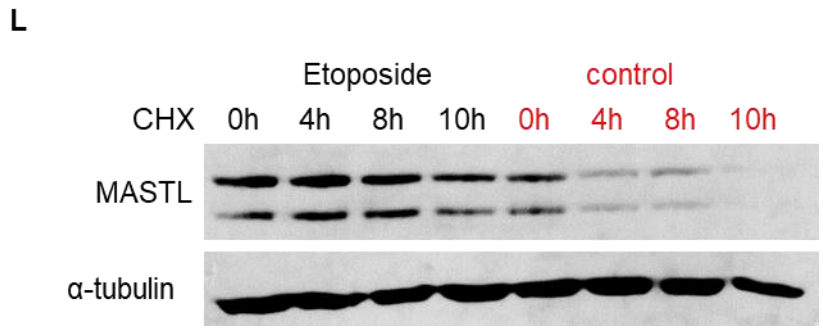

Figure 2.3. 1. MASTL upregulation induced by immuno-stimulus and DNA damage due to protein stability. (**A-D**) HaCaT cells were treated with 2μg/ml of poly I:C (**A**), 20ng/ml of IFN-α (**B**), 4μM of cisplatin (**C**), 1μM of etoposide (**D**) for indicated time period, then cell lysates were collected and MASTL expression was analyzed by western blot. (**E-G**) HeLa cells were treated with 10μg/ml of poly I: C alone (**E**), 20ng/ml of IFN-γ alone (**F**), or both poly I: C and IFN gamma (**G**) for indicated time period, then cell lysates were collected for western blot. (**H-J**) SCC38 cells were treated with 2μg/ml of poly I: C (**H**), 20ng/ml of IFN-α (**I**), 1μM of etoposide (**J**) for indicated time period, then cell lysates were collected and MASTL expression was analyzed by western blot. (**K-L**) SCC38 cells overexpressing CFP-MASTL (T-SCC38) were treated with 2μg/ml of poly I: C or not (**K**) or with 1μM of etoposide or not (**L**) for 36 hours, then followed by 20μg/ml of cycloheximide (CHX) for indicated hours; then cell lysates were collected for western blot.

2.3.2. MASTL regulates STAT1 phosphorylation through PP2A-B55α

As MASTL was upregulated after poly I:C and IFN-α/γ, important factors in the immune response, we wondered if MASTL would affect signal transducer and activator of transcription 1 (STAT1), an important downstream of the IFN receptor pathway [78], and interferon regulatory factor 3 (IRF3), which plays an important role in the innate immune system's response to viral infection and activates the transcription of IFN-α/β and other IFN-induced genes [79]. To verify this hypothesis, we firstly modified HeLa and MDA-MB-231 cell lines to stably overexpress CFP-tagged MASTL, which were renamed as T-HeLa and T-231 cells, respectively. Treatment with DNA damage drug or poly I: C and IFN-α in either HeLa or MDA-MB-231 cell lines did not change STAT1 protein level but induced more STAT1 phosphorylation at Y701 in a time-dependent manner, which was counteracted by overexpression of MASTL (Figure 2.3.2A-F). Interestingly, MASTL overexpression also reduced IRF3 protein level in HeLa cells (Figure 2.3.2A), which was due to impaired protein stability, as we demonstrate later in Figure 2.3.3C&D.

Then we further explored the detailed mechanism about how MASTL regulated STAT1 phosphorylation at Y701. As a novel kinase regulating mitotic entry, MASTL functions by phosphorylating and activating its substrates ARPP19/ENSA, which inhibits PP2A-B55α, a crucial phosphatase that antagonizes CDK1/cyclin B to promote mitotic exit [4]. Thus, we entertained the possibility of MASTL-ARPP19/ENSA-PP2A B55 axis regulation on STAT1 phosphorylation. Our data revealed that MASTL overexpression inhibited PP2A-B55α protein level (Figure 2.3.2G), while silencing ARPP19/ ENSA using specific siRNA in T-HeLa cells only slightly to moderately rescued STAT1 phosphorylation at Y701(Figure 2.3.2H), but re-overexpressing HA-tagged PPP2R2A/PP2A-B55α greatly induced STAT1 phosphorylation in T-HeLa cells,

regardless of DNA damage drug treatment (Figure 2.3.2I). These evidences indicated that MASTL regulated STAT1 phosphorylation at Y701 mainly through PP2A-B55α.

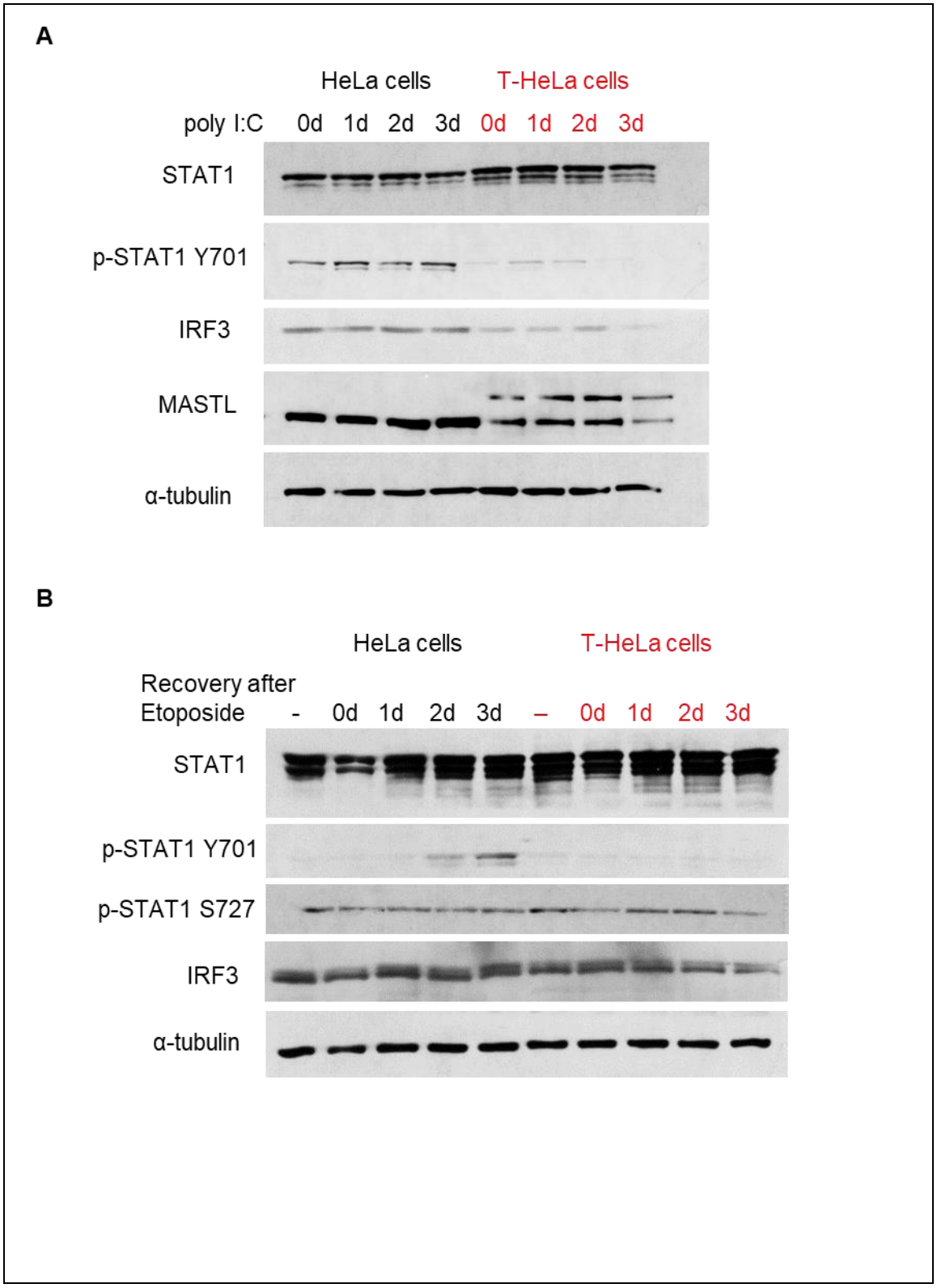

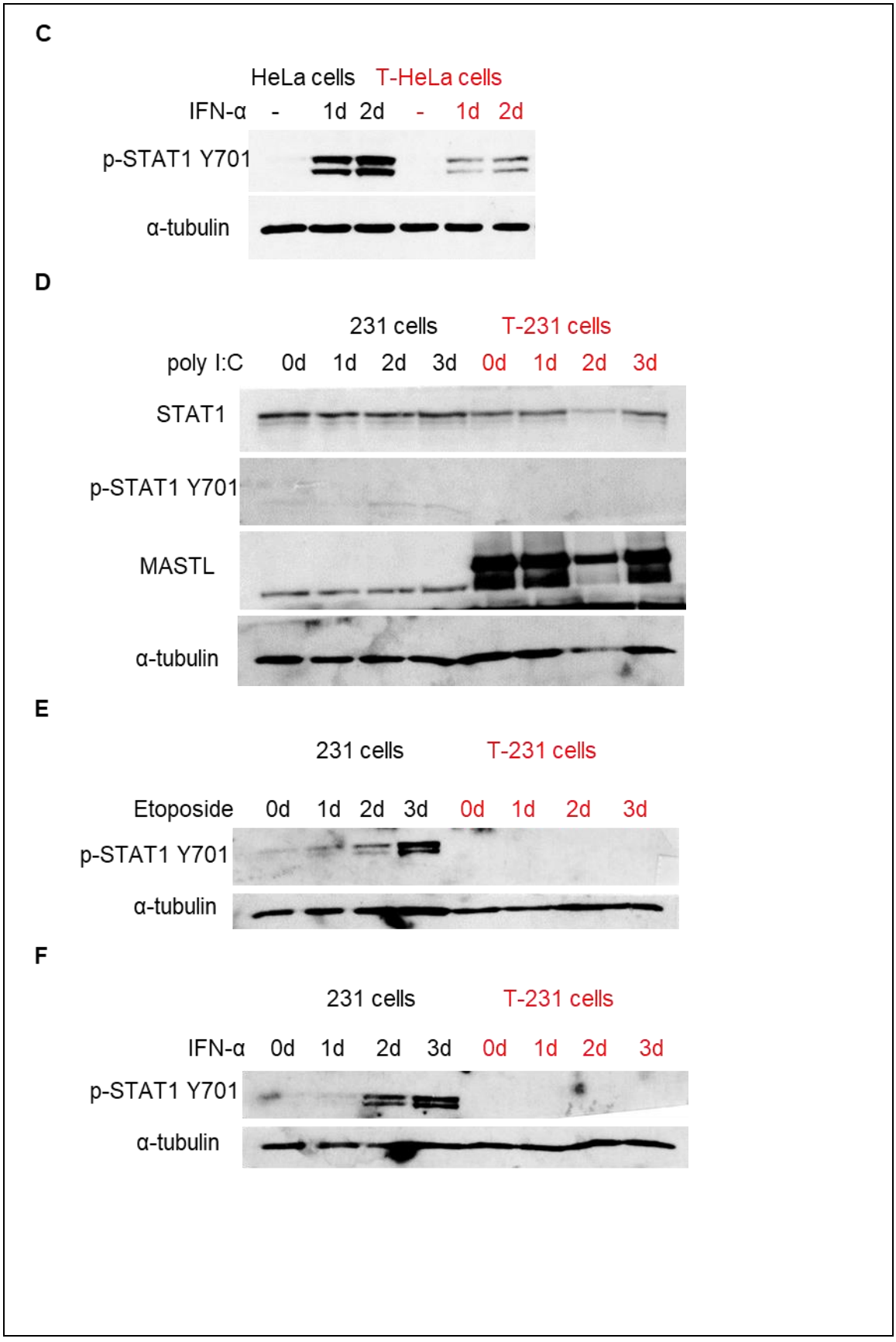
C
HeLa cells
T-HeLa cells
IFN-α - 1d 2d - 1d 2d
p-STAT1 Y701
α-tubulin
D
231 cells
T-231 cells
poly I:C 0d 1d 2d 3d 0d 1d 2d 3d
STAT1
p-STAT1 Y701
MASTL
α-tubulin
E
231 cells
T-231 cells
Etoposide 0d 1d 2d 3d 0d 1d 2d 3d
p-STAT1 Y701
α-tubulin
F
231 cells
T-231 cells
IFN-α 0d 1d 2d 3d 0d 1d 2d 3d
p-STAT1 Y701
α-tubulin

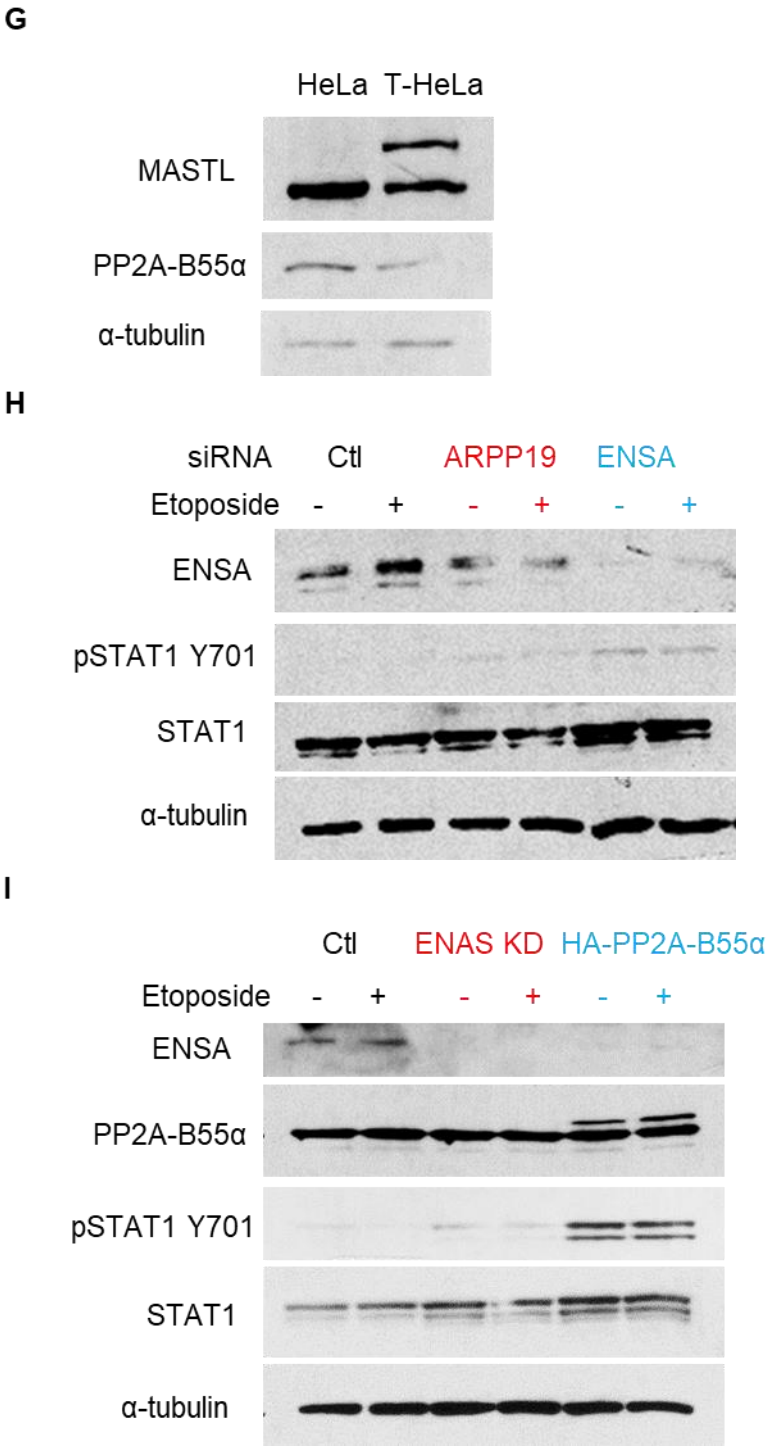

Figure 2.3. 2. MASTL regulates STAT1 phosphorylation through PP2A-B55α. HeLa and T-HeLa cells were treated with 2μg/ml of poly I: C (**A**), 1μM of etoposide (**B**), 20ng/ml of IFN-α (**C**) for up to 3 days; then cells were allowed for recovery up to 3 days; then cell lysates were collected by western blot. (**D-F)** MDA-MB-231 and T-231 cells were treated with 20ng/ml of poly I: C (**D**), 1μM of etoposide (**E**), 20ng/ml of

IFN-α (**F**) for up to 3 days; then cells were allowed for recovery up to 3 days; then cell lysates were collected by western blot. (**G**) HeLa and T-HeLa cell lysates were analyzed for MASTL, PP2A-B55α and α-tubulin by western blot; (**H**) T-HeLa cells were treated with control (Ctl) siRNA or siRNA targeting either ARPP19 or ENSA, followed with or without 1μM of etoposide overnight; (**I**) T-HeLa cells were treated with ENSA siRNA or transfected with HA-tagged PP2A-B55α, followed by treatment with or without 1μM of etoposide overnight; then cell lysates were collected by western blot.

2.3.3. MASTL-PP2A-B55α axis mediates cGAS-STING pathway to regulate STAT1 phosphorylation

cGAS - STING pathway is a component of the innate immune system that functions to detect the presence of cytosolic DNA and induce an innate immune response [80]. cGAS is also essential for cellular senescence induced by DNA damaging agents, including radiation and etoposide [80, 81]. We examined the MASTL-PP2A-B55α axis function on the cGAS-STING pathway. Our immunoblotting results showed that MASTL overexpression in HeLa and MDA-MB-231 cell lines reduced etoposide-induced STAT1 phosphorylation at Y701 and also inhibited the cGAS-STING pathway, including less protein levels of cGAS, STING, TBK1 and IRF3 (Figure 2.3.3A&B). Besides, overexpression of MASTL in HeLa cells induced more IRF3 degradation (Figure 2.3.3C&D), providing an explanation of reduced IRF3 signal in T-HeLa cells (Figure 2.3.3A & Figure 2.3.3A&B). Luckily, depleting MASTL with siRNA mildly induced more cGAS in HeLa cells (Figure 2.3.3E), while re-expressing HA-tagged PP2A-B55α in T-HeLa cells moderately rescued cGAS level but greatly restored STAT1 phosphorylation and induced STING phosphorylation in T-HeLa cells (Figure 2.3.3F). Moreover, we found that etoposide-induced STAT1 phosphorylation at Y701 was dependent on STING signal, as STING siRNA made such phosphorylation faded away

(Figure 2.3.3G). Taken together, our data demonstrated that MASTL-PP2A-b55α axis regulates STAT1 phosphorylation through cGAS-STING pathway.

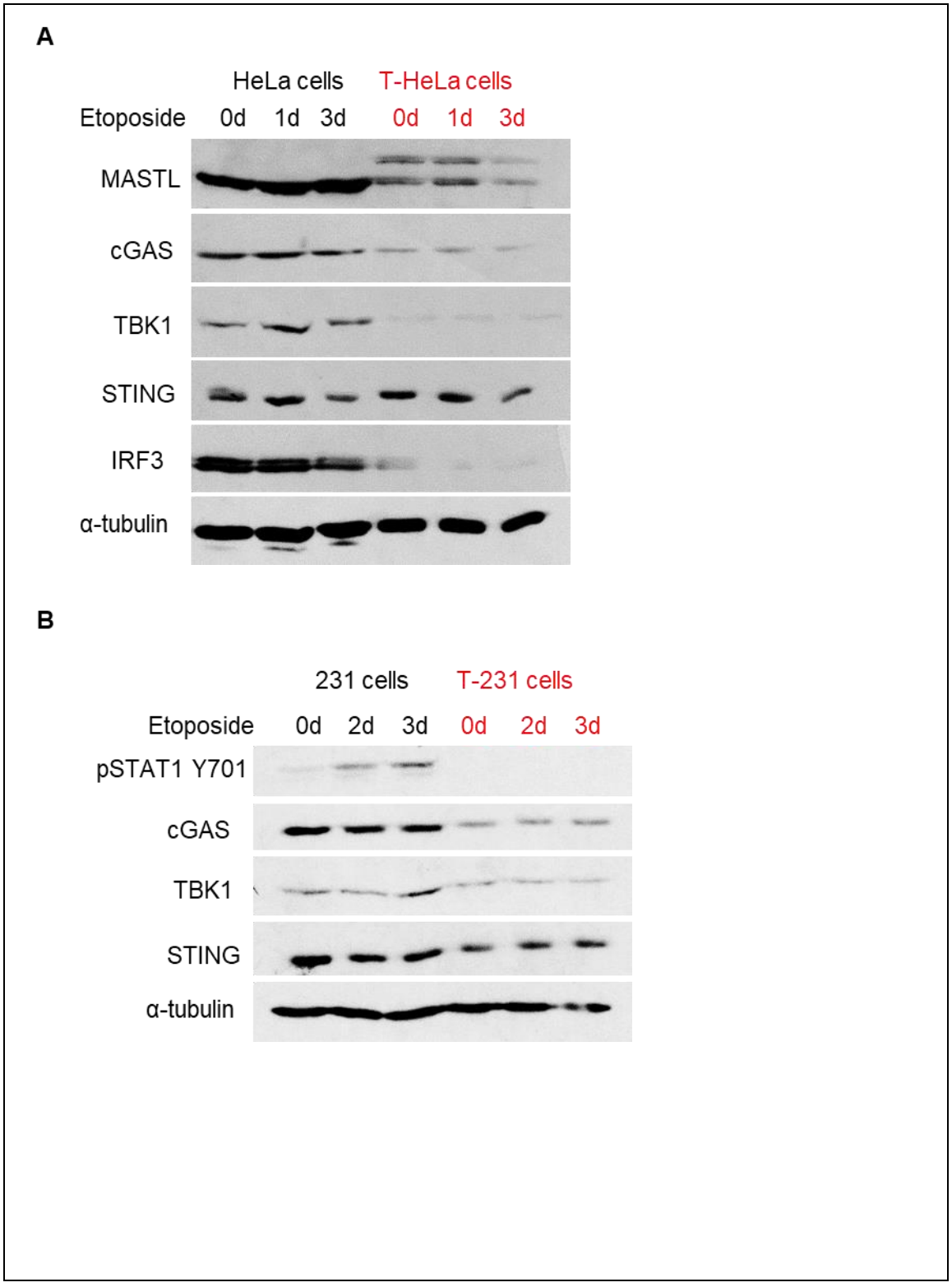

C

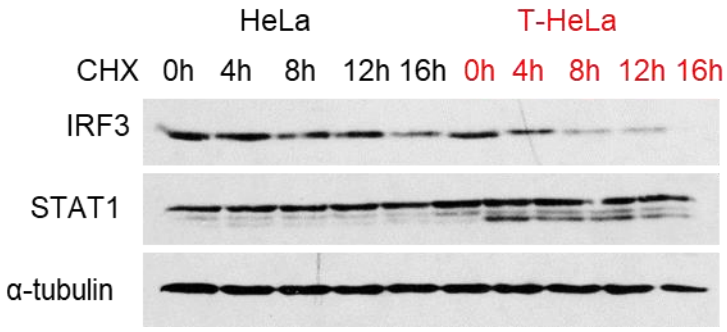
HeLa
T-HeLa
CHX 0h 4h 8h 12h 16h 0h 4h 8h 12h 16h
IRF3
STAT1
α-tubulin

D

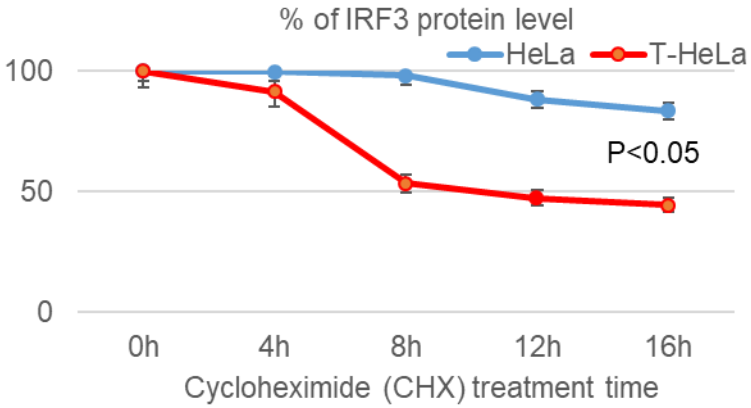
% of IRF3 protein level
HeLa
T-HeLa
100
50
0
P<0.05
0h
4h
8h
12h
16h
Cycloheximide (CHX) treatment time

E

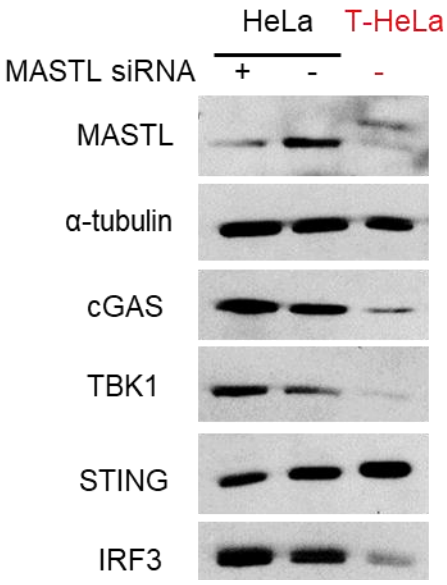
HeLa
T-HeLa
MASTL siRNA + - -
MASTL
α-tubulin
cGAS
TBK1
STING
IRF3

F

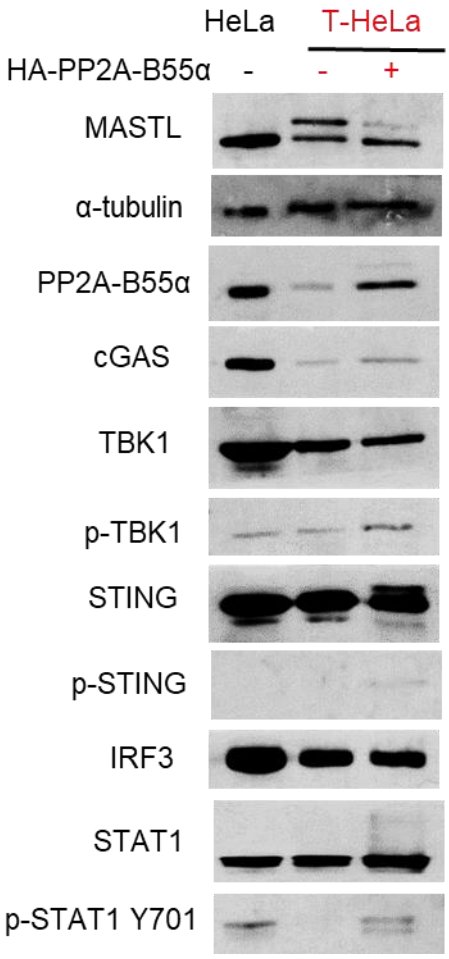
HeLa
T-HeLa
HA-PP2A-B55α - - +
MASTL
α-tubulin
PP2A-B55α
cGAS
TBK1
p-TBK1
STING
p-STING
IRF3
STAT1
p-STAT1 Y701

G

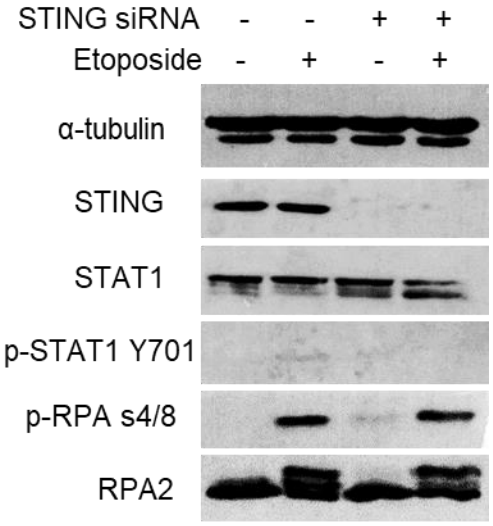
STING siRNA - - + +
Etoposide - + - +
α-tubulin
STING
STAT1
p-STAT1 Y701
p-RPA s4/8
RPA2

Figure 2.3. 3. MASTL-PP2A-B55α axis mediates cGAS-STING pathway to regulate STAT1 phosphorylation.

(**A**) HeLa and T-HeLa cells were treated with 1μM of etoposide for up to 3 days, then cell lysates were analyzed by western blot. (**B**) MDA-MB-231 and T-231 cells were treated with 1μM of etoposide for up to 3 days; then cell lysates were collected for western blot. (**C**) HeLa and T-HeLa cells were treated 20μg/ml of cycloheximide (CHX) for indicated hours, then cell lysates were collected for western blot. (**D**) Quantification of relative IRF3 protein level in panel (**C**), data were shown as mean ± standard deviation. Statistical analysis was performed using student's t-test. (**E**) HeLa cell lysates with or without MASTL siRNA and T-HeLa cell lysates were analyzed by western blot. (**F**) HeLa cell lysates, T-HeLa cell lysates with or without HA-tagged PP2A-B55α transfection, were analyzed by western blot. (**G**) HeLa cells were treated with or without STING siRNA for 24 hours, followed by 1μM of etoposide treatment overnight, then cell lysates were collected for immunoblotting analysis.

2.4. Discussion

Recent studies revealed that MASTL was inducible by inflammatory cytokines, including interleukin 6 (IL-6) and tumor necrosis factor alpha (TNF-a) in liver cancer cells [53]. Other studies also demonstrated high level of MASTL expression in various human cancers, which was related to poor patient survival, cancer invasion and resistance to chemotherapy [15-21, 54-56]. Subsequently it is important to uncover detailed mechanisms about how MASTL promotes tumor progression to overcome MASTL-associated tumor resistance, proposing better choices for cancer treatment.

Our current research studied MASTL's involvement in immunotherapy, which is most commonly used to treat allergies, autoimmune disorders and certain cancers [82]. Here we revealed that MASTL was inducible in response to DNA damaging drug, IFN and poly I: C in multiple human cancer cell lines (Figure 2.3.1A-J), consistent to previous

study induced by IL-6 [53]. Further protein degradation assay uncovered that the DNA damage- or poly I: C-induced MASTL upregulation was due to prolonged protein stability (Figure 2.3.1K&L).

Then we examined STAT1 activation during different treatment options in HeLa and MDA-MB-231 cell lines. Corresponding to previous study that DNA damage and oxidative stress upregulated STAT1 activation [62-65], our data showed that etoposide-induced DNA damage, as well as IFN and poly I: C treatments, triggered STAT1 phosphorylation at Y701, but causing no change to STAT1 protein level (Figure 2.3.2A, B&F). However, MASTL overexpression compromised upregulation of STAT1 phosphorylation at Y701 (Figure 2.3.2A-F) and reduced IRF3 protein level (Figure 2.3.2A & Figure 2.3.3A&B), but it did not affect STAT1 phosphorylation at S727 (Figure 2.2.2B). STAT1 modulates its downstream pathways via phosphorylation at Y701 or S727. Generally, STAT1 phosphorylation at Y701 is designated to work as a tumor suppressor that is involved in the JAK/STAT1 signaling pathway [69], while phosphorylation at S727 is related with tumor progression. Phosphorylation of STAT1 on S727 was prominently observed in uterine serous carcinoma and breast cancer [83, 84] and promotes autoimmune antibody-forming cells and germinal center responses, driving autoantibody production and systemic lupus erythematosus (SLE) development [85]. Our results that MASTL overexpression inhibited STAT1 phosphorylation at Y701, but not at S727 suggested a possible pathway that MASTL promotes tumor progression and cancer resistance to chemotherapy through STAT1.

As MASTL was known to inhibit PP2A-B55α function through activating ARPP19/ENSA [86], we wondered if PP2A- B55α played a role in MASTL-regulated STAT1 phosphorylation. As indicated in Figure 2.3.3G, PP2A- B55α protein level was decreased in T-HeLa cells, tempting us to investigate the effect of PP2A-B55α rescue in

T-HeLa cells on STAT1 phosphorylation at Y701. The obtained data showed that, independent of etoposide treatment, depletion of either ARPP19 or ENSA (Figure 2.3.2H) only slightly restored STAT1 phosphorylation, while re-expressing HA-tagged PP2A-B55α cells dramatically renovated STAT1 phosphorylation in T-HeLa (Figure 2.3.2I).

The cGAS/STING/TBK1/IRF3 innate immunity pathway also plays a pivotal role in the DNA damage-induced innate immune response and helps to maintain chromosomal stability [70]. Our data demonstrated that MASTL overexpression inhibited nearly every step of the cGAS-STING pathway in human cancer cell lines (Figure 2.3.3 A&B), which could be partially relieved by depleting MASTL (Figure 2.3.3E) or recovering PP2A-B55α (Figure 2.3.3F). Taken together, our results suggested that MASTL overexpression found in human cancers may help tumorous cells to evade immune-surveillance, thus promoting tumor invasion and metastasis, in a similar way that some pathogenic viruses use to antagonize host innate immune responses [87-89].

Previous studies showed that AKT kinase and beclin-1 autophagy protein suppresses cGAS-mediated antiviral immunity and that E3 ligase TRIM56 prompts cGAS dimerization and anti-DNA viral immunity [90]. In gastric cancer cells, MTMR2 upregulates ZEB1 to induce EMT by inactivating IFN-γ/STAT1 pathway [91]. FRK suppressed glioma through promoting STAT1 activation [68]. Consistent with that research, our current study revealed MASTL as a new factor negatively regulating the cGAS-STING pathway and its downstream IFN-induced STAT1 activation, proposing MASTL as a future target for antitumor immunotherapy and infection control. Nevertheless, more clinical evidence and future study are still needed to support this option.

CHAPTER 3: THE SM CORE COMPONENTS OF SMALL NUCLEAR RIBONUCLEOPROTEINS PROMOTE HOMOLOGOUS RECOMBINATION REPAIR*

3.0 Abstract

Double strand breaks (DSBs) are hazardous to the cell, where both DNA strands are severed. In response to DSBs, three mechanisms are used to repair DSBs in the cell: non-homologous end joining (NHEJ), homologous recombination (HR) and microhomology-mediated end joining (MMEJ). Sm core proteins, or simply Sm proteins, are a group of proteins that bind with small nuclear RNA (snRNA) to form small nuclear ribonucleoproteins (snRNPs), which aids RNA processing. Using mass spectrum assay, we found that Sm proteins were associated with DNA damage. Further micro-laser cut experiments revealed that the Sm proteins were recruited to DNA damage sites in cell nuclear, where they formed foci with other known DNA damage repair proteins, including gamma H2AX, phosphor-ATM s1981, PARP1 and phospho-53bp1. We later found that silencing Sm D3 or Sm B/B' induced more accumulation of gamma H2AX, phopho-RPA2, and impaired the HR repair efficiency with reduced protein levels of RAD51, CKH1 and/or BRCA1, but caused no change to these proteins mainly involved in NHEJ, such as FEN1, PARP1, MRE11, ku70/80 and DNA-PKcs. Lastly, our co-immunoprecipitation results demonstrated that Sm proteins were core components that associated with HR proteins, which promotes HR proteins stability to maintain DNA repair efficiency. In summary, our data exposed a novel function of Sm proteins as a regulator of DNA damage repair proteins to promote homologous recombination repair and maintain genome stability.

*The material presented in this chapter was previously submitted to *DNA Repair* for review.

3.1. Introduction

DNA damage happens in the cell every day naturally or due to exposure to chemotherapeutic drugs, which induces either single-strand breaks (SSBs) or double-strand breaks (DSBs). In particular, DSBs are more hazardous to the cell considering that both DNA strands are impacted. Two repair mechanisms are widely used in the cell to repair DSBs: the non-homologous end joining (NHEJ) and homologous recombination (HR). Unlike NHEJ, which is somewhat error-prone, the repair efficiency of HR is accurate with the need of an identical template [92]. Dysfunction of HR has been linked with some congenital disease [93, 94] and cancer formation [95-99].

In response to DSBs, numerous of proteins are activated and participating in chromatin remodeling and cell cycle arrest to promote efficient DNA repair. In the early steps of repair, PARP1 is recruited to DSBs sites [100-102], followed by later recruitment of the DNA repair enzyme MRE11 [103-105] to initiate DNA repair. H2AX phosphorylation is also involved in the early steps leading to chromatin de-condensation after DSBs [106-109]. After rapid chromatin remodeling, cell cycle checkpoints activation allows DNA repair to occur before the cell cycle progresses. ATM and ATR are two master kinases controlling checkpoints activation [49, 105, 110-112]. Once activated, they phosphorylate and activate downstream targets, including CHK1, CHK2, BRCA1, MDC1, and 53BP1, eventually leading to cell cycle arrest [111, 113-116].

In HR, after DSBs recognition and resection [117], the RPA protein, binds the 3' overhangs [118-120]. Then the Rad51 protein binds with the RPA-coated DNA, promoting searching for homology to the 3' overhang and strand invasion [121, 122]. Though much is known about HR importance in DSBs repair, it is still not clear the mechanism that regulates this important process.

Including mainly SmB, SmB′, SmN, SmD1, SmD2, SmD3, SmE, SmF and SmG, Sm proteins are a group of molecules, that bind with small nuclear RNA to form small nuclear ribonucleoproteins, or snRNPs, which play various roles in pre-mRNA processing and regulation [123]. The Sm proteins were first discovered as antigens targeted by so-called anti-Sm antibodies in a patient with a form of systemic lupus erythematosus [124]. Mutation of RNA binding protein in bacteria results in decreased growth rates and yields and increased sensitivity to ultraviolet light [125]. SmB upregulation or dysfunction has been observed in several human diseases, such as cervical cancer, hepatocellular carcinoma, non-small cell lung cancer (NSCLC), Crohn's disease, glioblastoma and cerebro-costo-mandibular syndrome [126-131]. Our recent proteomic assay revealed that Sm proteins were associated with DNA damage. However, it is ambiguous that what function Sm proteins have during DNA repair. Here we identified Sm proteins as DNA damage-associated proteins, which were recruited to DNA damage sites. Further experiments demonstrated that knockdown SNRPD3 or SNRPB reduced repair efficiency of HR, which was due to compromised HR repair protein stability of RAD51 and CHK1. We proposed a novel role of Sm proteins in DNA repair, which might throw new light to the therapeutic options for human disease.

3.2. Materials and Methods

3.2.1. Cell culture and transfection

Human cervix carcinoma (HeLa) and Human head and neck squamous cell carcinoma UM-SCC-38 cell lines were maintained at Dulbecco's modified Eagle medium (DMEM, Hyclone) with 10% fetal bovine serum (FBS, Hyclone). cDNA of human *Sm* genes and *RAD51* were synthesized by Twist Bioscience and then amplified and cloned into the pEGFP vector (Addgene). Transfection of plasmid DNA was performed using Lipofectamine 2000 (Invitrogen), following the protocol recommended by the

manufacturer. siRNAs targeting Sm genes were ordered from IDT company (Integrated DNA Technologies) and transfected into cells using Lipofectamine RNAi MAX (Invitrogen), a non-targeting siRNA was used as a control. The *Sm-D3* siRNA sequences are #1: 5'-3'GGUAUUCUGAGGAAUAA; 5'-3'ACUGAUGCUUAUUCCUCA, and #2: 5'-3'GUCUAUUGGUGUGCCGA; 5'-3'UACUUUAAUCGGCACACC. *Sm-B* siRNA sequences are: 5'-3'GAGAAUCUGGUCUCAAUG; 5' 3'CUACUGUCAUUGAGACCA.

3.2.1. Chromatin fractionation

As described in our previous study [132], HeLa cells were wash with PBS and trypsinized. One fifth of the cell pellet was resolved with Laemmli sample buffer (Bio-Rad), as input. The remaining cell pellet was resolved with buffer A (10mM Hepes, PH7.9; 10mM KCl; 1.5mM MgCl2; 0.34M sucrose; 10% Glycerol; 1mM DTT; 1mM protease inhibitor in sterilized ddH2O and 0.1% Triton X-100) on ice for 8 mins, then washed with triton X-100 free buffer A and resuspended in buffer B (3mM EDTA; 0.2mM EGTA; 1mM DTT and 1mM protease inhibitor in sterilized ddH2O) at room temperature for 30 mins. The chromatin fraction was then isolated by centrifugation, resolved with Laemmli sample buffer (Bio-Rad) and analyzed by immunoblotting.

3.2.2. Co-immunoprecipitation

For immunoprecipitation, RAD51 (Cell Signaling Technology #8875), Sm-B/B' (Santa Cruz Biotechnology, sc-271094), or GFP antibody (produced using full-length GFP protein) was conjugated on magnetic beads (Thermo Fisher Scientific) and incubated in human cell lysates. The beads were then re-isolated on a magnetic rack and analyzed by immunoblotting.

3.2.3. Immunoblotting

Sodium dodecyl sulfate-polyacrylamide gel electrophoresis (SDS-PAGE) and immunoblotting were carried out as previously described [133], using the following antibodies: KU80 (A302-627) and Sm-D3 (A303-954) from Bethyl Laboratories (Montgomery, TX); PARP1 (sc-74470), Sm-B/B' (sc-271094), Sm-D1 (sc-166650), ATM (sc-377293), DNA-PKcs (sc-390849), GFP (sc-9996), □-actin (sc-47778) and γ-H2AX (sc-517348) from Santa Cruz Biotechnology (Dallas, TX); FEN1 (ab109132), H2B (ab1790-100) and α-tubulin (ab7291) from Abcam (Cambridge, MA); CHK1 (#2345), phospho-ATM (#13050) and γ-H2AX (#9718) from Cell Signaling Technology (Beverly, MA).

3.2.4. I-PPOI assay and Chromatin immunoprecipitation

Gnomic DSBs are induced by I-PPOI digestion, as in previous studies [134, 135]; chromatin immunoprecipitation was performed using the simple ChIP enzymatic chromatin IP kit (CST#9003), following the protocol recommended by the manufacturer. Briefly, HeLa cells were transfected with control plasmid or pBABE-HA-ER-IPpoI (a gift from Michael Kastan via Addgene; plasmid # 32565), followed by 4-hydroxytamoxifen (4-OHT) treatment. Cells were crosslinked in 1% formaldehyde solution for 10 minutes with briefly swirling at room temperature, then quenched with glycine. Then cell nuclei were isolated by centrifugation, digested with Micrococcal Nuclease, and processed by sonication. The resulted cross-linked chromatin was incubated with Sm-B/B' antibody, or negative control Normal rabbit IgG at 4ºC overnight. ChIP-grade protein G magnetic beads were added into the reactions, and the chromatin DNA in the IP was eluted, purified, and quantified by PCR analysis.

3.2.5. HR and NHEJ repair assays

Homologous recombination and nonhomologous end joining assays were performed as in our previous studies [43, 136]. Briefly, HR was measured in a HeLa-derived cell line that was stably integrated with a DR-GFP reporter cassette. DSBs were induced in these cells by expressing I-SceI endonuclease. In these cells, GFP is expressed only after DSBs introduced by I-SceI endonuclease are repaired by HR, and the level of full-length GFP (and control α-tubulin) expression was quantified by immunoblotting and NIH ImageJ. The NHEJ assay was performed in U2OS-EJ5 cells. The cells were transfected with an expression vector of I-SceI endonuclease. In these cells, GFP is expressed only after DSBs introduced by I-SceI endonuclease are repaired by NHEJ, and the level of GFP expression, normalized to control α-tubulin, was quantified by immunoblotting.

3.2.6. Immunofluorescence and laser micro-irradiation

HeLa cells were seeded on microscope cover glasses and fixed with 3% formaldehyde with 0.1% Triton X-100 for 30 min, followed by treatment with 0.05% Saponin and blocking in 5% goat serum. Primary antibodies were diluted in 5% goat serum and incubated with the cover-glasses overnight at cold room. The cells were then incubated with Alexa Fluor secondary antibodies (Invitrogen) for 1 hour at room temperature. The nuclei of cells were stained with 4', 6-diamidino-2-phenylindole (DAPI). The stained cells were imaged using a Zeiss Axiovert 200M inverted fluorescence microscope at the UNMC College of Dentistry. HeLa cells seeding on dishes with bottom glasses were transfected with GFP-tagged Sm components for laser micro-irradiation, which was performed using 405 nm laser under the Zeiss Axiovert 200M Microscope with Marianas Software (Intelligent Imaging Innovations, Inc Denver, CO).

3.2.7. DNA binding and mass spectrum assay

As described in our previous studies [43, 136], biotin-labeled double strand DNA fragment (dsDNA, 300 bp) was generated using biotin-11-ddUTP (Thermo Scientific) incorporation. Biotin-labeled DNA (produced as above) or biotin dA-dT (Invitrogen) was conjugated on streptavidin magnetic beads (New England Biolabs) and incubated in *Xenopus* egg extracts or HeLa cell lysates. The beads were re-isolated using a magnet rack, washed five times, and resolved in SDS-PAGE gels, and submitted for mass spectrum analysis at the Taplin mass spectrometry facility, Harvard.

3.2.8. Statistical analysis

Each experiment was carried out at least three times and the results were shown as the mean values and standard deviations. Unpaired two-tailed Student's t-test was used to analyze statistical significance. A P-value<0.05 was considered statistically significant.

3.3. Results

3.3.1. Sm proteins are associated with DNA damage and recruited to DNA damage sites

As described in our previous studies [43, 136], a 300 bp double stranded DNA fragment and a 70-mer dA-dT double stranded oligonucleotide were used as DNA DSB-mimicking templates to isolate potential DSB-associated proteins. These studies were performed in both HeLa cell lysate and *Xenopus* egg extract, a cell-free system well-defined for DNA damage repair and signaling [137]. The associated proteins were analyzed by mass spectrometry for identification. Interestingly, these experiments recovered multiple members of the Sm core proteins [138] (Figure 3.3.1A & B). The identification of Sm proteins was consistent between HeLa cell lysate and *Xenopus* egg extract, and between the two different DSB-mimicking templates (Fig 3.3.1B).

To confirm the role of these Sm proteins in the cellular DNA damage response, we showed in HeLa cells that GFP-tagged Sm-D3 protein was recruited to DNA damage sites within one minute after laser micro-irradiation (Figure 3.3.1C), indicating Sm-D3 as an early responder to DNA damage. A similar pattern of DNA damage recruitment was seen for other components of the Sm core, including Sm-B, Sm-D1, Sm-G and Sm-F (Figure 3.3.1D). Next, we asked if the rapid recruitment of Sm-D3 to laser-induced DNA damage sites was dependent on known upstream players of the DNA damage response, or on active RNA synthesis. As shown in Figure 3.3.1E, Sm-D3 recruitment to the laser track was independent of ATM/ATR kinase activities which play an important role in DNA damage signaling and repair, or PARP1-mediated PARylation which rapidly detects DNA damage and initiates DNA repair [102]. The recruitment of Sm-D3 was also independent of RNA synthesis, as disruption of RNA synthesis using 8-aminoadenosine did not impact the recruitment of Sm-D3 to the laser track (Figure 3.3.1E). These results suggested that Sm proteins either directly recognize DNA damage, or are recruited by another, yet unknown upstream factor.

As laser micro-irradiation induces a variety of DNA damage, we used the I-PPOI endonuclease system to specifically generate DNA DSBs in the genomic DNA. The chromatin immunoprecipitation assay following I-PPOI digestion demonstrated that Sm-B protein was indeed associated with the I-PPOI substrate genomic locus, in a manner that was dependent on I-PPOI induction (Figure 3.3.1F). Furthermore, we used immunofluorescent staining to study the DNA damage localization of endogenous Sm proteins. Our data confirmed that Sm-B and Sm-D1 proteins co-localized with well-established DNA damage response markers, including ATM phosphorylation and γ-H2AX, in cells treated with etoposide, hydroxyurea, or cisplatin (Figure 3.3.1G-L).

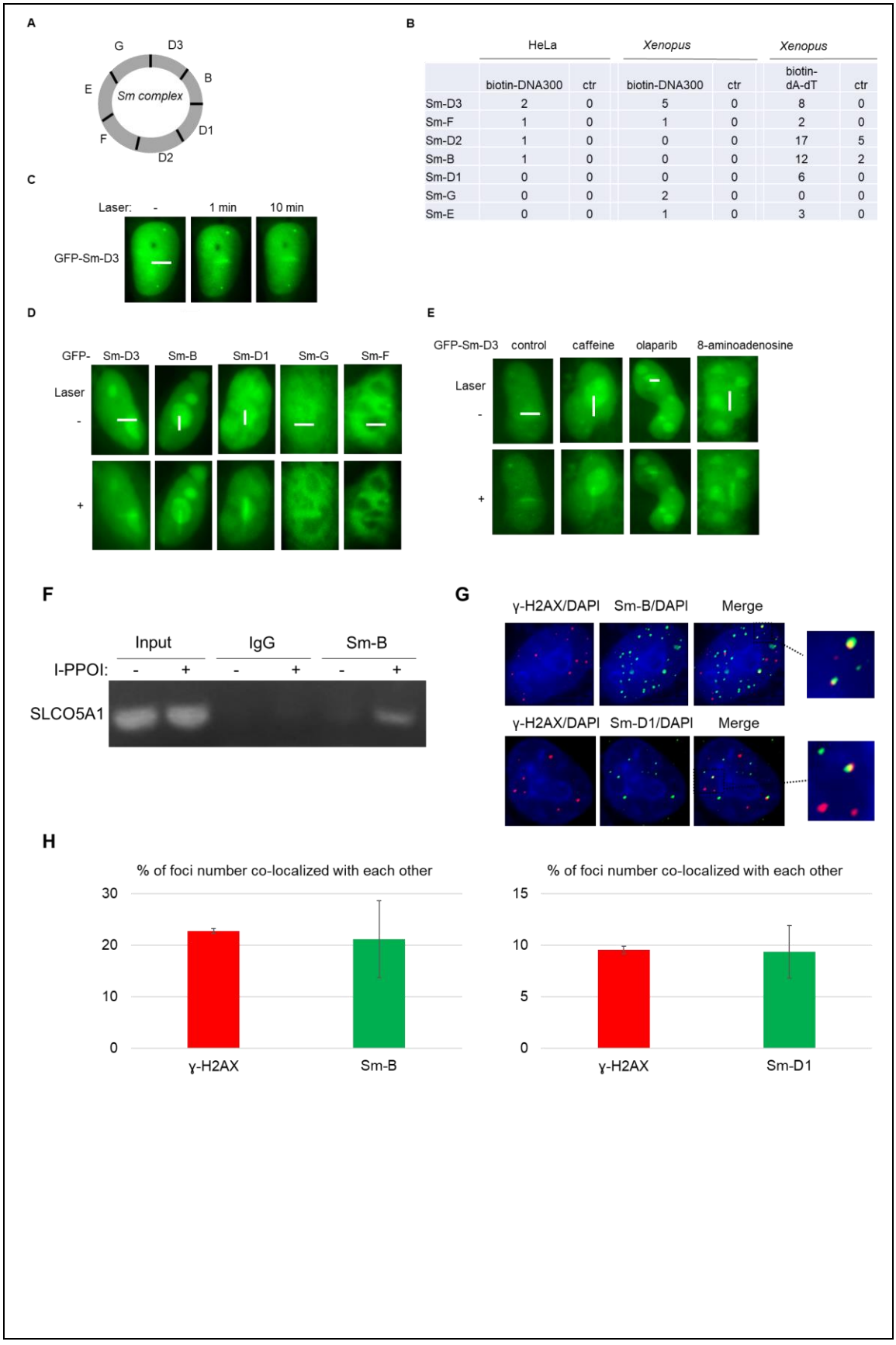

	HeLa		*Xenopus*		*Xenopus*	
	biotin-DNA300	ctr	biotin-DNA300	ctr	biotin-dA-dT	ctr
Sm-D3	2	0	5	0	8	0
Sm-F	1	0	1	0	2	0
Sm-D2	1	0	0	0	17	5
Sm-B	1	0	0	0	12	2
Sm-D1	0	0	0	0	6	0
Sm-G	0	0	2	0	0	0
Sm-E	0	0	1	0	3	0

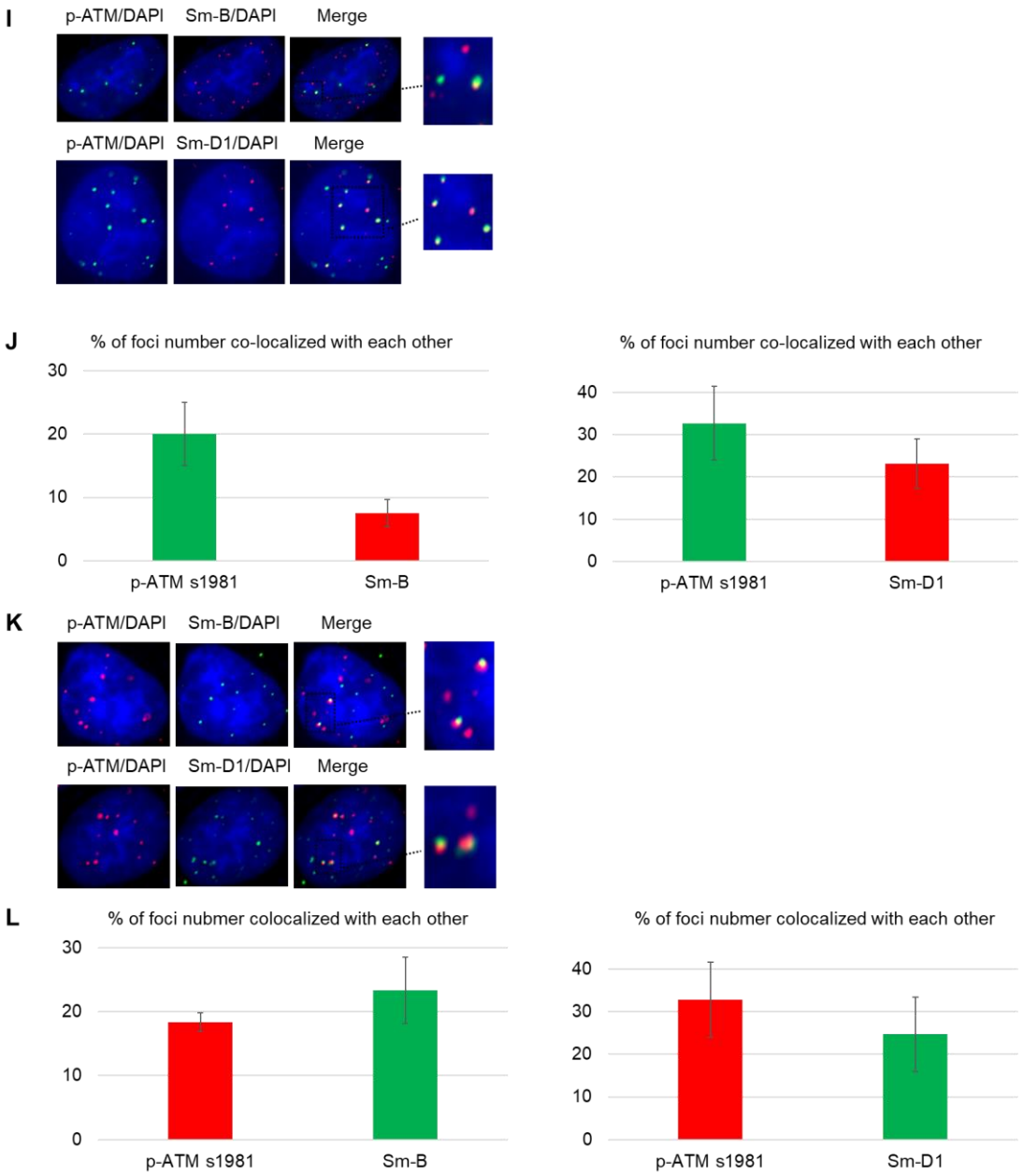

Figure 3.3. 1. Sm proteins are recruited to DNA damage sites.
(**A**) A diagram of the Sm core protein complex. (**B**) As described in Materials and Methods, biotin-coated double-strand DNA templates were incubated in HeLa cell lysate or *Xenopus* egg extracts. Co-purified proteins were analyzed by mass spectrometry, and the identified Sm core proteins are shown, with the numbers of their peptides identified by mass spectrometry. Ctr: control pull-down. (**C**) HeLa cells expressing GFP-tagged Sm-D3 were subjected to laser micro-irradiation as described in Materials and Methods. The fluorescent signal of GFP is shown at the indicated time points. The laser track is marked by a white line. (**D**) HeLa cells expressing GFP-tagged Sm core proteins were subjected to laser micro-irradiation as described in Materials and Methods. The fluorescent signals of GFP are shown. The laser track is marked by a white line. (**E**) The recruitment of GFP- Sm-D3 to

laser tracks was shown as in panel (**C**). These cells were pre-treated with ATM/ATRi (caffeine, 4mM), PARPi (olaparib, 10μM), or 8-aminoadenosine (10μM), 1hr before laser irradiation. Consistent results were observed in >10 cells for each treatment. (**F**) As described in the Materials and Methods, ChIP assay was performed in HeLa cells with or without I-PPOI induction, at the SLCO5A1 gene locus. The input, IgG IP, and Sm-B IP products were analyzed by PCR and shown. Data from Feifei Wang. (**G, H**) HeLa cells were treated with 1μM of etoposide for 3hrs, and then analyzed by immunofluorescence. The partial co-localization of Sm-B or Sm-D1 with γ-H2AX is shown in panel (**G**). The number of foci co-localized with each other were counted and quantified as shown in panel (**H**). Consistent results were observed in >10 cells for each treatment. (**I, J**) HeLa cells were treated with 2μM of hydroxyurea overnight, and analyzed by immunofluorescence. The partial co-localization of Sm-B or Sm-D1 with phospho-ATM Ser-1981 is shown in panel (**I**). The number of foci co-localized with each other were counted and quantified as shown in panel (**J**). Consistent results were observed in >10 cells for each treatment. (**K, L**) HeLa cells were treated with 1μM of cisplatin for 3hrs, and then analyzed by immunofluorescence. The partial co-localization of Sm-B or Sm-D1 with phospho-ATM Ser-1981 is shown in panel (**K**). The number of foci co-localized with each other were counted and quantified as shown in panel (**L**). Consistent results were observed in >10 cells for each treatment. Statistical analysis was performed using Excel and data were shown as mean± standard deviation.

3.3.2. Sm proteins are required for DSB repair via homologous recombination

We sought to investigate the role of Sm proteins in DSB repair. Interestingly, deletion of Sm-D3 using independent siRNAs caused accumulation of γ-H2AX, as measured by immunoblotting (Figure 3.3.2A). The similar phenotype was also observed with depletion of Sm-B (Figure 3.3.2B). Moreover, measurement of γ-H2AX foci formation by immunofluorescence confirmed that Sm-D3 depletion increased the level of γ-H2AX (Figure 3.3.2C&D); γ-H2AX induction was alleviated by re-expression of siRNA-resistant, recombinant Sm-D3 (Figure 3.3.2E&F), confirming that the phenotype was caused by specific depletion of Sm-D3.

A potential reason for the accumulation of endogenous DNA damage is DNA repair deficiency. We further assessed the impact of Sm proteins on DNA repair, particularly DSB repair via NHEJ and HR. Using a well-established, intra-chromosomal, I-SceI-induced reporter system [139], we measured the repair efficiency of HR and

NHEJ in control and Sm-D3 depleted cells. Interestingly, Sm-D3 depletion reduced HR repair activity by approximately 50% (Figure 3.3.2G), while causing no reduction in NHEJ repair (Figure 3.3.2H).

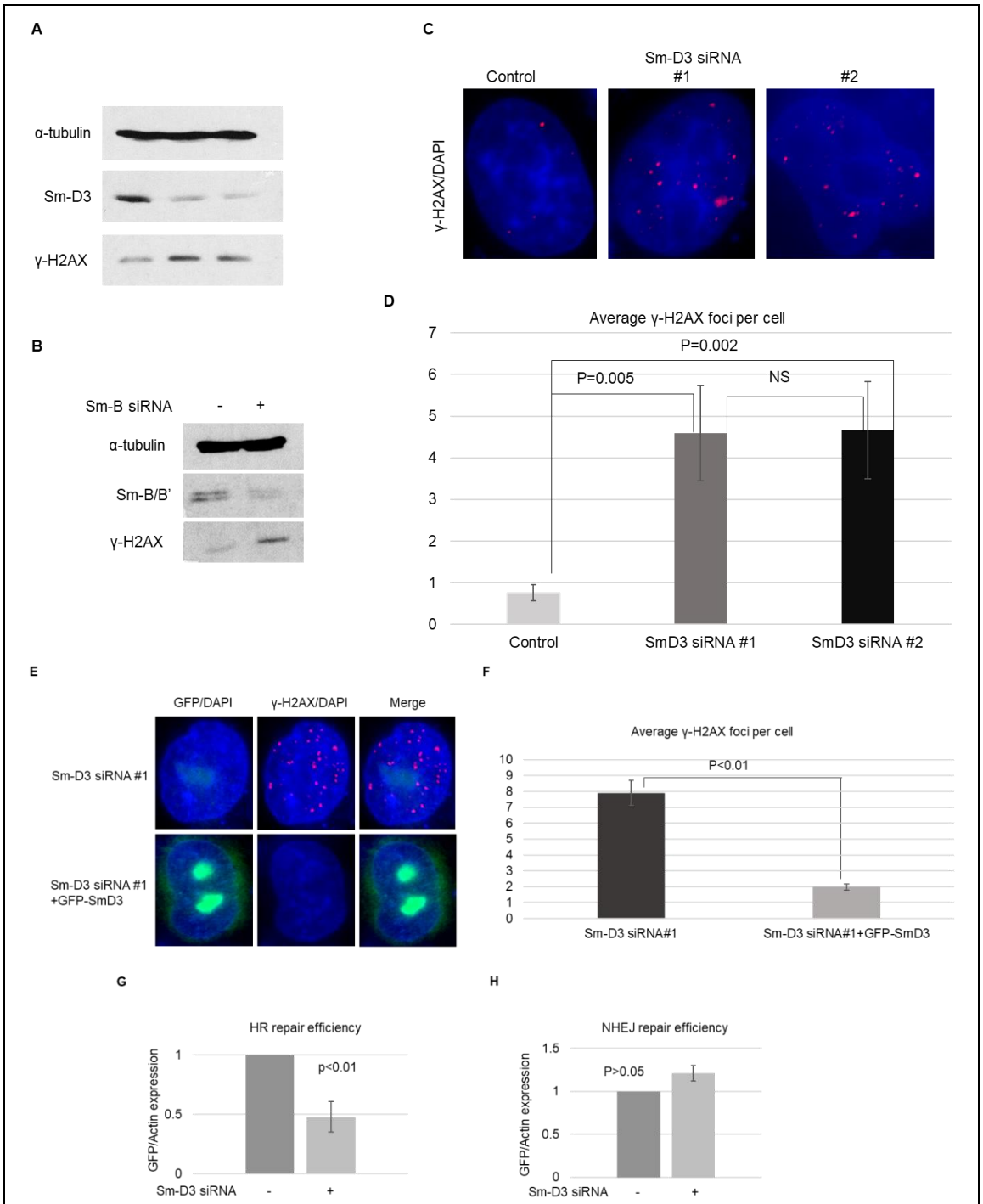

Figure 3.3. 2. Sm proteins are required for DSB repair via homologous recombination. (**A**) HeLa cells were treated with control siRNA (-) or Sm-D3 siRNAs (#1 and #2) for 2 days, and then harvested and analyzed by immunoblotting.

(**B**) HeLa cells were treated with control siRNA (-) or Sm-B siRNAs, and analyzed by immunoblotting. (**C, D**) HeLa cells were treated control siRNA (-) or Sm-D3 siRNAs (#1 and #2) as in panel (A), cells were analyzed by immunofluorescence for γ-H2AX. The γ-H2AX foci number per cell was counted and quantified and shown as panel (**D**).More than 100 cells were counted in each treatment. More than 100 cells were counted in each treatment. (**E, F**) HeLa cells were treated with Sm-D3 siRNA (#1), and co-transfection with GFP-Sm-D3. 2 days after siRNA treatment, cells were analyzed by immunofluorescence for γ-H2AX foci. GFP and DAPI signals are shown in panel (**E**). The γ-H2AX foci number per cell was counted and quantified as shown in panel (**F**), more than 50 cells were counted. (**G, H**) HR and NHEJ assays were performed as described in the Materials and Methods. Cells were first treated with control siRNA or Sm-D3 siRNA, followed by co-transfection with I-SceI endonuclease. The repair efficiency of HR in HeLa (**G**), and NHEJ in U2OS (H), was measured by the expression level of GFP, normalized to that of β-actin. The mean values and standard deviations, calculated from three independent experiments, were shown. Statistical analysis was conducted using unpaired 2-tailed Student's t-test, only p value <0.05 was considered as significant difference while $p >0.05$ as no difference (NS).

3.3.3 Sm-D3 depletion reduced the expression level of RAD51 and CHK1

As we discovered the importance of Sm-D3 in the HR repair pathway, we furthered explored its effects on the expression levels of HR factors. Sm-D3 depletion using two independent siRNAs reduced the protein level of RAD51 and CHK1, but not CHK2 or PARP1, in HeLa cells (Figure 3.3.3A). This result was also confirmed in UM-SCC38 cells where Sm-D3 knockdown reduced the protein level of RAD51 and CHK1, but not CHK2, ATM, DNA-PKcs, FEN1, PARP1, or KU80 (Figure 3.3.3B). Furthermore, re-expression of siRNA resistant Sm-D3 rescued RAD51 reduction from Sm-D3 depletion in UM-SCC38 or HeLa cells (Figure 3.3.3C&D).

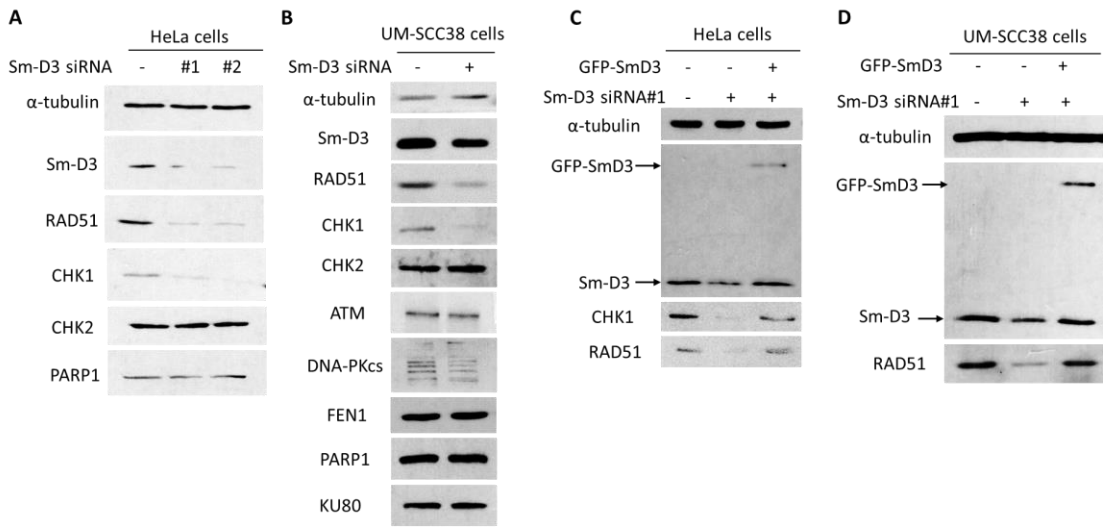

Figure 3.3. 3. Sm-D3 depletion reduced the expression level of RAD51.

(**A**) HeLa cells were treated with control siRNA (-) or Sm-D3 siRNAs (#1 and #2) for 2 days. Cells were then harvested and analyzed by immunoblotting for α-tubulin, Sm-D3, RAD51, CHK1, CHK2 and PARP1 by immunoblotting. (**B**) UM-SCC38 cells were treated with control siRNA (-) or Sm-D3 siRNAs (#1), and analyzed for the indicated DNA repair proteins. (**C, D**) HeLa cells (**C**) or UM-SCC38 cells (**D**) were treated with control siRNA or Sm-D3 siRNA (#1), and reconstituted with siRNA-resistant GFP-Sm-D3, as indicated. Cell lysates were analyzed by immunoblotting.

3.3.4. Sm-D3 associates with RAD51, and is required for its protein stability

Sm proteins are known to mediate mRNA processing, and can thereby, modulate gene expression, such as that of RAD51 or CHK1. However, we speculated that Sm proteins may directly participate in the DNA damage response, as suggested by their recruitment to DNA damage sites. Along this line, our reciprocal co-immunoprecipitation assays revealed an association between Sm-D3 and RAD51 (Figure 3.3.4A&C). We also confirmed the associations of Sm-B with RAD51 and CHK1 (Figure 3.3.4B&C). In addition, such associations between Sm proteins and RAD51 were independent of DNA,

as DNase I treatment didn't disrupted such association (Figure 3.3.4D); neither did DNA damaging agent, such as hydroxyurea, change their interactions (Figure 3.3.4E).

Strikingly, depletion of Sm-D3 accelerated the degradation of both GFP-tagged, recombinant, and endogenous RAD51 in HeLa cells (Figure 3.3.4F, 4G, 4I&4K). In this assay, new protein synthesis was inhibited by cycloheximide, and protein turnover indicated protein stability. The result was consistent with increased RAD51 ubiquitylation in cells depleted of Sm-D3 (Figure 3.3.4H&4L). Depletion of Sm-D3 also similarly reduced the protein stability of CHK1 (Figure 3.3.4I&4J). Thus, Sm-D3 influenced the level of RAD51 and CHK1 at the post-translational level, by preventing these proteins from proteolysis. Finally, our chromatin fractionation assay revealed that Sm-D3 depletion much more profoundly reduced the protein levels of CHK1 and RAD51 in the chromatin-bound fraction, in comparison to those in the whole cell lysate (Figure 3.3.4M-O). Together, the results support a model that the recruitment of Sm proteins to damaged chromatin plays an important role in HR by stabilizing RAD51 and CHK1 at the sites of DNA damage.

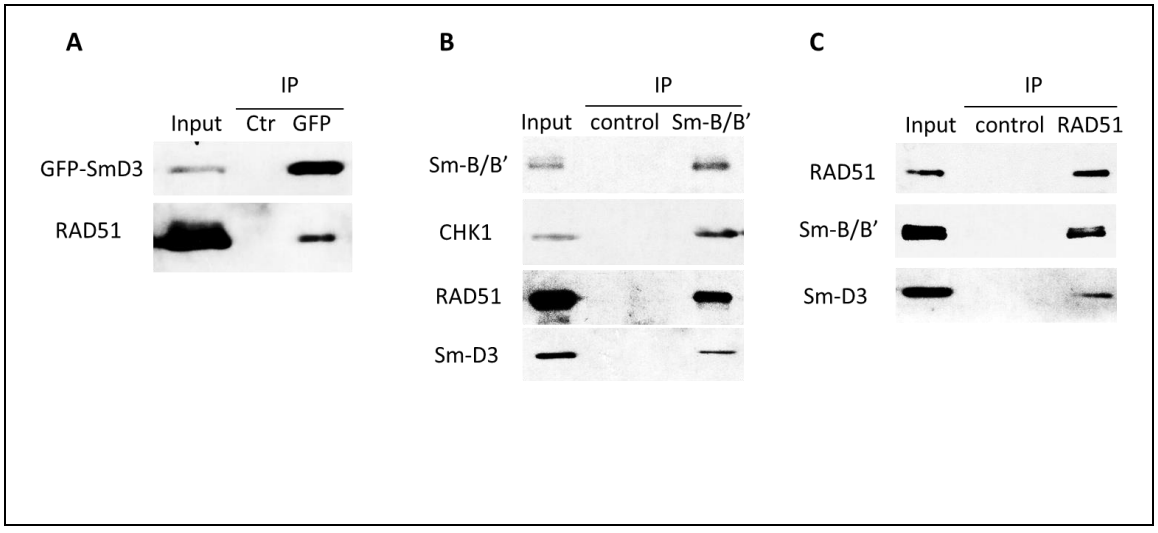

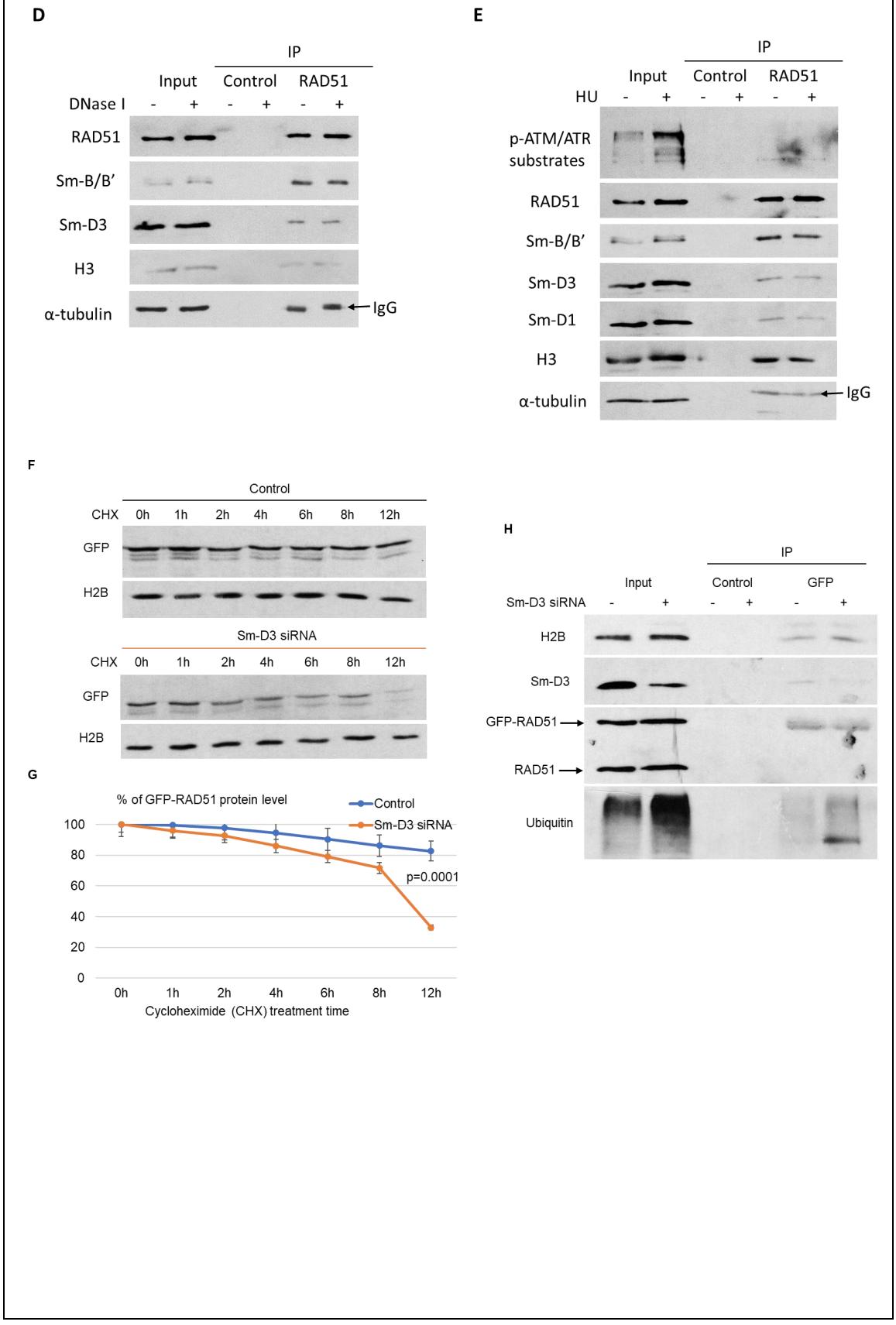
D
IP
Input
Control
RAD51
DNase I - + - + - +
RAD51
Sm-B/B'
Sm-D3
H3
α-tubulin
IgG
E
IP
Input
Control
RAD51
HU - + - + - +
p-ATM/ATR substrates
RAD51
Sm-B/B'
Sm-D3
Sm-D1
H3
α-tubulin
IgG
F
Control
CHX 0h 1h 2h 4h 6h 8h 12h
GFP
H2B
Sm-D3 siRNA
CHX 0h 1h 2h 4h 6h 8h 12h
GFP
H2B
G
% of GFP-RAD51 protein level
Control
Sm-D3 siRNA
100
80
60
40
20
0
p=0.0001
0h 1h 2h 4h 6h 8h 12h
Cycloheximide (CHX) treatment time
H
IP
Input
Control
GFP
Sm-D3 siRNA - + - + - +
H2B
Sm-D3
GFP-RAD51
RAD51
Ubiquitin

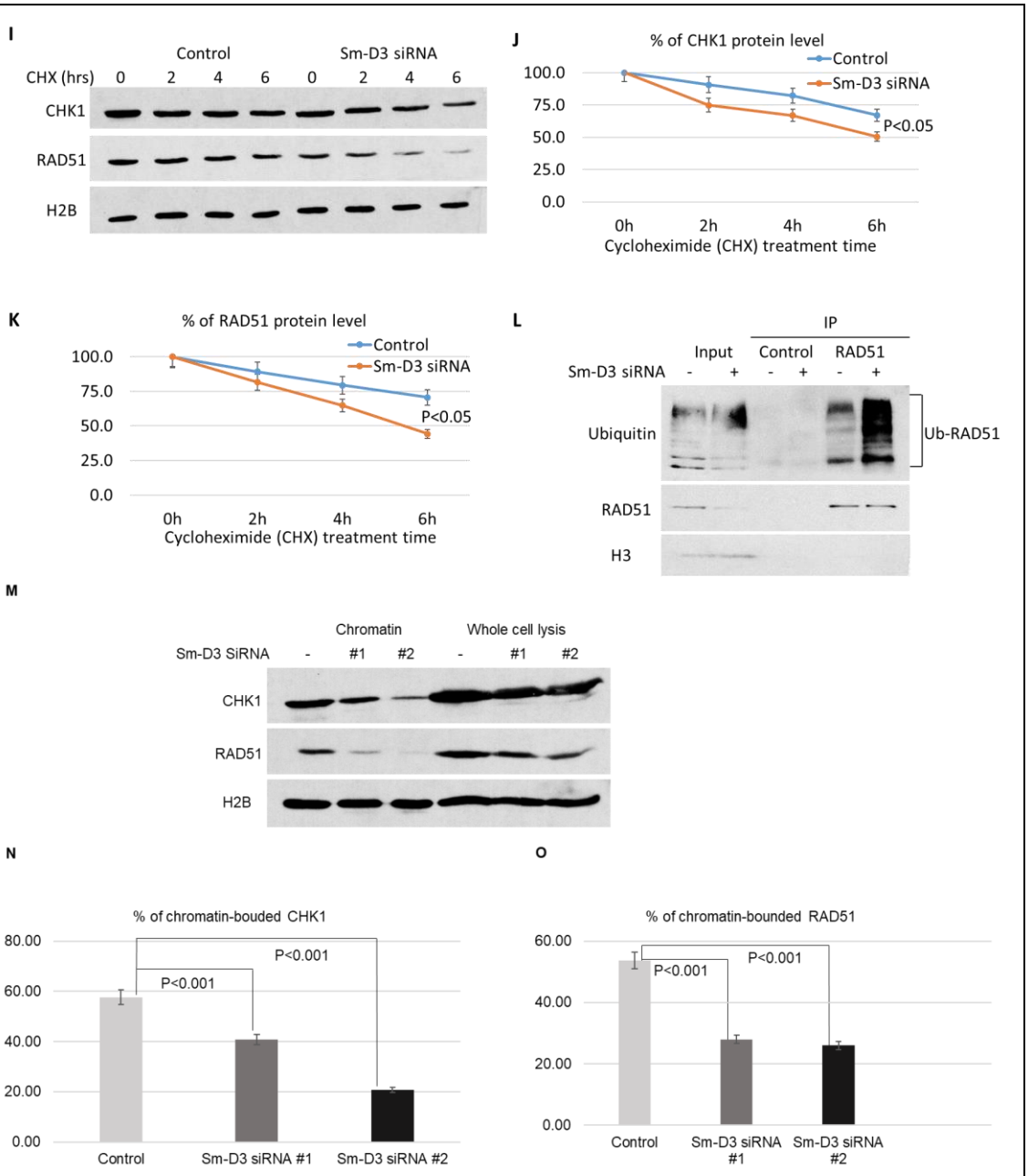

Figure 3.3. 4. Sm-D3 associates with RAD51 and is required for its protein stability. (**A**) Immunoprecipitation (IP) was performed in HeLa cells, as described in Materials and Methods. The input, control (empty magnetic beads) IP, and GFP-Sm-D3 IP samples were analyzed by immunoblotting for GFP and RAD51. (**B**) UM-SCC38 cell lysates were used for IP using Sm-B/B' antibody or control (empty magnetic beads). The input and IP samples were analyzed by immunoblotting. (**C**) Control or RAD51 IP was performed in HeLa cell lysates, then cell lysates input and IP samples were analyzed by immunoblotting. (**D**) HeLa cell lysates were incubated with or without DNase I (200 units/ml) (New England Biolabs) at 37℃ for 30mins before immune-precipitation with RAD51 antibody or control (empty magnetic beads),

then cell lysates input and IP samples were analyzed by immunoblotting. (**E**) HeLa cells were treated with or without 2mM of hydroxyurea (HU) overnight before ready use for immune-precipitation with RAD51 antibody or control (empty magnetic beads), then cell lysates input and IP samples were analyzed by immunoblotting. (**F**) HeLa cells were pre-treated with control (the upper panel) or Sm-D3 siRNA (the lower panel) for 5hrs, and then co-transfected with GFP-RAD51 plasmid DNA. After 24-hour incubation, cells were treated with 20μg/ml of cycloheximide (CHX), and incubated for indicated times. Cell lysates were collected and analyzed by immunoblotting for the expression of GFP and H2B. (**G**) Quantification of GFP-H2B ration in panel (**F**) is shown. (**H**) HeLa cells were pre-treated with control or Sm-D3 siRNA for 5hrs, then co-transfected with GFP-RAD51 plasmid DNA, and incubated for another 24hrs. After 4-hour treatment with 50mM of MG132, cell lysates were harvested for IP using anti-GFP antibody or control empty magnetic beads. The input, control IP and GFP IP samples were analyzed by immunoblotting. (**I**) HeLa cells were pre-treated with control or Sm-D3 siRNA for 1 day, followed by 20μg/ml of cycloheximide (CHX) treatment for indicated times. Then cell lysates were collected and analyzed by immunoblotting for CHK1, RAD51 and H2B. (**J, K**) Quantification of CHK1-H2B ration (**J**) and RAD51-H2B ration (**K**) in panel I were shown. (**L**) HeLa cells were pre-treated with control or Sm-D3 siRNA for 2 days. Then 4-hour treatment of 50mM of MG132 was introduced before cell lysates were harvested for IP using anti-RAD51 antibody or control empty magnetic beads. The input, control IP and RAD51 IP samples were analyzed by immunoblotting. (**M**) HeLa cells were treated with control siRNA (-) or Sm-D3 siRNAs (#1 and #2) for 2 days. Cells were treated with 1mM of hydroxyurea overnight and cell lysates were harvested for chromatin fractionation. The whole cell lysis and chromatin-bounded portion were analyzed by immunoblotting. (**N, O**) Quantification of chromatin-bounded CHK1 (**N**) and chromatin-bounded RAD51 (**O**), normalized to those in whole cell lysis, in panel (**M**). The mean values and standard deviations, calculated from at least three independent experiments, were shown. Statistical analysis was conducted using unpaired 2-tailed Student's t-test.

3.4. Discussion

As the core components of the small nuclear ribonucleoproteins (snRNPs), Sm proteins play many important roles in the post-transcriptional regulation of gene expression, including spliceosome assembly and pre-mRNA splicing [140]. Interestingly, adding to these known functions of Sm proteins, we reported here a direct involvement of Sm proteins in DNA repair (Figure 3.3.1& Figure 3.3.2). First, we showed that Sm proteins associated with DSB-mimicking structures in human cell lysates and *Xenopus* egg extracts (Figure 3.3.1B). Second, Sm proteins were recruited to DNA damage sites in human cells (Figure 3.3.1C, D&F); the recruitment of Sm proteins to DNA damage occurred within one minute (Figure 3.3.1C); and such recruitment was independent of ATM/ATR or PARP activities (Figure 3.3.1E). Functionally, our study found that Sm proteins were required for efficient DNA DSB repair via HR (Figure 3.3.2G), and depletion of Sm proteins led to accumulation of endogenous DSBs (Figure 3.3.2A-D).

Mounting evidence in recent studies characterized the involvement of many RNA binding and processing proteins, as well as RNA synthesis *per se*, in DNA repair, especially HR. Several genome-wide screens identified a large number of RNA binding and processing proteins as factors that mediate HR and prevent genomic instability [141-146]. Although this can be attributed partially to the role of these proteins in regulation of gene expression, the direct involvement of these proteins in DNA repair has been indicated by the recruitment of these proteins to DNA damage. In fact, a broad spectrum of RNA processing enzymes, including RNA endonucleases, RNA helicases, RNA polymerases II and III components, and RNA splicing factors, have been directly connected to HR [143, 145-147]. Hand in hand with these findings is the emerging theory of DNA damage response RNA. Interestingly, it has been proposed that RNA molecules may be synthesized at DNA damage sites, to serve as a template to guide

HR, to facilitate the recruitment of downstream repair factors, and to enhance the stability of 3'-single strand DNA overhang [147-149].

The involvement of RNA binding and processing proteins in DNA repair is also highlighted by the formation and resolution of R-loops. R-loop defines DNA/RNA hybrids that can occur during transcription and are normally maintained in homeostasis through balanced formation and removal [150, 151]. R-loops can be formed at DNA damage sites to promote DNA repair. However, mis-regulated R-loops is an important source of genomic instability [152, 153]. On this note, a number of RNA binding proteins are required for the resolution of R-loops, and their depletion leads to accumulation of DNA damage-induced R-loops [154-157].

In this study, we revealed a role of Sm protein in regulation of RAD51 and CHK1 (Figure 3.3.3 & Figure 3.3.4). Sm proteins associated with RAD51 and CHK1 (Figure 3.3.4A-C). Depletion of Sm-D3 reduced the protein levels of CHK1 and RAD51 (Figure 3.3.3A&B), consistent with increased ubiquitination and compromised protein stability (Figure 3.3.4F-I). Interestingly, depletion of Sm-D3 more profoundly impact the level of chromatin-associated RAD51 and CHK1 (Figure 3.3.4J-L), which is consistent with the direct recruitment of Sm proteins to DNA damage (Figure 3.3.1C, D&F). Together, our results defined a new role of Sm proteins in binding and stabilizing HR proteins, and thereby promoting DNA repair. These findings indicate a new and unexpected mechanism for these RNA processing proteins in DNA repair. However, there are many important questions remain to be further investigated, for example, do Sm proteins interact with the ubiquitination enzymes and prevent them from degrading repair proteins on damaged chromatin; if other RNA binding and processing factors play similar functions in DNA repair; and what is the implication of these findings to the involvement of Sm proteins in human diseases.

BIBLIOGRAPHY

1. Vigneron, S., et al., The master Greatwall kinase, a critical regulator of mitosis and meiosis. Int J Dev Biol, 2016. **60**(7-8-9): p. 245-254.
2. Diril, M.K., et al., Loss of the Greatwall Kinase Weakens the Spindle Assembly Checkpoint. PLoS Genet, 2016. **12**(9): p. e1006310.
3. Hermida, D., et al., Molecular Basis of the Mechanisms controlling MASTL. Mol Cell Proteomics, 2019.
4. Castro, A. and T. Lorca, Greatwall kinase at a glance. J Cell Sci, 2018. **131**(20).
5. Ma, S., et al., Greatwall dephosphorylation and inactivation upon mitotic exit is triggered by PP1. J Cell Sci, 2016. **129**(7): p. 1329-39.
6. Rogers, S., et al., PP1 initiates the dephosphorylation of MASTL, triggering mitotic exit and bistability in human cells. J Cell Sci, 2016. **129**(7): p. 1340-54.
7. Della Monica, R., et al., Fcp1 phosphatase controls Greatwall kinase to promote PP2A-B55 activation and mitotic progression. Elife, 2015. **4**.
8. Heim, A., A. Konietzny, and T.U. Mayer, Protein phosphatase 1 is essential for Greatwall inactivation at mitotic exit. EMBO Rep, 2015. **16**(11): p. 1501-10.
9. Soeda, S., et al., RSK-MASTL Pathway Delays Meiotic Exit in Mouse Zygotes to Ensure Paternal Chromosome Stability. Dev Cell, 2018. **47**(3): p. 363-376 e5.
10. Reshi, I., et al., AKT regulates mitotic progression of mammalian cells by phosphorylating MASTL leading to PP2A inactivation. Mol Cell Biol, 2020.
11. Risal, S., et al., MASTL is essential for anaphase entry of proliferating primordial germ cells and establishment of female germ cells in mice. Cell Discov, 2017. **3**: p. 16052.
12. Johnson, H.J., et al., In vivo inactivation of MASTL kinase results in thrombocytopenia. Exp Hematol, 2009. **37**(8): p. 901-8.

13. Hurtado, B., et al., Thrombocytopenia-associated mutations in Ser/Thr kinase MASTL deregulate actin cytoskeletal dynamics in platelets. J Clin Invest, 2018. **128**(12): p. 5351-5367.

14. Pavey, S., et al., Multiple interaction nodes define the postreplication repair response to UV-induced DNA damage that is defective in melanomas and correlated with UV signature mutation load. Mol Oncol, 2020. **14**(1): p. 22-41.

15. Cetti, E., et al., Mitosis perturbation by MASTL depletion impairs the viability of thyroid tumor cells. Cancer Lett, 2019. **442**: p. 362-372.

16. Uppada, S.B., et al., MASTL induces Colon Cancer progression and Chemoresistance by promoting Wnt/beta-catenin signaling. Mol Cancer, 2018. **17**(1): p. 111.

17. Zhuge, B.Z., et al., MASTL is a potential poor prognostic indicator in ER+ breast cancer. Eur Rev Med Pharmacol Sci, 2017. **21**(10): p. 2413-2420.

18. Tian, J., Y. Lin, and J. Yu, E2F8 confers cisplatin resistance to ER+ breast cancer cells via transcriptionally activating MASTL. Biomed Pharmacother, 2017. **92**: p. 919-926.

19. Rogers, S., et al., MASTL overexpression promotes chromosome instability and metastasis in breast cancer. Oncogene, 2018. **37**(33): p. 4518-4533.

20. Alvarez-Fernandez, M., et al., Therapeutic relevance of the PP2A-B55 inhibitory kinase MASTL/Greatwall in breast cancer. Cell Death Differ, 2018. **25**(5): p. 828-840.

21. Nagel, R., et al., Genome-wide siRNA Screen Identifies the Radiosensitizing Effect of Downregulation of MASTL and FOXM1 in NSCLC. Mol Cancer Ther, 2015. **14**(6): p. 1434-44.

22. Wang, L., et al., Mastl kinase, a promising therapeutic target, promotes cancer recurrence. Oncotarget, 2014. **5**(22): p. 11479-89.

23. Howley, P.M., Warts, cancer and ubiquitylation: lessons from the papillomaviruses. Trans Am Clin Climatol Assoc, 2006. **117**: p. 113-26; discussion 126-7.

24. Wang, Y., et al., HECT E3 ubiquitin ligases - emerging insights into their biological roles and disease relevance. J Cell Sci, 2020. **133**(7).

25. Khatri, N. and H.Y. Man, The Autism and Angelman Syndrome Protein Ube3A/E6AP: The Gene, E3 Ligase Ubiquitination Targets and Neurobiological Functions. Front Mol Neurosci, 2019. **12**: p. 109.

26. Dodge, A., et al., Generation of a Novel Rat Model of Angelman Syndrome with a Complete Ube3a Gene Deletion. Autism Res, 2020. **13**(3): p. 397-409.

27. Kuhnle, S., et al., Angelman syndrome-associated point mutations in the Zn(2+)-binding N-terminal (AZUL) domain of UBE3A ubiquitin ligase inhibit binding to the proteasome. J Biol Chem, 2018. **293**(47): p. 18387-18399.

28. Khatri, N., et al., The Autism Protein Ube3A/E6AP Remodels Neuronal Dendritic Arborization via Caspase-Dependent Microtubule Destabilization. J Neurosci, 2018. **38**(2): p. 363-378.

29. Wolyniec, K., et al., E6AP ubiquitin ligase regulates PML-induced senescence in Myc-driven lymphomagenesis. Blood, 2012. **120**(4): p. 822-32.

30. Birch, S.E., et al., Expression of E6AP and PML predicts for prostate cancer progression and cancer-specific death. Ann Oncol, 2014. **25**(12): p. 2392-7.

31. Gamell, C., et al., E6AP Promotes a Metastatic Phenotype in Prostate Cancer. iScience, 2019. **22**: p. 1-15.

32. Paul, P.J., et al., Restoration of tumor suppression in prostate cancer by targeting the E3 ligase E6AP. Oncogene, 2016. **35**(48): p. 6235-6245.

33. Sailer, C., et al., Structural dynamics of the E6AP/UBE3A-E6-p53 enzyme-substrate complex. Nat Commun, 2018. **9**(1): p. 4441.

34. Drews, C.M., N. Brimer, and S.B. Vande Pol, Multiple regions of E6AP (UBE3A) contribute to interaction with papillomavirus E6 proteins and the activation of ubiquitin ligase activity. PLoS Pathog, 2020. **16**(1): p. e1008295.

35. Wang, Y., et al., Identifying the ubiquitination targets of E6AP by orthogonal ubiquitin transfer. Nat Commun, 2017. **8**(1): p. 2232.

36. Mishra, M., et al., Nano-LC based proteomic approach identifies that E6AP interacts with ENO1 and targets it for degradation in breast cancer cells. IUBMB Life, 2019. **71**(12): p. 1896-1905.

37. Kim, J.Y., et al., Induction of E6AP by microRNA-302c dysregulation inhibits TGF-beta-dependent fibrogenesis in hepatic stellate cells. Sci Rep, 2020. **10**(1): p. 444.

38. Pyeon, D., et al., HIV-1 Impairment via UBE3A and HIV-1 Nef Interactions Utilizing the Ubiquitin Proteasome System. Viruses, 2019. **11**(12).

39. Gulati, T., et al., Proteotranscriptomic Measurements of E6-Associated Protein (E6AP) Targets in DU145 Prostate Cancer Cells. Mol Cell Proteomics, 2018. **17**(6): p. 1170-1183.

40. Martinez-Noel, G., et al., Network Analysis of UBE3A/E6AP-Associated Proteins Provides Connections to Several Distinct Cellular Processes. J Mol Biol, 2018. **430**(7): p. 1024-1050.

41. Wolyniec, K., et al., The E6AP E3 ubiquitin ligase regulates the cellular response to oxidative stress. Oncogene, 2013. **32**(30): p. 3510-9.

42. Levav-Cohen, Y., et al., E6AP is required for replicative and oncogene-induced senescence in mouse embryo fibroblasts. Oncogene, 2012. **31**(17): p. 2199-209.

43. Zhu, S., et al., Kinesin Kif2C in regulation of DNA double strand break dynamics and repair. Elife, 2020. **9**.

44. Sanjana, N.E., O. Shalem, and F. Zhang, Improved vectors and genome-wide libraries for CRISPR screening. Nat Methods, 2014. **11**(8): p. 783-784.

45. Liu, X.D., et al., PBRM1 loss defines a nonimmunogenic tumor phenotype associated with checkpoint inhibitor resistance in renal carcinoma. Nat Commun, 2020. **11**(1): p. 2135.

46. Wang, L., et al., Monoclonal antibodies against Xenopus greatwall kinase. Hybridoma (Larchmt), 2011. **30**(5): p. 469-74.

47. Peng, A., L. Wang, and L.A. Fisher, Greatwall and Polo-like kinase 1 coordinate to promote checkpoint recovery. J Biol Chem, 2011. **286**(33): p. 28996-9004.

48. Ren, D., et al., Cell cycle-dependent regulation of Greatwall kinase by protein phosphatase 1 and regulatory subunit 3B. J Biol Chem, 2017. **292**(24): p. 10026-10034.

49. Yan, S., M. Sorrell, and Z. Berman, Functional interplay between ATM/ATR-mediated DNA damage response and DNA repair pathways in oxidative stress. Cell Mol Life Sci, 2014. **71**(20): p. 3951-67.

50. Yamamoto, T.M., et al., Regulation of Greatwall kinase by protein stabilization and nuclear localization. Cell Cycle, 2014. **13**(22): p. 3565-75.

51. Fatima, I., A.B. Singh, and P. Dhawan, MASTL: A novel therapeutic target for Cancer Malignancy. Cancer Med, 2020. **9**(17): p. 6322-6329.

52. Raghu, D., et al., E6AP promotes prostate cancer by reducing p27 expression. Oncotarget, 2017. **8**(26): p. 42939-42948.

53. Cao, L., et al., Inflammatory cytokine-induced expression of MASTL is involved in hepatocarcinogenesis by regulating cell cycle progression. Oncol Lett, 2019. **17**(3): p. 3163-3172.

54. Vera, J., et al., Greatwall promotes cell transformation by hyperactivating AKT in human malignancies. Elife, 2015. **4**.

55. Sun, X.J., et al., Mastl overexpression is associated with epithelial to mesenchymal transition and predicts a poor clinical outcome in gastric cancer. Oncol Lett, 2017. **14**(6): p. 7283-7287.

56. Yoon, Y.N., et al., MASTL inhibition promotes mitotic catastrophe through PP2A activation to inhibit cancer growth and radioresistance in breast cancer cells. BMC Cancer, 2018. **18**(1): p. 716.

57. Jung, S.R., et al., Contribution of STAT1 to innate and adaptive immunity during type I interferon-mediated lethal virus infection. PLoS Pathog, 2020. **16**(4): p. e1008525.

58. Schindler, C., D.E. Levy, and T. Decker, JAK-STAT signaling: from interferons to cytokines. J Biol Chem, 2007. **282**(28): p. 20059-63.

59. Zenke, K., M. Muroi, and K.I. Tanamoto, IRF1 supports DNA binding of STAT1 by promoting its phosphorylation. Immunol Cell Biol, 2018. **96**(10): p. 1095-1103.

60. Cheon, H., et al., IFNbeta-dependent increases in STAT1, STAT2, and IRF9 mediate resistance to viruses and DNA damage. EMBO J, 2013. **32**(20): p. 2751-63.

61. Moore, T.C., et al., Control of early Theiler's murine encephalomyelitis virus replication in macrophages by interleukin-6 occurs in conjunction with STAT1 activation and nitric oxide production. J Virol, 2012. **86**(19): p. 10841-51.

62. Butturini, E., et al., STAT1 drives M1 microglia activation and neuroinflammation under hypoxia. Arch Biochem Biophys, 2019. **669**: p. 22-30.

63. Sato, H., et al., DNA double-strand break repair pathway regulates PD-L1 expression in cancer cells. Nat Commun, 2017. **8**(1): p. 1751.

64. Hagiwara, Y., et al., Analysis of programmed death-ligand 1 expression in primary normal human dermal fibroblasts after DNA damage. Hum Immunol, 2018. **79**(8): p. 627-631.

65. Blazanin, N., et al., Activation of a protumorigenic IFNgamma/STAT1/IRF-1 signaling pathway in keratinocytes following exposure to solar ultraviolet light. Mol Carcinog, 2019. **58**(9): p. 1656-1669.

66. Ah-Koon, L., et al., Cellular response to alkylating agent MNNG is impaired in STAT1-deficients cells. J Cell Mol Med, 2016. **20**(10): p. 1956-65.

67. Ryan, N., et al., STAT1 inhibits T-cell exhaustion and myeloid derived suppressor cell accumulation to promote antitumor immune responses in head and neck squamous cell carcinoma. Int J Cancer, 2020. **146**(6): p. 1717-1729.

68. Hua, L., et al., Activation of STAT1 by the FRK tyrosine kinase is associated with human glioma growth. J Neurooncol, 2019. **143**(1): p. 35-47.

69. Goodman, M.L., et al., Progesterone Receptor Attenuates STAT1-Mediated IFN Signaling in Breast Cancer. J Immunol, 2019. **202**(10): p. 3076-3086.

70. Ragu, S., G. Matos-Rodrigues, and B.S. Lopez, Replication Stress, DNA Damage, Inflammatory Cytokines and Innate Immune Response. Genes (Basel), 2020. **11**(4).

71. Basit, A., et al., The cGAS/STING/TBK1/IRF3 innate immunity pathway maintains chromosomal stability through regulation of p21 levels. Exp Mol Med, 2020.

72. Lohard, S., et al., STING-dependent paracriny shapes apoptotic priming of breast tumors in response to anti-mitotic treatment. Nat Commun, 2020. **11**(1): p. 259.

73. Motwani, M., S. Pesiridis, and K.A. Fitzgerald, DNA sensing by the cGAS-STING pathway in health and disease. Nat Rev Genet, 2019. **20**(11): p. 657-674.

74. Ma, F., et al., LncRNA NEAT1 Interacted With DNMT1 to Regulate Malignant Phenotype of Cancer Cell and Cytotoxic T Cell Infiltration via Epigenetic Inhibition of p53, cGAS, and STING in Lung Cancer. Front Genet, 2020. **11**: p. 250.

75. Thomsen, M.K., et al., The cGAS-STING pathway is a therapeutic target in a preclinical model of hepatocellular carcinoma. Oncogene, 2020. **39**(8): p. 1652-1664.

76. Shouse, G.P., X. Cai, and X. Liu, Serine 15 phosphorylation of p53 directs its interaction with B56gamma and the tumor suppressor activity of B56gamma-specific protein phosphatase 2A. Mol Cell Biol, 2008. **28**(1): p. 448-56.

77. Guinn, Z.P. and T.M. Petro, IFN-gamma synergism with poly I:C reduces growth of murine and human cancer cells with simultaneous changes in cell cycle and immune checkpoint proteins. Cancer Lett, 2018. **438**: p. 1-9.

78. Baris, S., et al., Severe Early-Onset Combined Immunodeficiency due to Heterozygous Gain-of-Function Mutations in STAT1. J Clin Immunol, 2016. **36**(7): p. 641-8.

79. Collins, S.E., R.S. Noyce, and K.L. Mossman, Innate cellular response to virus particle entry requires IRF3 but not virus replication. J Virol, 2004. **78**(4): p. 1706-17.

80. Yang, H., et al., cGAS is essential for cellular senescence. Proc Natl Acad Sci U S A, 2017. **114**(23): p. E4612-E4620.

81. Kwon, J. and S.F. Bakhoum, The Cytosolic DNA-Sensing cGAS-STING Pathway in Cancer. Cancer Discov, 2020. **10**(1): p. 26-39.

82. Kennedy, L.B. and A.K.S. Salama, A review of cancer immunotherapy toxicity. CA Cancer J Clin, 2020. **70**(2): p. 86-104.

83. Zeng, X., et al., Phosphorylation of STAT1 serine 727 enhances platinum resistance in uterine serous carcinoma. Int J Cancer, 2019. **145**(6): p. 1635-1647.

84. Nakayama, Y., et al., PhosphoSTAT1 expression as a potential biomarker for antiPD1/antiPDL1 immunotherapy for breast cancer. Int J Oncol, 2019. **54**(6): p. 2030-2038.

85. Chodisetti, S.B., et al., Serine Phosphorylation of the STAT1 Transactivation Domain Promotes Autoreactive B Cell and Systemic Autoimmunity Development. J Immunol, 2020. **204**(10): p. 2641-2650.

86. Kumm, E.J., et al., The Cell Cycle Checkpoint System MAST(L)-ENSA/ARPP19-PP2A is Targeted by cAMP/PKA and cGMP/PKG in Anucleate Human Platelets. Cells, 2020. **9**(2).

87. Eaglesham, J.B. and P.J. Kranzusch, Conserved strategies for pathogen evasion of cGAS-STING immunity. Curr Opin Immunol, 2020. **66**: p. 27-34.

88. Li, K., et al., Avian oncogenic herpesvirus antagonizes the cGAS-STING DNA-sensing pathway to mediate immune evasion. PLoS Pathog, 2019. **15**(9): p. e1007999.

89. Lee, J.K., et al., Human cytomegalovirus IE86 protein aa 136-289 mediates STING degradation and blocks the cGAS-STING pathway. J Microbiol, 2020. **58**(1): p. 54-60.

90. Saeed, A., et al., Regulation of cGAS-Mediated Immune Responses and Immunotherapy. Adv Sci (Weinh), 2020. **7**(6): p. 1902599.

91. Jiang, L., et al., MTMR2 promotes invasion and metastasis of gastric cancer via inactivating IFNgamma/STAT1 signaling. J Exp Clin Cancer Res, 2019. **38**(1): p. 206.

92. Ceccaldi, R., B. Rondinelli, and A.D. D'Andrea, Repair Pathway Choices and Consequences at the Double-Strand Break. Trends Cell Biol, 2016. **26**(1): p. 52-64.

93. Lamb, N.E., et al., Association between maternal age and meiotic recombination for trisomy 21. Am J Hum Genet, 2005. **76**(1): p. 91-9.

94. Liu, Y. and L.Y. Lu, BRCA1 and homologous recombination: implications from mouse embryonic development. Cell Biosci, 2020. **10**: p. 49.

95. Luo, G., et al., Cancer predisposition caused by elevated mitotic recombination in Bloom mice. Nat Genet, 2000. **26**(4): p. 424-9.

96. Modesti, M. and R. Kanaar, Homologous recombination: from model organisms to human disease. Genome Biol, 2001. **2**(5): p. REVIEWS1014.

97. Powell, S.N. and L.A. Kachnic, Roles of BRCA1 and BRCA2 in homologous recombination, DNA replication fidelity and the cellular response to ionizing radiation. Oncogene, 2003. **22**(37): p. 5784-91.

98. Biswas, K. and S.K. Sharan, RAD52 S346X Variant Reduces Breast Cancer Risk in BRCA2 Mutation Carriers. Mol Oncol, 2020.

99. Pires, E., P. Sung, and C. Wiese, Role of RAD51AP1 in homologous recombination DNA repair and carcinogenesis. DNA Repair (Amst), 2017. **59**: p. 76-81.

100. Yang, G., et al., Super-resolution imaging identifies PARP1 and the Ku complex acting as DNA double-strand break sensors. Nucleic Acids Res, 2018. **46**(7): p. 3446-3457.

101. Schuhwerk, H., et al., Kinetics of poly(ADP-ribosyl)ation, but not PARP1 itself, determines the cell fate in response to DNA damage in vitro and in vivo. Nucleic Acids Res, 2017. **45**(19): p. 11174-11192.

102. Ray Chaudhuri, A. and A. Nussenzweig, The multifaceted roles of PARP1 in DNA repair and chromatin remodelling. Nat Rev Mol Cell Biol, 2017. **18**(10): p. 610-621.

103. Shibata, A., et al., DNA double-strand break repair pathway choice is directed by distinct MRE11 nuclease activities. Mol Cell, 2014. **53**(1): p. 7-18.

104. Oh, J. and L.S. Symington, Role of the Mre11 Complex in Preserving Genome Integrity. Genes (Basel), 2018. **9**(12).

105. Wang, Z., et al., MRE11 UFMylation promotes ATM activation. Nucleic Acids Res, 2019. **47**(8): p. 4124-4135.

106. Tarrade, S., et al., Histone H2AX Is Involved in FoxO3a-Mediated Transcriptional Responses to Ionizing Radiation to Maintain Genome Stability. Int J Mol Sci, 2015. **16**(12): p. 29996-30014.

107. Feng, Y.L., et al., H2AX facilitates classical non-homologous end joining at the expense of limited nucleotide loss at repair junctions. Nucleic Acids Res, 2017. **45**(18): p. 10614-10633.

108. Luczak, M.W. and A. Zhitkovich, Monoubiquitinated gamma-H2AX: Abundant product and specific biomarker for non-apoptotic DNA double-strand breaks. Toxicol Appl Pharmacol, 2018. **355**: p. 238-246.

109. Moeglin, E., et al., Uniform Widespread Nuclear Phosphorylation of Histone H2AX Is an Indicator of Lethal DNA Replication Stress. Cancers (Basel), 2019. **11**(3).

110. Marechal, A. and L. Zou, DNA damage sensing by the ATM and ATR kinases. Cold Spring Harb Perspect Biol, 2013. **5**(9).

111. Kemp, M.G., DNA damage-induced ATM- and Rad-3-related (ATR) kinase activation in non-replicating cells is regulated by the XPB subunit of transcription factor IIH (TFIIH). J Biol Chem, 2017. **292**(30): p. 12424-12435.

112. Menolfi, D. and S. Zha, ATM, ATR and DNA-PKcs kinases-the lessons from the mouse models: inhibition not equal deletion. Cell Biosci, 2020. **10**: p. 8.

113. Ray, A., et al., NER initiation factors, DDB2 and XPC, regulate UV radiation response by recruiting ATR and ATM kinases to DNA damage sites. DNA Repair (Amst), 2013. **12**(4): p. 273-83.

114. Lima, M., et al., Dual inhibition of ATR and ATM potentiates the activity of trabectedin and lurbinectedin by perturbing the DNA damage response and homologous recombination repair. Oncotarget, 2016. **7**(18): p. 25885-901.

115. Roitinger, E., et al., Quantitative phosphoproteomics of the ataxia telangiectasia-mutated (ATM) and ataxia telangiectasia-mutated and rad3-related (ATR) dependent DNA damage response in Arabidopsis thaliana. Mol Cell Proteomics, 2015. **14**(3): p. 556-71.

116. Ray, A., et al., ATR- and ATM-Mediated DNA Damage Response Is Dependent on Excision Repair Assembly during G1 but Not in S Phase of Cell Cycle. PLoS One, 2016. **11**(7): p. e0159344.

117. Mimitou, E.P. and L.S. Symington, Nucleases and helicases take center stage in homologous recombination. Trends Biochem Sci, 2009. **34**(5): p. 264-72.

118. Rechkunova, N.I. and O.I. Lavrik, Photoreactive DNA as a Tool to Study Replication Protein A Functioning in DNA Replication and Repair. Photochem Photobiol, 2020. **96**(2): p. 440-449.

119. Soniat, M.M., et al., RPA Phosphorylation Inhibits DNA Resection. Mol Cell, 2019. **75**(1): p. 145-153 e5.

120. Domingo-Prim, J., et al., EXOSC10 is required for RPA assembly and controlled DNA end resection at DNA double-strand breaks. Nat Commun, 2019. **10**(1): p. 2135.

121. Godin, S.K., M.R. Sullivan, and K.A. Bernstein, Novel insights into RAD51 activity and regulation during homologous recombination and DNA replication. Biochem Cell Biol, 2016. **94**(5): p. 407-418.

122. Huang, T.H., et al., The Histone Chaperones ASF1 and CAF-1 Promote MMS22L-TONSL-Mediated Rad51 Loading onto ssDNA during Homologous Recombination in Human Cells. Mol Cell, 2018. **69**(5): p. 879-892 e5.

123. Li, X., et al., Genome-wide identification and expression analyses of Sm genes reveal their involvement in early somatic embryogenesis in Dimocarpus longan Lour. PLoS One, 2020. **15**(4): p. e0230795.

124. Mahler, M., M.J. Fritzler, and M. Bluthner, Identification of a SmD3 epitope with a single symmetrical dimethylation of an arginine residue as a specific target of a subpopulation of anti-Sm antibodies. Arthritis Res Ther, 2005. **7**(1): p. R19-29.

125. Tsui, H.C., H.C. Leung, and M.E. Winkler, Characterization of broadly pleiotropic phenotypes caused by an hfq insertion mutation in Escherichia coli K-12. Mol Microbiol, 1994. **13**(1): p. 35-49.

126. Zhu, L., X. Zhang, and Z. Sun, SNRPB promotes cervical cancer progression through repressing p53 expression. Biomed Pharmacother, 2020. **125**: p. 109948.

127. Peng, N., et al., c-Myc-mediated SNRPB upregulation functions as an oncogene in hepatocellular carcinoma. Cell Biol Int, 2020. **44**(5): p. 1103-1111.

128. Liu, N., et al., SNRPB promotes the tumorigenic potential of NSCLC in part by regulating RAB26. Cell Death Dis, 2019. **10**(9): p. 667.

129. Wang, H., et al., Identification of Antibody Against SNRPB, Small Nuclear Ribonucleoprotein-Associated Proteins B and B', as an Autoantibody Marker in Crohn's Disease using an Immunoproteomics Approach. J Crohns Colitis, 2017. **11**(7): p. 848-856.

130. Correa, B.R., et al., Functional genomics analyses of RNA-binding proteins reveal the splicing regulator SNRPB as an oncogenic candidate in glioblastoma. Genome Biol, 2016. **17**(1): p. 125.

131. Bacrot, S., et al., Mutations in SNRPB, encoding components of the core splicing machinery, cause cerebro-costo-mandibular syndrome. Hum Mutat, 2015. **36**(2): p. 187-90.

132. Peng, A., et al., Repo-man controls a protein phosphatase 1-dependent threshold for DNA damage checkpoint activation. Curr Biol, 2010. **20**(5): p. 387-96.

133. Fisher, L.A., et al., Phosphatase 1 nuclear targeting subunit is an essential regulator of M-phase entry, maintenance, and exit. J Biol Chem, 2014. **289**(34): p. 23745-52.

134. Bonath, F., et al., Next-generation sequencing reveals two populations of damage-induced small RNAs at endogenous DNA double-strand breaks. Nucleic Acids Res, 2018. **46**(22): p. 11869-11882.

135. van Sluis, M. and B. McStay, A localized nucleolar DNA damage response facilitates recruitment of the homology-directed repair machinery independent of cell cycle stage. Genes Dev, 2015. **29**(11): p. 1151-63.

136. Zhu, S., et al., Protein phosphatase 1 and phosphatase 1 nuclear targeting subunit-dependent regulation of DNA-dependent protein kinase and non-homologous end joining. Nucleic Acids Res, 2017. **45**(18): p. 10583-10594.

137. Lupardus, P.J., C. Van, and K.A. Cimprich, Analyzing the ATR-mediated checkpoint using Xenopus egg extracts. Methods, 2007. **41**(2): p. 222-231.

138. Kambach, C., et al., Crystal structures of two Sm protein complexes and their implications for the assembly of the spliceosomal snRNPs. Cell, 1999. **96**(3): p. 375-87.

139. Gunn, A. and J.M. Stark, I-SceI-based assays to examine distinct repair outcomes of mammalian chromosomal double strand breaks. Methods Mol Biol, 2012. **920**: p. 379-91.

140. Will, C.L. and R. Luhrmann, Spliceosome structure and function. Cold Spring Harb Perspect Biol, 2011. **3**(7).

141. Adamson, B., et al., A genome-wide homologous recombination screen identifies the RNA-binding protein RBMX as a component of the DNA-damage response. Nat Cell Biol, 2012. **14**(3): p. 318-28.

142. Herr, P., et al., A genome-wide IR-induced RAD51 foci RNAi screen identifies CDC73 involved in chromatin remodeling for DNA repair. Cell Discov, 2015. **1**: p. 15034.

143. Tanikawa, M., et al., The spliceosome U2 snRNP factors promote genome stability through distinct mechanisms; transcription of repair factors and R-loop processing. Oncogenesis, 2016. **5**(12): p. e280.

144. Paulsen, R.D., et al., A genome-wide siRNA screen reveals diverse cellular processes and pathways that mediate genome stability. Mol Cell, 2009. **35**(2): p. 228-39.

145. Ouyang, J., L. Lan, and L. Zou, Regulation of DNA break repair by transcription and RNA. Sci China Life Sci, 2017. **60**(10): p. 1081-1086.

146. Dutertre, M., et al., DNA damage: RNA-binding proteins protect from near and far. Trends Biochem Sci, 2014. **39**(3): p. 141-9.

147. Bader, A.S., et al., The roles of RNA in DNA double-strand break repair. Br J Cancer, 2020. **122**(5): p. 613-623.

148. Wei, L., et al., DNA damage during the G0/G1 phase triggers RNA-templated, Cockayne syndrome B-dependent homologous recombination. Proc Natl Acad Sci U S A, 2015. **112**(27): p. E3495-504.

149. Liu, S., et al., RNA polymerase III is required for the repair of DNA double-strand breaks by homologous recombination. Cell, 2021. **184**(5): p. 1314-1329 e10.

150. Belotserkovskii, B.P., et al., R-loop generation during transcription: Formation, processing and cellular outcomes. DNA Repair (Amst), 2018. **71**: p. 69-81.

151. Hegazy, Y.A., C.M. Fernando, and E.J. Tran, The balancing act of R-loop biology: The good, the bad, and the ugly. J Biol Chem, 2020. **295**(4): p. 905-913.

152. Crossley, M.P., M. Bocek, and K.A. Cimprich, R-Loops as Cellular Regulators and Genomic Threats. Mol Cell, 2019. **73**(3): p. 398-411.

153. Skourti-Stathaki, K. and N.J. Proudfoot, A double-edged sword: R loops as threats to genome integrity and powerful regulators of gene expression. Genes Dev, 2014. **28**(13): p. 1384-96.

154. Alfano, L., et al., Depletion of the RNA binding protein HNRNPD impairs homologous recombination by inhibiting DNA-end resection and inducing R-loop accumulation. Nucleic Acids Res, 2019. **47**(8): p. 4068-4085.

155. Nishida, K., et al., RNA Binding Proteins and Genome Integrity. Int J Mol Sci, 2017. **18**(7).

156. Li, L., et al., DEAD Box 1 Facilitates Removal of RNA and Homologous Recombination at DNA Double-Strand Breaks. Mol Cell Biol, 2016. **36**(22): p. 2794-2810.

157. Meng, X., S. Yang, and V.J.A. Camp, The Interplay Between the DNA Damage Response, RNA Processing and Extracellular Vesicles. Front Oncol, 2019. **9**: p. 1538.